FABRICATION OF STIMULI RESPONSIVE AND CONDUCTING

POLYMERIC NANOTUBES BY CHEMICAL VAPOR DEPOSITION:

LOADING/RELEASE AND SENSOR STUDIES

by

Efe Armagan

Submitted to the Graduate School of Engineering and Natural Sciences

In partial fulfillment of the requirements for the degree of

Master of Science

Sabanci University

June, 2016

FABRICATION OF STIMULI RESPONSIVE AND CONDUCTING

POLYMERIC NANOTUBES BY CHEMICAL VAPOR DEPOSITION:

LOADING/RELEASE AND SENSOR STUDIES

APPROVED BY:

Asst. Prof. Dr. Gözde Özaydın-İnce
(Thesis Supervisor)

....

Asst. Prof. Dr. Fevzi Çakmak Cebeci

....

Assoc. Prof. Dr. Gökhan Demirel

....
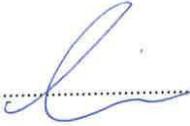
DATE OF APPROVAL: 25/07/2016

FABRICATION OF STIMULI RESPONSIVE AND CONDUCTING POLYMERIC

NANOTUBES BY CHEMICAL VAPOR DEPOSITION: LOADING/RELEASE AND

SENSOR STUDIES

Efe Armagan

MAT, Master of Science Thesis, 2016

Thesis Supervisor: Asst. Prof. Gozde Ozaydin-Ince

Keywords: Stimuli Responsive Polymer Nanotubes, Initiated Chemical Vapor Deposition, Conducting Polymer Nanotubes, Oxidative Chemical Vapor Deposition,

Abstract

Nanostructures have been the great candidates for many engineering applications due to their unique physical properties, for example; high surface to volume ratio compared to bulk structures. Integration of distinct polymer systems to nanostructures of different shapes, i.e nanofibers, nanorods, nanotubes or nanospheres, has enabled researchers to obtain various functional surfaces with the characteristic advantages of these nanostructures. In this study, we separately present the hard-templated nanotube fabrication of single and coaxial stimuli responsive and conducting polymer for drug delivery and humidity sensors application. Nanotubes of stimuli responsive polymers, poly(methacrylic acid) p(MAA) , poly(N-isopropylacrylamide) p(NIPAAm) and poly(hydroxyethylmethacrlyate) p(HEMA), are achieved by initiated chemical vapor deposition (iCVD) technique whereas conducting polymer nanotubes, polyaniline (PANI), are fabricated via oxidative chemical vapor deposition (oCVD). The loading-release capacity and kinetics of single and coaxial stimuli responsive polymeric nanotubes are investigated by monitoring UV-VIS intensity change of model dye molecule, phloroglucinol (Phl). The sensor sensitivity of conducting polymeric nanotubes is studied by analyzing conductivity change of nanotubes under various humid conditions. Furthermore, iCVD and oCVD polymers, which are respectively pHEMA and PANI in this thesis, are combined for coaxial nanotube fabrication in order to enhance the sensitivity of humidity sensors.

UYARIYA DUYARLI POLİMERİK VE İLETKEN POLİMERİK NANOTÜPLERİN

KİMYASAL BUHAR BİRİKTİRME YÖNTEMİ İLE ÜRETİMİ :

YÜKLEME/SALINIM VE SENSÖR ÇALIŞMALARI

Efe Armağan

MAT, Yüksek Lisans Tezi, 2016

Tez Danışmanı: Yard. Doç. Dr. Gözde Özaydın-İnce

Özet

Nanoyapılar kendilerine özgü fiziksel özelliklerinden dolayı, örneğin yüksek yüzey alanı hacim oranı, mühendislik uygulamalarında önem kazanmaya başlamışlardır. Nanofiber, nanoçubuk, nanotüp veya nanoküre gibi farklı şekillerdeki nanoyapılara çeşitli polimer sistemlerinin entegre edilmesiyle birlikte araştırmacılar nanoyapıların fiziksel avantajlarını kullanarak değişik biçimlerde fonksiyonel yüzeyler elde etmeyi başarmışlardır. Bu çalışmada, sert kalıp yöntemi kullanılarak tek veya eş-eksenli olarak elde edilen uyarıya duyarlı polimerik ve iletken polimerik nanotüplerin üretimi, ayrıca ilaç taşınımı ve nem sensörü uygulamaları için yapılan çalışmalar sunulacaktır. Uyarıya duyarlı polimerik nanotüpler, poli(methacrylic acid) p(MAA) , poli(N-isopropylacrylamide) p(NIPAAm) and poli(hydroxyethylmethacrlyate) p(HEMA), başlatıcılı kimyasal buhar biriktirme (iCVD) tekniği ile sentezlenmiştir. Buna karşın iletken polimerik nanotüpler, Polianilin (PANI) oksidatif buhar biriktirme (oCVD) metodu ile üretilmiştir. Tek ve eşeksenli uyarıya duyarlı polimerik nanotüplerin ilaç yükleme ve salma kapasitesi ile birlikte bu işlem sırasındaki kinetikleri incelenmiştir. İletken polimerik nanotüplerin sensör hassasiyeti farklı ortam nemliliğindeki öziletkenlik değişimlerinin analiz edilmesiyle hesaplanmıştır. Bu çalışmanın devamında iCVD ve oCVD polimerleri (bu çalışmada pHEMA ve PANI) kullanılarak eş-eksenli polimerik nanotüpler elde edilmiş olup bu yapıların sensör hassasiyeti üzerine etkisi incelenmiştir.

ACKNOWLEDGEMENT

My family (Kadri Armağan, Gülden Armağan and Emre Armağan) for their limitless support and courage during my whole life, To all of you, Thank you.

Efe Armağan

TABLE OF CONTENTS

CONCLUSION

BIBLIOGRAPHY

LIST OF FIGURES

LIST OF TABLES

LIST OF SYMBOLS AND ABBREVIATIONS

iCVD   Initiated Chemical Vapor Deposition

oCVD   Oxidative Chemical Vapor Deposition

pNIPAAM   Poly (N-isopropylacrylamide)

pHEMA   Poly (2-hydroxyethylmethacrylate)

pMAA   Poly (Methacrylic Acid)

PANI   Polyaniline

EGDMA   Ethylene Glycol dimethacrylate

TBPO   Tert-butyl Peroxide

Phl   Phloroglucinol

FTIR   Fourier Transform Infrared Spectroscopy

SEM   Scanning Electron Microscopy

UV-VIS   Ultraviolet-visible Spectroscopy

XRD   X-Ray Diffraction

AAO   Aluminum Anodic Oxide

nm   Nanometer

°C   Degree Celsius

θ Theta

P_m Monomer Vapor Pressure

P_{sat} Monomer Saturation Pressure

S/cm   Siemens/centimeter

Ω Ohm

Sccm   Standart Cubic Centimeters per Minute

mTorr   Millitorr

SRP   Stimuli Responsive Polymer

CP   Conducting Polymer

To My Beloved Family

CHAPTER 1

INTRODUCTION

1.1 Stimuli Responsive Polymers

Stimuli Responsive Polymers (SRP) can be classified as polymers whose physiochemical properties change with environmental stimuli. Even small external stimuli alteration may suddenly causes a huge change in these polymers' molecular basis resulting in large modification of polymer's response to the environment. The origin of external stimuli alteration, which triggers various behaviors of SRP to different environments, might be either chemical or physical. Chemical stimuli can be pH, chemical agent, ion concentration whereas physical triggers may be temperature, humidity, wavelength of light, electrical or magnetic field and applied force. Due to slight variation in these chemical or physical stimuli, polymer can undergo some changes, such as conformations, water retention capacity, adhesiveness and surface or charge state etc. Furthermore, these changes are mostly reversible and polymer losses all new physiochemical properties with the removal of external stimuli. The tremendous response to environmental alteration and reversibility make SRP polymers very unique for various applications for instance drug delivery, sensors, bioseparators and food packaging.

1.2 Stimuli Responsive Polymers: Types and Applications

Stimuli Responsive Polymers are entitled with regard to which external stimuli affects their physiochemical properties. There are several types of SRP polymers which are commonly classed as temperature responsive polymers, pH responsive polymers, water/moisture responsive polymers (hydrogels), light responsive polymers etc. For example, poly(vinyl cinnamate) (pVCIN) is one of the polymer which is classified as light responsive polymer. Since, ultraviolet light suddenly alters pVCIN's molecular and bond structure, it is possible to play with crosslinker ratio by changing wavelength of incoming light [1]. Fig.1 also demonstrates the structural changes of pVCIN with regard to incoming light energy. Thus, pVCIN enables to obtain various surface modifications (hydrophobicity/hydrophilicity) or mechanical properties with respect to wavelength of light. However, pH responsive polymers, temperature responsive polymers and hydrogels were used as SRP polymers in this thesis.
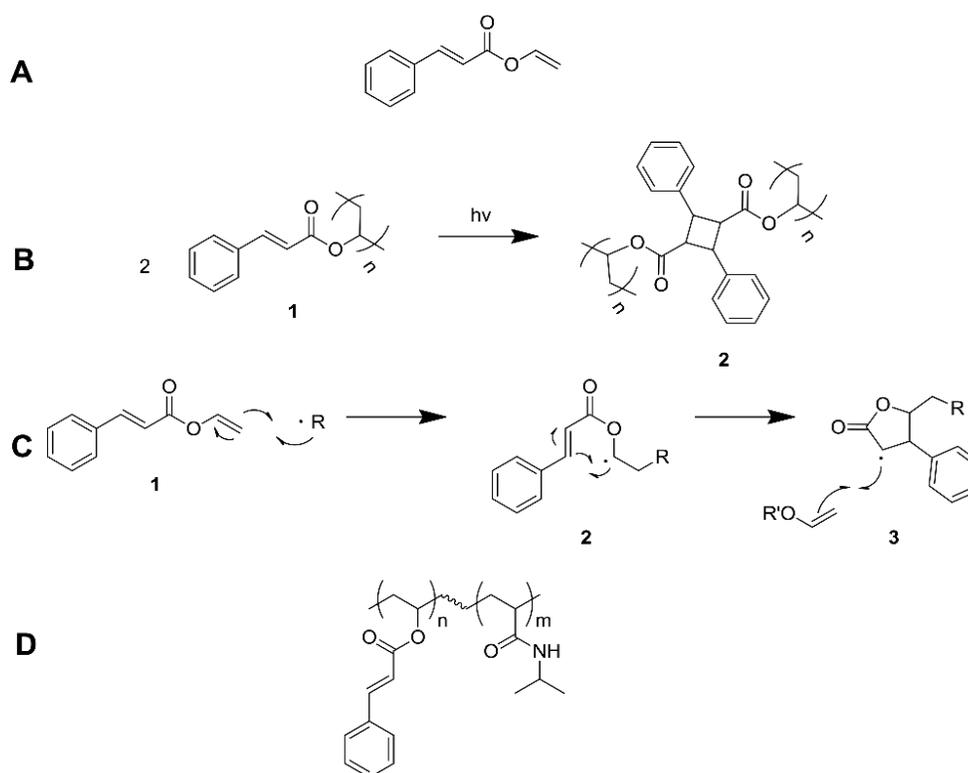
Figure 1: Illustration of pVCIN's structural modification with respect to incoming UV light[1]. A) VCIN monomer B) Dimerization of VCIN monomer exposed to UV light C) Cyclization of VCIN D) Copolymer of VCIN

1.2.1 pH Responsive Polymers

pH responsive polymers are able to display different physiochemical properties in regard to pH level of environment due to ionizable pendant group in the polymer structure. Polymer chain conformation, polymer volume and solubility can vary with ambient acidity or basicity. Volumetric expansion or shrinkage make pH responsive materials very popular in different applications. This behavior is mainly due to presence of a weakly ionizable functional group that accepts or donates protons with regard to ambient pH level. pH responsive polymers show a transition from collapsed state to expanded state at the exact point of acid dissociation constant (pK_a) due to osmotic pressure change. The main reason behind volumetric modification is presence of acid or basic group in the polymer structure. At pK_a value, electrical charge of these acid or basic groups can drastically change so that electrostatic repulsion between each polymer chain is affected by the change of number of charged groups in polymer structure that causes volumetric expansion or shrinkage in polymer network.

pH responsive polymers are divided into two classes in terms of availability of side groups, which are entitled as weak polyacids and weak polybases. Weak polyacidic pH responsive polymers possess acidic side groups, such as carboxylic acid or sulfonic acid and their low pK_a values makes them a good candidate showing volumetric transition at lower pH ambient. In other words, weak polyacidic polymers accept protons at low pH whereas donate protons at high pH., therefore, many negatively charged group forms in the whole polymer chain that results in strong electrostatic repulsion between polymer chain and volumetric expansion happens at high pH ambient [2]. The most known examples of weak polyacidic pH responsive polymers are poly(acrylic acid), poly (methacrylic acid) and polysulfonamides [3]. On the other hand, pH responsive materials having weak base groups displays an opposite trend. Their base groups (ammonium salts) are protonated at high pH whereas they include positively charged pendant groups at neutral or low pH. Thus, polybases are in the swollen state at lower pH due to large electrostatic repulsion forces between positively charged functional groups of polymer chains. Poly (4-vinylpyridine), poly (2-vinylpyridine) and poly (vinylamine) are the most common examples of polybasic pH responsive polymers.

In recent years with the advances in nanotechnology, pH responsive polymers has gained increasing interest due to wide range of applications especially in biotechnology, such as drug delivery, gene carriers or food industry. For example, Liu et al. [4] demonstrates the use of pH responsive micelles for cancer chemotherapy by triggering the drug release location of micelles with respect to acidity of tumor tissue.

In this thesis, poly (methacrylic acid), known as weak polyacid, was used as pH responsive polymers. It swells under high pH conditions due to deprotonation of the carboxy groups which causes a net electrostatic repulsion force among the polymer molecules and shrinks at low pH due to protonation of the carboxy group [5].

1.2.2 Thermo-Responsive Polymers

Thermo-responsive polymers are highly sensitive to the temperature, they abruptly alter their microstructural and physiochemical properties with regard to ambient temperature. In recent years, they are most widely used and safest group of stimuli responsive polymer for especially drug delivery system and biomaterials due to great microstructural reversibility and ease of stimulus change. Thermo-responsive polymers show the transition between hydrophobic state and hydrophobic state at the temperature point called "critical solution temperature". Lower critical solution temperature (LCST) phenomena is commonly seen for thermo-responsive polymers. When polymer solution temperature is below LCST, it is soluble and possesses hydrophilic behavior. However, as solution temperature raises and becomes higher than LCST, hydrophobic interactions dominate and polymer chain collapse [7]. On the other hand, the polymer which has upper critical solution temperature (UCST) point behaves oppositely compared to LCST polymers. Above UCST point, the polymer is dissolved in solvent whereas it forms globular shape below UCST.

The theory behind transition between hydrophilicity and hydrophobicity is balance between interactions of polymer-polymer chains, polymer-solvent molecules and solvent-solvent molecules. Flory-Huggins solution theory (equation 1) explains the mechanism of microstructural change of thermo-responsive polymers in the solution.

$$\frac{\Delta G_{mix}}{RT} = \frac{\emptyset_1}{m_1} \ln\emptyset_1 + \frac{\emptyset_2}{m_2} \ln\emptyset_2 + \chi \emptyset_1\emptyset_2 \qquad (1)$$

where ΔG_{mix} is Gibbs free energy, T is temperature, R is universal gas constant, m is number of occupied lattice sites per molecule, $\emptyset$ is volume fraction of the polymer and solvent and χ is interaction parameter. χ value is highly temperature dependent so that as temperature changes, dominancy of interaction parameter also varies. At the critical point where interaction parameter makes ΔG_{mix} zero, polymer's microstructural changes occur. Therefore, as ΔG_{mix} goes to positive, polymer chains collapse and forms globular shape vice versa when interaction parameter decreases with respect to ambient temperature, ΔG_{mix} become negative, so thermo-responsive polymer are soluble in that temperature.

The well-known examples of LCST type thermo-responsive polymers are poly (N-isopropyacrylamide) (pNIPAAm), poly (N,N'- diethyl acrylamide), poly (dimethylamino ethyl metharcylate), poly (2-carboxy isopropyl acrylamide) and poly (N-(L)-(1-hydroxymethyl) propyl methacrylamide) [8]. Some famous thermo-responsive polymers and their LCST point are also listed in Table 1.

Abbreviation	Name	LCST (^{0}C)
PNIPAAm	Poly(N-isopropylacrylamide)	32
PVCL	Poly(N-vinylcaprolactam)	31
PPO	Poly(proprylene oxide)	10-20
PVME	Poly(vinyl methyl ether)	33.8
MC	Methylcellulose	50
EHEC	Ethyl(hydroxyethyl)cellulose	65
PDMA	Poly(2-dimethylamino)ethyl methacrylate)	50
PEMA	Poly(N,N-ethylmethylacrylamide)	70
PNPAm	Poly(N-n-propylacrylamide)	25
PBMEAm	Poly(N,N-bis(2-methoxyethyl) acrylamide)	49
HPC	Hydroxypropylcellulose	42

Table 1: List of common LCST thermo-responsive polymers and their LCST point[8]

In this thesis, p(N-isopropylacrylamide) (pNIPAAm) was used as thermo-responsive polymeric material. pNIPAAm is a thermoresponsive polymer which demonstrates a phase segregation above the lower critical solution temperature (LCST) of approximately 32 °C [9,10]. Below LCST, hydrogen bonds form between the hydrophilic amide groups and water molecules, whereas above LCST the hydrogen bonds between amide groups of the pNIPAAm chains exposing the hydrophobic isopropyl groups [11]. Fig. 2 demonstrates the molecular structure of pNIPAAm and how polymer chain reacts as ambient temperature varies. This transition from hydrophilic to hydrophobic behavior above LCST can be used as a trigger in wide areas, such as controlled release mechanisms, making pNIPAAm one of the most commonly used polymers especially in drug delivery systems. Studies focusing on drug delivery applications of pNIPAAm generally involve bulk polymers or nanospheres, loaded with drug that is released as the polymer shrinks when heated [12-14].
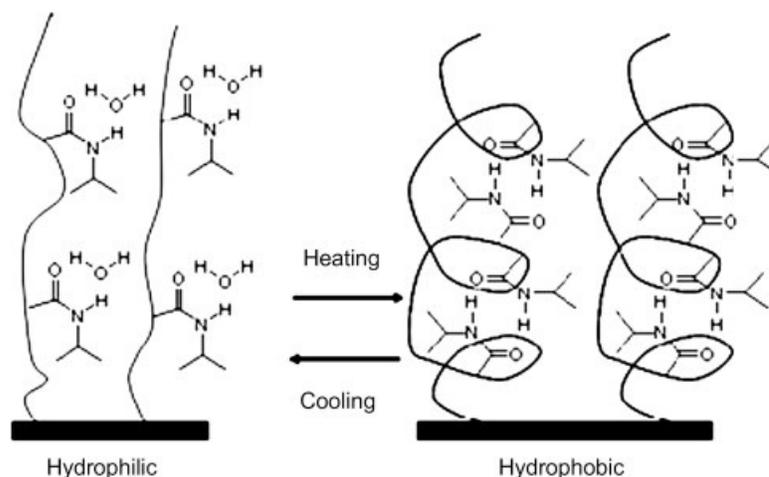
Fig 2: Illustration of physiochemical change of pNIPAAm with regard to temperature alteration [15].

1.2.3 Hydrogels: pHEMA

Poly(hydroxy ethylmethacrylate) (pHEMA) belongs to the class of water responsive hydrogels. pHEMA, like the other hydrogels, can be defined as a hydrophilic material which is insoluble in water when crosslinked. These tremendous properties make pHEMA an extensively used polymer for biotechnology such as drug delivery or contact lenses. In recent years with the advances in nanotechnology, pHEMA has been used as nano-sized materials due to its non-toxicity, ease of fabrication, biocompatibility and

exceptional swelling ratio in water. Most basically, pHEMA swells in water ambient whereas it gives back all intake water in dry ambient. This transition occurs because of orientation of pHEMA side groups and backbone. Fig. 3 shows molecular structure of HEMA monomer and pHEMA polymer. When pHEMA is in water, pHEMA hydroxyl (-OH) group orients outward and forms stronger hydrogen bonding with water molecules. Thus, polymer network intakes water and swells. However, as ambient become drier, hydrophobic methyl groups orient outward so that hydrophobic interactions dominate the whole polymer chains, resulting in deswelling of pHEMA.
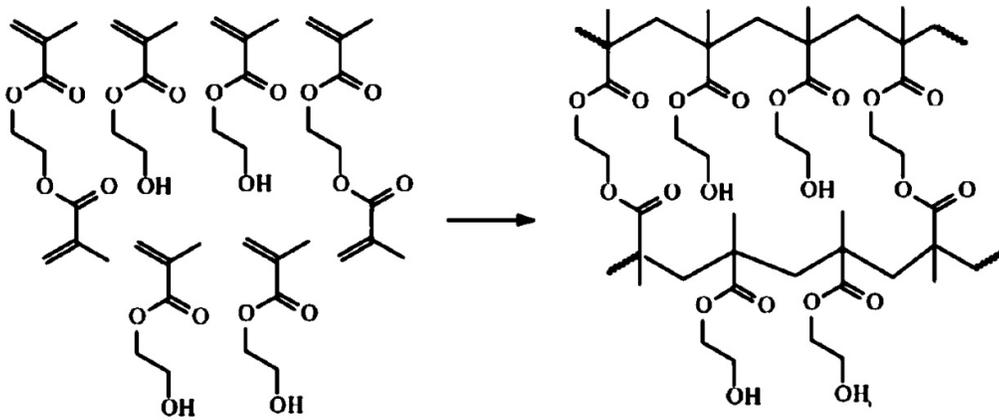
Fig 3: Representation of HEMA monomer (left) and formation of pHEMA (right) after polymerization

Flory-Rehner Theory thermodynamically explains the swelling-deswelling mechanisms of hydrogels in different environmental conditions. According to this theory, total Gibbs Free Energy (ΔG_{total}) (equation 2) is summation of free energy caused by elastic forces ($\Delta G_{elastic}$) and free energy caused by mixing (ΔG_{mixing}). Koetting et al. [16] states that "Flory–Rehner theory posits that hydrogel equilibrium is attained through a balance of enthalpic mixing, which promotes swelling, and the elastic forces imposed by the crosslinked hydrogel chains, which promotes contraction."

$$\Delta G_{total} = \Delta G_{elastic} + \Delta G_{mixing} \qquad (2)$$

Furthermore, Peppas and Merrill [17] developed new equations (equation 3 and 4) about the variation of mesh size of polymer network with regard to ambient moisture by using Flory-Rehner Theory. The model basically describe the molecular weight of polymer chain between each crosslink points that remains the same for neutral polymer although ambient humidity changes. However, the hydrogels contain ionizable functional group which force the polymer chain swelling when encounters aqueous medium.

$$\frac{1}{Mc} = \frac{2}{Mn} - \frac{\frac{v}{V1}[\ln(1+vs)+vs+x(vs^2)[1-\frac{Mr}{2Mc}vs^{\frac{2}{3}}]^3}{(vs^{\frac{1}{3}}-0.5vs)[1+\frac{Mr}{2Mc}vs^{\frac{1}{3}}]^2} \tag{3}$$

where v is specific volume, x is the Flory-Huggins interaction parameter, V_1 is the molar volume of water, v_s is the ratio of dry thickness to wet thickness and M_n is number average molecular weight of polymer. However, M_n is large enough to assume that first term goes to zero.

$$\xi = Q^{1/3}\left[2Cn\left(\frac{Mc}{Mr}\right)\right]^{1/2} l \tag{4}$$

where ξ is the mesh size, Q is swelling ratio, l is C-C bond length (1.54 A°), C_n is characteristic ratio. By contrasting ξ of polymer chain at water and dry ambient, it is possible to comment on how much hydrogel swells or deswells.

1.3 Conducting Polymers

For years, polymers are known as insulator materials, however, for the first time Shirakawa et al. [20] discovered that intrinsically organic polymer, polyacetylene, become electrically conducting material when doped with redox reaction. The conductivity of polyacetylene reaches 10^3 S/cm after redox doping whereas it is initially lower than 10^{-5} S/cm. The remarkable increase in polyacetylene conductivity attributes to its conjugated structure with alternating single and double bonds which provides p-orbital for a continuous orbital overlap. Although metal's electrical conductivity only depends on its free electrons, conducting polymers have one more significant property besides number of charge carriers that is orbital overlapping which enables charge

carriers move along polymer chains.

Many conducting polymers are insulator before redox doping so that they should be treated with doping steps which create p-type or n-type charge carriers that is required for electrical conduction. P-type charge carriers are produced at the end of oxidation reaction whereas n-type carriers are formed in consequence of reduction of polymer chain. Since, conductivity depends on number of charge carriers, carrier mobility and electron charge, organic polymer conductivity remarkably increases after oxidation/reduction reactions because of rise in number of charge carriers. Due to thermodynamically favorable process, formation of negative or positive charged sites in polymer chains causes lattice distortion which is called polaron or bipolaron. Donor type conducting polymers (n-type) have negatively charged polaron /bipolaron in molecular structure vice versa acceptor type conducting polymers (p-type) have positively charged polaron/bipolaron [21].

Doping concentration of conducting polymer can be higher than inorganic based semiconductors. Some polymers, having great conductivity level, may comprise up to 50% oxidized or reduced components in their polymeric structures. Besides, conducting polymers are reversible in terms of their extrinsic conductivity. By eliminating charged particles and creating neutral states, conducting polymers may return to insulators. Removal of p-type charge carriers can be caused by reacting the polymer with electron donors, for example reducing agents. Conversely, oxidizing agents lead to elimination of n-type charge carriers that result in insulators instead of conducting polymers. The reversibility between insulators and conductors are the key property for some applications, such as organic transistors or rechargeable batteries [22].

The formation of charged states after doping of conducting polymer leads to charge transfer and movement along polymer chain which results in local distortion and relaxation. This distortion and relaxation changes the geometry of polymer chains at charged state compared to undoped states that induces the formation of intermediate electronic states between band gap which modifies the π electrons mobility. Conducting polymers are divided into two classes based on energy degeneracy and location of these intermediate electronic states which are degenerate CP and non-degenerate CP. For example, polyacetylene is one of the degenerate CP because two geometric structures

exactly have the same total energy in the ground state (Fig. 4). Also, the defect formed after doping step divides polyacetylene two part which have the same energy. The energy point where separate the system into two is called "soliton" (Fig 5.)
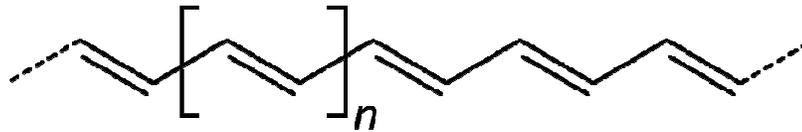
Fig 4. : Demonstration of molecular structure of trans-polyacetylene chain. Although location of all double bonds change, the total energy remains the same that leads to degeneracy.
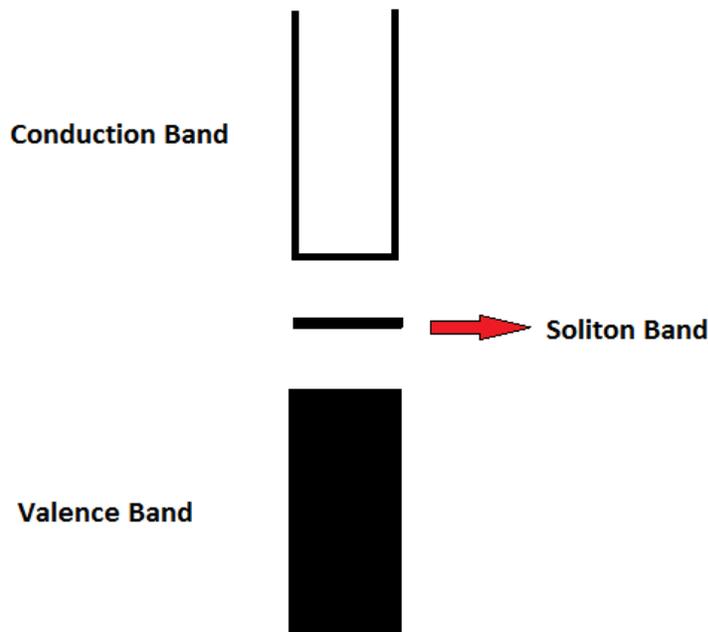
Fig. 5: Schematic of band structure of degenerate conducting polymer

The heterocyclic conducting polymer, such as polypyrrole, polyaniline, polythiophene, PEDOT or polyselenophene are non-degenerate polymers due to the energy difference between two ground states so that their band structure are completely dissimilar to polyacetylene. Instead of soliton bands, non-degenerate conducting polymers have polarons or bipolarons, depending on doping concentration, in their band structure at the stable defect state [23]. Fig 6. illustrates the change in band structure of non-degenerate conducting polymer with increasing amount of dopant. When dopant concentration is around 1%-1.5%, formation of polaron band in band structure occurs.

However, as dopant concentration raises to 2%-10%, spin concentration becomes vanished due to addition of new charge carriers between conduction and valence electrons. Thus, spinless bipolaron bands are created at the end of dopant supplementation.
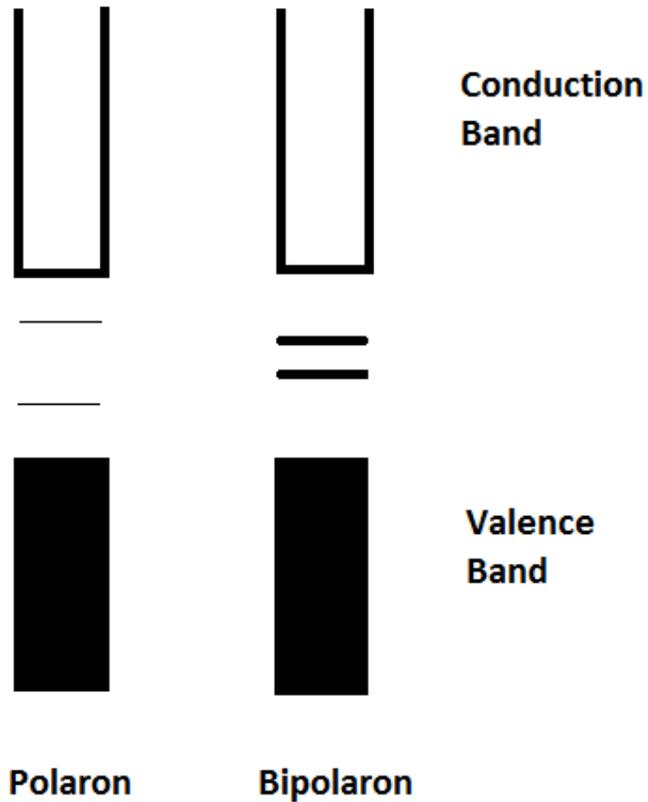
Fig. 6 : Representation of polaron and bipolaron band structure in non-degenerate conducting polymers.

Some commonly used conducting polymers, their band gap and conductivities are listed in Table 2.

Polymer (Discovered Date)	Band Gap (eV)	Conductivity (S/cm)
Polyacetylene (1977)	1.5	10^3 -$2*10^5$
Polypyrole (1979)	3.1	2- $3*10^2$
Polythiophene (1981)	2	10- 250
Polyaniline (1980)	3.2	1-130

Table 2 : List of the common used conducting polymers, their band gap and conductivities.

Among many conducting polymers, PANI is one of the commonly used polymer due to superiority of some properties compared to the other conducting polymers. Firstly, thermal stability is better than other common polymers. It enables the researchers use PANI for various applications which require elevated temperatures. Secondly, the electrical conductivity is good enough to take place in applications requiring intermediate conductivity (1-100 S/cm). In terms of economic perspective, PANI is cheaper and can be easily synthesized by different polymerization technique. Furthermore, PANI has several stable states which depend on doping level so that it is applicable to transfer PANI from one state to another state by reacting with various solutions. This reversibility brings the advantage of on-off state in terms of conductivity that is key requirement especially for transistor-like applications.

PANI's molecular structure has benzenoid and quinoid groups in polymer chain, the oxidation level of PANI denoted as 1-y in Fig. 7. PANI can form 3 distinct molecular state with respect to y value. According to that, when y becomes 1, PANI can exist as fully reduced form which is called leucomeraldine (LE), however, as oxidation level increases and 1-y value raises, quinoid structures forms in PANI chains. At exactly

y=0.5, half oxidized emeraldine base (EB) exists whereas as oxidation level arises, PANI reaches its maximum oxidized state which is called pernigraniline (y=0). However, protonated form of emeraldine base, called as emeraldine salt (ES), conducts electricity. Its electrical conductivity shifts between 1-130 S/cm [24,25]. Fig 8. summarizes polymer structure of   all oxidized and reduced state of PANI (leucomeraldine, emeraldine and pernigraniline).
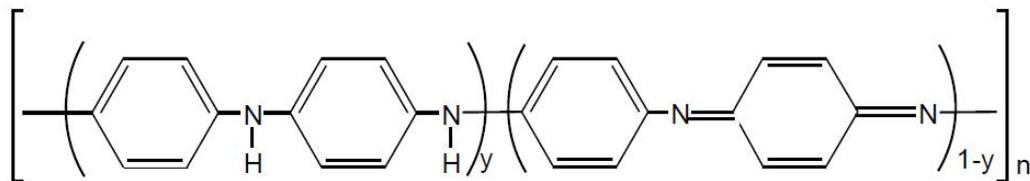
Fig 7. : Demonstration of the PANI structure with respect to oxidation level (1-y) [26]
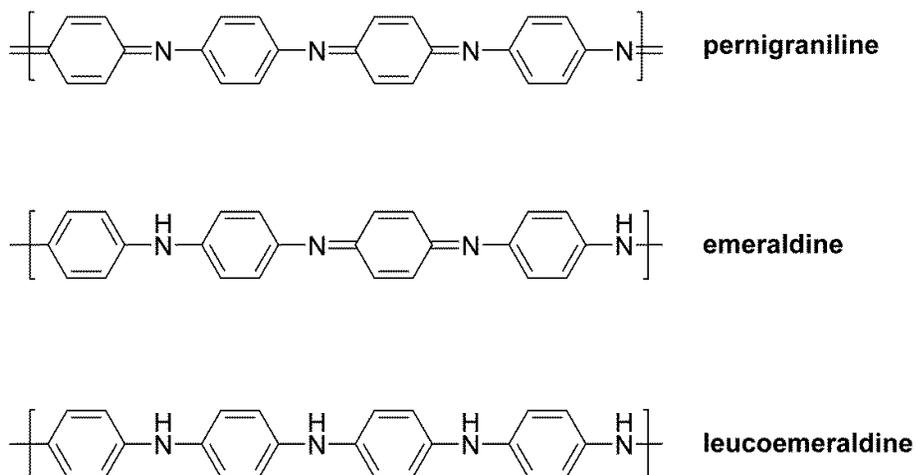
Fig. 8 : Fully oxidized (pernigraniline), half oxidized (emeraldine) and fully reduced (leucomeraldine) state of PANI

1.4 Nanotubes

In recent years with the advances in nanotechnology, the use of nanostructure material has gained increasing interest in various applications, such as biotechnology, food industry, sensors or photovoltaics [27-32]. The unique advantages of nanostructures make these materials very popular in the research. These advantages are high surface-to-volume ratio which provides greater contact area with the other materials that brings better response and response rate. For example, the nanostructure configuration provides more sensitivity and minimized diffusion constant due to greater surface-to-volume ratio [33]. Besides, the nanoscale systems have different and unique properties in the molecular and atomic level compared to bulk and thin film systems. Particularly, these differences affects the electronic, optical and magnetic properties of the materials. The better confinement of the materials in the nanostructures increases the electrical conductivity that is key for sensor applications to obtain greater sensitivity. Furthermore, the recent studies show that using nanostructures in photovoltaics significantly enhances the performance and efficiency of the devices due to high control over material's band gap and lower recombination possibility between holes and electrons. Polymeric nanostructures have been commonly used rather than the other materials due to their prominent advantages, for example; cost-effectiveness, ease of fabrication and tremendous biocompatibility that make polymeric nanostructures become very popular in different areas [34,35]

Nanoporous materials belong to the class of nanostructure materials that includes nanotubes, nanocapsules and nanoporous cylinder arrays [36,37]. Due to their greater nanospace inside the structure, these materials are commonly used to release, capture or store the nanomaterials. Thus, nanoporous materials are the good candidate in the application of catalysis, drug delivery, sensors, gas storage and separation systems. Among the nanoporous materials above, the nanotubes are the most popular structures because of having circular nanospaces. Firstly, the open mouth structure of nanotubes makes the inner surface accessible for various nanosized materials. Secondly, the larger inner surface, due to its circular shape, provides the better loading amount of nanosized materials that enables these materials to use as a nanocarriers in the application of drug delivery, sensor or membrane systems. Thirdly, the control over size of nanotube's openings and length brings the advantage of selectivity for penetrant molecules. In other words, the undesired molecules can be eliminated by changing the size and length.

Fourthly, existence of two separated surface of nanotubes (inner and outer surfaces) can provide different surface functionalization of these surfaces that may also enhance the device efficiency and bioselectivity in various applications.

1.4.1 SRP Nanotubes

Stimuli Responsive Polymers (SRP) which respond to a stimulus change by changing their physiochemical properties are preferred for fabrication of nanostructures to achieve better control over application dependent performance. Besides, the biocompatible nature of SRP polymers make these materials very unique in the application of biomedical devices and food industry [38,39].

In the SRP based nanosystems the release of the molecules is triggered by a change in the stimuli which leads to physical changes in the polymer chain. Furthermore, by tuning the chemical composition of the polymers, the response rate can be adjusted depending on the application. Extensive studies on the fabrication of SRP nanostructures of different shapes, such as spheres, rods, or tubes, exist in the literature [40-43] In recent years , great number of study about drug delivery using nanostructures was reported. For example, Garcia-Millan et al. [44] improved drug loading-release capacity by optimizing pHEMA composition and nanostructure using water during the polymerization. Chang et al. synthesized nanoporous pNIPAAm to study the effect of porous size on total release amount [45]. However, the performance of nanorods, nanofibers or the other closed nanostructures is limited in drug delivery application due to lack of nanospace and surface functionalization Therefore, SRP nanotubes are frequently chosen for fabrication of drug delivery system. Baochun et al. [46] used pH responsive pMAA in the fabrication of butadiene-styrene nanotubes for better store and release performance. Chen et al. [47] fabricated crosslinked poly (glycidyl methacrylate) polymeric nanotubes functionalized with pNIPAAm as a drug carrier for anti-cancer treatment. Furthermore, Cavallaro et al. [48] used pNIPAAm as a grafting material on outer surface of halloysite nanotubes that enhances the adsorption of drug molecules. However, the nanotubes are generally synthesized using solution polymerization techniques. Due to wetting effect and wettability, the solution polymerization bring some limitations for the fabrication of nanotubes. For example, fully conformal nanotubes cannot be obtained after the polymerization. Furthermore, the fabrication of

polymeric nanotubes having high aspect ratio is not facile using solutions in the polymerization. Besides, mixing monomer in the solvent can cause contamination and impurity in the final nanotube concentration. Therefore, for the fabrication of templated nanotubes, chemical vapor phase deposition techniques are preferred due to conformal coatings that can be achieved.

In recent years, there are many studies about the fabrication of SRP nanostructures using chemical vapor deposition technique. McInnes et al. [49] used chemical vapor deposited pMAA thin films to cap the pores pSi pores that is loaded with drug molecules. Ozaydin-Ince et al. [50] achieved the fabrication of pHEMA nanotube forest using Aluminum Anodic Oxide (AAO) template to show the better loading-release capacity due to greater swelling of pHEMA nanotubes rather than flat film. Armagan et al. [51,52] reported the fabrication of pH responsive polymeric nanotubes and single/coaxial polymeric nanotubes using initiated chemical vapor deposition (iCVD).

In this thesis, AAO membranes and Si wafers are used as templates and are conformally coated with SRP polymers (pMAA, pHEMA and pNIPAAm) using iCVD for the fabrication of single and coaxial nanotubes. The aim of the study is to tune the release rates by fabricating single nanotubes and incorporating different SRPs in the nanotubes.

1.4.2 CP Nanotubes

In last decades, great attention has been attracted for conducting polymer in the fabrication of nanostructures due to its good electrical conductivity, high flexibility, environmental and thermal stability, ease of production and low cost. The higher electrical conductivity of CP made nanostructures due to better polymer confinement and regularity make these materials very popular in various semiconductor based applications. CP based nanostructures; such as nanowires, nanorods, nanotubes or nanospheres have been extensively studied through solution based techniques, either chemical polymerization or electrochemical polymerization [53-58] especially in light emitting diodes, photovoltaic cells, supercapacitors, sensors and drug delivery [59-64]. Similarly to SRP nanotubes, CP nanotubes are commonly used especially in the application of sensors and actuators due to high surface-to-volume ratio that provides better adsorption of penetrant materials. For example, Kwon et al. [65] reported the fabrication of multidimensional PEDOT nanotubes for ultrasensitive chemical nerve

16

agent sensing. On the other hand, Ishpal et al. [66] fabricated polypyrrole nanotubes in order to analyze sensing mechanism in the ammonia environment. Moreover, polythiophene-carbon composite nanotubes were fabricated to use as sensors for chemical warfare agents [67]. However, use of solvents is a major drawback for homogeneity and conformal coatings, especially on high aspect ratio templates, due to wetting effect and surface tension that affects the electrical conductivity and performance of CP based device. Thus, vapor phase polymerization techniques have emerged for conducting polymer deposition that facilitates the fabrication of conformal polymeric nanostructures [68,69].

Due to its great thermal and air stability, electrical conductivity, ease of fabrication, economic advantage and reversibility, PANI is widely used polymer in various nano-applications, such as supercapacitors, sensors, solar cell and membrane [70-73]. PANI is a good candidate material for sensor application due to the change of oxidation/reduction level which affects electrical conductivity responding to environmental conditions, for example humidity or pH. Liu et al. fabricates PANI nanofibers ammonia sensors whose electrical conductivity varies with NH_3 concentration, enhances the sensitivity of ammonia sensor up to 0.88 mV/ppm [74]. There are also numerous studies which are about the effect of pH change on PANI sensor [71, 75]. For PANI humidity sensors, for the first time Zeng et al. shows the reverse resistance change of PANI nanofibers depending on humidity level [76]. Lin et al. fabricates electrospun PANI nanofibers and introduces hydrophilic material into PANI to improve the sensitivity of humidity sensors [77]. Parvatikar et al. indicates PANI composites are also useful for detection of humidity level [78].

In this thesis, PANI nanotubes and PANI+ SRP coaxial nanotube fabrication were achieved using oxidative chemical vapor deposition (oCVD) in order to control and enhance the sensitivity of humidity sensor.

CHAPTER 2

EXPERIMENTAL PROCEDURE and CHARACTERIZATION

2.1 pH Responsive Polymeric Single Nanotube Fabrication

Chemical Vapor Deposition (CVD) is one of the important technique for fabrication high quality thin films. The CVD synthesized thin films are widely used in several areas such as biomedical devices, MEMS, membranes, drug delivery etc. These areas require high compositional purity and retention of polymer functionality. Therefore, CVD offers better synthesizing conditions rather than liquid based techniques, for instance spin coating or dip coating.

In CVD techniques, evaporated gas molecules are the reactive materials during the polymerization so that these methods have several advantages over solution based polymerization techniques. Firstly, all CVD methods enable great thickness control in thin film fabrication. Thus, it is feasible to obtain ultra-thin polymer coating after deposition. Secondly, elimination of wetting effect and wettability, due to all dry environment in CVD, provides tremendous thin film conformality that is not possible to fabricate as conformal as CVD with solution polymerization. Therefore, the substrates having complex geometrical patterns can be conformally coated by CVD techniques.

The other major advantage of CVD is retention of polymer functional groups which is vital for applications based on stimuli responsive polymers whose key properties comes

from functional pendant groups. The main reason behind retention is lower energy transfer into reaction chamber during polymerization due to low temperature environment [79]. Consequently, many stimuli responsive polymers may be deposited by CVD in order to be used as hydrophilic/hydrophobic materials, bio/chemical resistance, high swelling response, tunable mechanical performance and tunable copolymer concentration. Furthermore, it is very facile to avoid unwanted and side reactions due to low temperature chamber conditions that increases the thin film purity which is also key for several applications.

Initiated Chemical Vapor Deposition (iCVD) is in the class of hot wire chemical vapor deposition technique. The main difference of iCVD is decomposing of initiator molecules into radicals when confronting hot filament wires in the iCVD chamber which launches free radical polymerization by reacting with monomers. Radical molecules and evaporated monomers are adsorbed by iCVD stage cooled with water chiller system. Then, adsorbed radicals and monomers suddenly start polymerization reaction on the chamber stage. As mentioned, iCVD is one of free radical polymerization based CVD system. Thus, there are 3 stages during polymerization that are initiation, propagation and termination. It is possible to make analogy between iCVD and the other polymerization techniques based on free radical polymerization. However, the main difference between is existence of adsorption and desorption phenomena, which should be taken into consideration in iCVD.

As described earlier, iCVD has an advantage of retention of polymer functional groups during polymerization due to relatively low temperature ambient. The initiators, commonly used in iCVD, are decomposed into radical molecules at around 150-300 °C so that iCVD chamber does not radiationally heat up too much compared to the other polymerization techniques that preserves monomers' functional group while polymerizing. The main requirement of initiator using in iCVD is their high volatility and low decomposition temperature. Thus, the common iCVD initiators can be listed as; tert-butyl peroxide (TBPO), triethylamide (TEA) and tert-amyl peroxide (TAPO) [80].

iCVD is gas phase vapor deposition technique, so monomers are delivered in the gas phase to the vacuum reactor. In order to send monomers into chamber in the gas phase, all monomers should have enough vapor pressure. Thus, some monomers are heated up to the certain temperature in order to obtain ideal vapor pressure which is between 1-10

Torr for iCVD monomers whereas some of them can be used at room temperature.

There are several iCVD parameters that affect the reaction kinetics during polymerization. Firstly, as described earlier, the monomers and radicals are adsorbed by cooled stage so that stage temperature determines the amount of adsorbed molecules per unit time and has an effect on deposition rate. Basically, as stage temperature decreases, the number of adsorbed monomer or radical molecules increase on the stage that leads to higher deposition rate rather than deposition at high stage temperature. The other two parameters affecting polymerization and deposition rate are reactor pressure and monomer/initiator flowrate. Herein, it is very crucial to define two concepts which highly depend on pressure and flowrate. First term is monomer vapor pressure (P_m) that shows the pressure of evaporated monomer molecules at given temperature. Second one is monomer saturation pressure (P_{sat}) which represents the maximum vapor pressure of monomer at certain temperature. Classius-Clapeyron equation is used in order to calculate P_{sat} value that depend on reactor stage temperature and reactor pressure. By varying stage temperature and pressure, P_{sat} value alters and it leads to different deposition kinetics than before. However, P_m only depends on monomer flow rate and even slight changes in monomer flow rate can make huge differences in P_m which is also key for deposition rate. In general, as P_m/P_{sat} ratio increases, the deposition rate also ascends at certain value. The increase of P_m/P_{sat} ratio can be achieved by lowering stage temperature, raising reactor pressure or boosting monomer flow rate. However, although it is theoretically possible to increase P_m/P_{sat} to 1, condensation and liquidification of monomers begin to occur on reactor stage beyond $P_m/P_{sat} =0.8$. Conversely, thin film deposition cannot start if P_m/P_{sat} ratio is below than 0.1 due to insufficient amount of monomer and initiator molecules in the reactor. Therefore, the deposition can be achieved at $0.1 < P_m/P_{sat} < 0.8$.
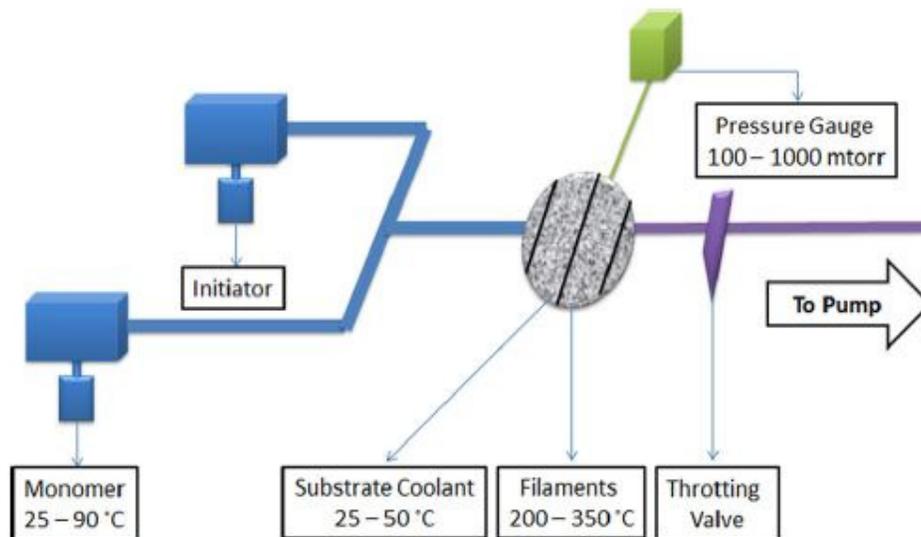
Fig. 9: Components of iCVD system and its working conditions [81]

In pH responsive polymer deposition, the iCVD system which is converted from basic custom-made plasma vapor deposition chamber of 20 liters was used. The system contains monomer and initiator pipelines/ jars, stage chiller system, pressure controller by butterfly valve, oil-vacuum system, temperature controllers for filaments and monomer jars, and laser system for thickness determination. Fig. 11 demonstrates the part and connection system of home-made iCVD chamber in SUNUM /Sabanci University. The monomer pipelines are always kept at elevated temperature, between 90°C and 110 °C in order to avoid condensation of evaporated monomer molecules before reaching iCVD reactor. The heating of both monomer pipelines and jars are provided by plastic heating cable and wrapped by aluminum foil to remove energy loss and obtain better heating at the jar and pipeline part. In order to cool the stage, LabO branded water chiller is used that has connection from chiller to bottom of chamber where sample stage locates. The stage temperature can be adjusted between 10°C and 50°C which is optimal range for iCVD deposition. The chamber pressure is modified by monitoring capacitance manometer (MKS) and manually adjusting the vacuum opening (Edwards, Speedivalve). Initiator or nitrogen's flowrate is automatically measured by flowrate controller system (Aalborg MFC). The filaments are heated up to required temperature with the help of power supplier (Sorensen, Ametek) which changes the

voltage or current through the filament wires. Laser system (HeNe laser with 632 nm) ,placed at the top of iCVD reactor, is used in order to monitor thickness of thin film coated on substrate.
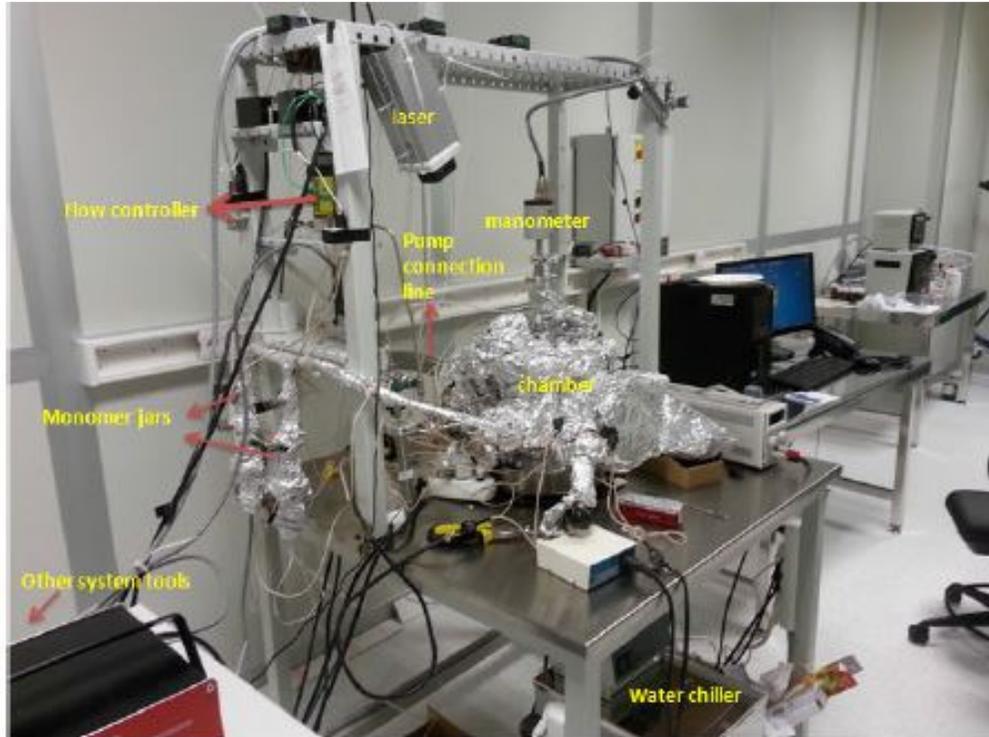
Figure 10: Component of iCVD system in Sabancı University

For pH responsive polymer deposition, the monomers methacrylic acid (MAA, Aldrich, 98%) and ethylene glycol dimethacrylate (EGDMA, Aldrich, 98%) and the initiator tert-butyl peroxide (TBPO, Aldrich, 98%) were used as received. The initiator was kept at room temperature while MAA and EGDMA were heated to 75 °C and 85 °C respectively. The deposition flowrates of monomer/initiator, stage temperature and chamber pressure were decided according to P_m/P_{sat} ratio ,which should be between 0.1 and 0.7 as shown in previous chapter, by using specific excel file. After waiting for stabilization of temperature, flow rates of monomers and initiators were calculated by closing the vacuum outlet and monitoring the pressure change at every 2 seconds. The flowrates used during deposition were 1 sccm for MAA, 0.1 sccm for EGDMA, 0.8 sccm for TBPO and 1 sccm for nitrogen gas (N_2). Nitrogen gas was passed through iCVD reactor to clean the system and use as carrier gas for more homogenous coating.

In next step, a quarter of silicon wafer (Wafer World) and AAO membranes were placed inside of calibrated iCVD chamber while stage temperature was arising. In this study, the main aim of using AAO membranes is fabricating polymer nanotube forest by eliminating AAO non-porous part of membrane. Figure 11 indicates basic schematic of how nanotubes produced after removal of AAO. By depositing polymer into AAO channels, hollow shape polymeric structure can be obtained. Then, the removal of AAO in NaOH or HCl solution creates polymeric nanotubes. However, the iCVD deposition on AAO should be slower than on flat surface due to the fact that AAO pore openings should not close with rapid polymer deposition which may prevent the nanotube fabrication. Therefore, low P_m/P_{sat} ratio, close to 0.1, was selected for all depositions. The AAO membranes had pores of 200 nm diameter with an aspect ratio of 200:1. Polymer thin film deposited on Si substrates were used for characterization of the pH response of the polymer films, whereas the AAO membranes were used for nanotube fabrication and drug delivery study. AAO membranes and Si substrates were placed next to each other in the deposition chamber and were coated simultaneously. After reaching base pressure of iCVD reactor, the chamber pressure was set to 180 mTorr and subsequently filament temperature (T_f) was increased to 245 °C that started the polymerization reaction. The thickness of coating was monitored by 632 nm HeNe laser source. Laser interferometer measured the periodic laser intensity change with increasing of film thickness.. Besides pH responsive polymer coating, for the deposition of p(EGDMA) control sample and nanotubes, pure p(EGDMA) was coated on AAO templates at flowrates of 0.12 and 0.8 sccm for EGDMA and TBPO respectively. The other deposition conditions were kept the same during the polymerization. The all deposition flowrates are summarized in Table 3.

	MAA flowrate (sccm)	EGDMA flowrate (sccm)	TBPO flowrate (sccm)	Nitrogen flowrate (sccm)
pMAA	1	0.1	0.8	1
pEGDMA	-	0.12	0.8	-

Table 3: Flowrates of pMAA and pEGDMA during single nanotube fabrication

After iCVD deposition, the polymer coated AAO templates were immersed into 1 M HCl solution for 24 hours to etch the AAO membranes and release the nanotubes. Then, the remaining polymer nanotubes were rinsed three times at DI water and dried for 24 hours before characterization.
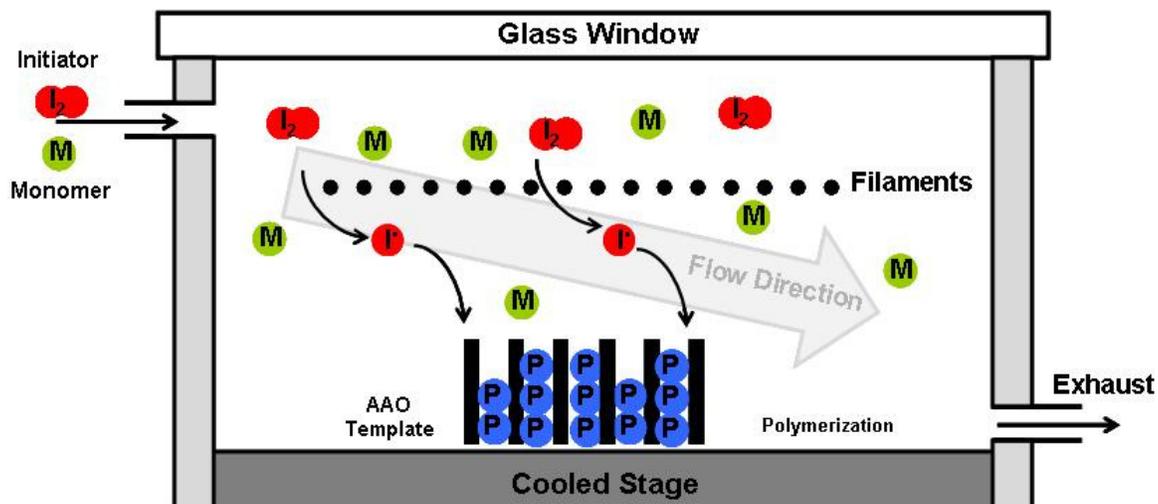
Figure 11: Fabrication of AAO templated nanotubes in iCVD [82]

2.2 Stimuli Responsive Polymeric Coaxial Nanotube Fabrication

For stimuli responsive polymeric coaxial nanotube deposition, the same deposition procedure was followed as fabrication of pH responsive single nanotubes. AAO templates and flat Si substrates were coated with crosslinked pNIPAAm, pNIPAAm + pHEMA, pNIPAAm + pMAA and pEGDMA polymers by using iCVD technique. Similarly to previous deposition, the pEGDMA polymer was used to fabricate the control samples. Si wafers and AAO templates were coated simultaneously; placed next to each other in the chamber. Flat Si substrates were used for chemical identification whereas AAO templates were used for nanotube fabrication.

The monomers NIPAAm (Aldrich, 97%), MAA (Aldrich, 99%) , HEMA (Aldrich, 99%) , the crosslinker EGDMA (Aldrich, 98%) and TBPO (Aldrich, 98%) were used as received, without further purification. NIPAAm, MAA, HEMA and EGDMA monomers were heated up to 80 ℃, 75 ℃, 70 ℃ and 85 ℃ respectively, in jars outside the chamber and delivered into the system in the vapor phase. For all depositions, the substrate and filament temperatures were 35 ℃ and 240 ℃, respectively and the

chamber pressure was maintained at 450 mTorr. The flowrates used during deposition were 1.1 sccm for NIPAAm, 0.7 sccm for HEMA and 1 sccm for MAA, however EGDMA and TPBO flowrates vary with type of monomer. EGDMA flowrate was 0.07 sccm for NIPAAm deposition, 0.1 sccm for HEMA and 0.1 sccm for MAA coating whereas 2 sccm, 1 sccm and 0.8 sccm TBPO were respectively used for NIPAAm, HEMA and MAA deposition. For control sample preparation, 0.15 sccm EGDMA and 0.8 sccm TBPO was used. Nitrogen flowrate was kept at 1 sccm for all deposition, except control sample, to clean the system and use as carrier gas for more homogenous coating. Table 4 lists the flowrates of all monomers used in the deposition.

	NIPAAm flowrate (sccm)	HEMA flowrate (sccm)	MAA flowrate (sccm)	EGDMA flowrate (sccm)	TBPO flowrate (sccm)	Nitrogen flowrate (sccm)
pNIPAAm	1.1	-	-	0.07	2	1
pHEMA	-	0.7	-	0.1	1	1
pMAA	-	-	1	0.1	0.8	1
pEGDMA	-	-	-	0.15	0.8	-

Table 4: Flowrates of monomers for iCVD depositions of different polymers.

For coaxial nanotube fabrication, outer layer of nanotubes was selected as pNIPAAm so that the pNIPAAm polymer was coated firstly. Then, all pNIPAAm coated AAO membranes are treated by oxygen plasma etcher (BRAND) at 50 Watt for 30 seconds in order to etch the top layer that reopens the membrane pores. Subsequently, the inner layer deposition was carried out by coating either pHEMA or pMAA. For the fabrication of closed-end nanotubes, the coated AAO templates were first loaded with dye molecules, and another layer of pNIPAAM polymer was deposited on top to cap the tube openinings. Finally, all coated opened-end or closed-ended AAO membranes (pNIPAAm+pHEMA, pNIPAm+pMAA, pNIPAAm and pEGDMA) were immersed into 1 M HCl solution for 24 hours to remove AAO membranes and obtain polymeric nanotube forest.

2.3 Flat SRP Film Characterization

FTIR Analysis:

Polymer coated Si wafer and bare Si wafer were used for FTIR measurement. The measurement was taken by FTIR (Thermo Fisher Scientific, Model NICOLET iS10). Before beginning spectra acquisition, N_2 gas was passed through FTIR chamber to remove residual air inside that enables to get better resolution spectra. Firstly, polymer coated Si wafer was placed into FTIR and measurement was carried out in between 400 cm^{-1} and 4000 cm^{-1} with 4 cm^{-1} resolution and 256 scans. Subsequently, bare Si wafer's measurement was conducted by following the same procedure. Eventually, spectra of coated Si wafer was subtracted from bare Si wafer to only analyze the spectra of polymer thin film.

Ellipsometry Analysis:

For ellipsometry analysis, Ellipsometer (M-2000, J.A Woollam) was used in order to analyze film thickness and swelling ratio of polymer films. Firstly, calibration process was performed by placing bare Si wafer onto ellipsometer stage. Then, the software (WVASE32, J.A Woollam) automatically checked the signal intensity whether the device is healthy or not. When calibration was done, polymer coated Si wafer was located onto stage. The acquisition parameters were manually entered to the software. The incident angles were adjusted as 65°, 70° and 75°within the region of 250 nm and 800 nm wavelength. After the acquisition completed, the data was fitted to find film thickness or roughness by using Cauchy-Urbach isotropic model, which is the most suitable model for SRP polymers, and entering initial guess of thickness or refractive index of polymer films.

For swelling analysis, the ellipsometer measurement was performed at single angle (75°) in contrast to static measurement explained previous paragraph. Firstly, the thickness of coated Si wafer was measured in air for 5 minutes. Afterwards, pMAA was placed into dynamic measurement equipment of ellipsometer, then 0.0064 M KOH (pH=8) and 0.00102 M HCl (pH 4) were separately poured on coated Si wafer. For pHEMA swelling measurement, only DI water was dropped on sample. For pNIPAAm, DI water was dropped on sample and substrate temperature varied between 25 °C and 45 °C in order to see the response of temperature responsive pNIPAAm. Subsequently, the device had obtained the data for 25 minutes. The fitting of data in air and in different

solution were separately done by using Cauchy-Urbah model and combined in the software in order to see the change of thickness with time.

2.4 Loading- Release Capacity and Kinetics Characterization

Scanning Electron Microscopy:

In this study, Field Emission SEM (Zeiss, SUPRA VP 35) was used to understand whether the nanotube fabrication was achieved or not. Furthermore, nanotube wall thickness was calculated by acquiring SEM images. The accelerating voltage of 4 kV and working distance of 6-7 mm was selected for all SEM measurements. The reason of lower voltage choice is to avoid damaging the polymer sample.

UV-VIS Study:

For loading and release study, the model molecule phloroglucinol (Phl) was used instead of drug molecules due to ease of accessibility and low price. The importance of Phl is having the molecular structure which shows UV excitation peak at 267 nm. Thus, it is achievable to calculate the loading or release capacity of nanotubes filled by Phl by following the change of UV-VIS intensity at the wavelength of 267 nm. When dye concentration arises in the solution which is analyzed in UV light, the intensity also increases in UV spectra and vice versa.

Before starting the loading & release study, the concentration of Phl solution was optimized considering maximum allowable intensity which UV-VIS equipment (Shimadzu, UV-VIS 3150) can measure. According to that, 0.003 M Phl solution was prepared. Subsequently, the stability of the Phl dye was tested by monitoring the changes in the UV-VIS intensity as a function of time for a solution at constant concentration. It was observed that the intensity did not change up to 72 hours at DI water, pH values of 4 and 8 and temperature of 25 °C and 40 °C, confirming that the absorbance of the dye remained the same.

For pMAA single polymeric nanotubes' loading, the polymer nanotubes were immersed in dye solution at pH 8 (KOH) for 24 hours at 25 °C. At the end of 24 hours, the dye concentration of the solution was measured to find the approximate value of the loaded dye inside nanotubes. Herein, the maximum intensity (I_{max}) which is measured at 0.003 M Phl solution was taken as reference value. All UV-VIS intensity measured after

nanotubes are loaded by Phl (I_{load}) is linearly correlated with the maximum intensity. The formula showing how to calculate loading concentration (C_{load}) of polymer nanotubes is given below;

$$\frac{I_{max} - I_{load}}{I_{max}} * 0.003 = C_{load} \qquad (5)$$

For coaxial polymeric nanotubes' loading, three pNIPAAM nanotubes abbreviated as NI1, NI2 and NI3 were respectively loaded in DI water dye solution at following conditions; NI1 at pH 7 and 25 °C, NI2 at pH 7 and 40 °C, NI3 at pH 7 and 25 °C. pNIPAAm+ pHEMA coaxial nanotubes, denoted as NIHE1, NIHE2 and NIHE3 was respectively immersed in DI water dye solution with 25 °C, 40 °C and 25 °C. Finally, pNIPAAm + pMAA nanotubes entitled as NIMA1, NIMA2 and NIMA3 was respectively immersed in 25 °C, 40 °C and 25 °C KOH dye solution with constant pH value of 8. All loaded coaxial nanotubes stayed in dye solution for 24 hours. Then, dye solutions were analyzed with UV-VIS and the same procedure was applied in order to calculate loaded dye concentration. There is only exception for closed-end nanotubes that loading was performed prior to etching of the AAO template.

For release experiment of single pMAA nanotubes, Phl loaded nanotubes were first washed three times with DI water and then immersed in pure HCl or KOH solution at pH 4 or pH 8. The release of dye as a function of time was monitored using UV-VIS spectroscopy by taking 6 mL of solution. The release concentration ($C_{release}$) was calculated with similar method as explained in calculation of loading concentration. The measured intensity ($I_{release}$) in UV-VIS spectroscopy was linearly proportioned with the maximum intensity of Phl dye and multiplied by 0.003 M, resulting in released dye concentration. The equation giving release concentration is given below;

$$\frac{I_{release}}{I_{max}} * 0.003 = C_{release} \qquad (6)$$

For release experiment of coaxial nanotubes, before starting UV-VIS measurement, the nanotube samples were rinsed three times with DI water to remove the excess dye solution. Subsequently, the polymer nanotubes were immersed in DI water at different

28

temperatures and pH values. The change in dye concentration in water was monitored by taking 6 mL of solution and measuring the concentration using UV-VIS periodically over time. The details of the loading and release conditions of coaxial nanotubes are provided in Table 5. Moreover, the stability studies were performed by repeating the loading and release experiments 3 times for each set of samples and the change in the release performance of the polymer nanotubes was monitored.

Samples	Polymers	Loading		Release	
		pH	Temperature (°C)	pH	Temperature (°C)
NI1	pNIPAAm	7	25	7	25
NI2	pNIPAAm	7	40	7	25
NI3	pNIPAAm	7	25	7	40
NIHE1	pNIPAAm + pHEMA	7	25	7	25
NIHE2	pNIPAAm + pHEMA	7	40	7	25
NIHE3	pNIPAAm + pHEMA	7	25	7	40
NIMA1	pNIPAAm + pMAA	8	25	4	25
NIMA2	pNIPAAm + pMAA	8	40	4	25
NIMA3	pNIPAAm + pMAA	8	25	4	40

Table 5: Dye Loading and release conditions for coaxial nanotubes

2.5 Conducting Polymeric Nanotube Fabrication

As described earlier, oxidative chemical vapor deposition (oCVD) is in the class of step-growth based deposition techniques. In other words, the polymer thin film fabricated by oCVD, unlikely in iCVD, is polymerized via step-growth polymerization. The main purpose of oCVD is realizing the production of conducting polymeric thin film which is composed of heterocyclic monomers, such as aniline, thiophene, pyrrole or 3-4 ethylenedioxythiophene (EDOT). Similarly to iCVD, the deposition parameters are reactor pressure, monomers' flowrate and stage temperature. However, since oCVD is non-hot wire chemical vapor deposition method, there is no parametric term called as filament temperature. Basically, the monomer and oxidant molecules spontaneously react and deposit polymer thin film without any initiation requirement, such as photon and temperature. Fig. 10 illustrates the component of oCVD reactor where conducting thin film deposition take places. Either solid oxidant, such as Iron (III) Chloride, Copper (II) Chloride, Iron (III) tosylate [83-85], or liquid oxidant, vanadium oxytrichloride, bromine or antimony pentachloride [86-88], can be used in order to both start the

reaction with monomers and provide extra doping to as-obtained polymer thin film for enhancement in electrical conductivity. Solid oxidants are placed into resistively heated ceramic crucible inside the chamber whereas liquid oxidant are kept in the glass jar outside the chamber. By obtaining enough vapor pressure from solid and liquid oxidant either heated up to certain temperature or kept at room temperature, the evaporated oxidant molecules are sent to the stage which looks towards oxidant's inlet. Simultaneously, the evaporated monomer molecules, which again have enough vapor pressure, flow into oCVD chamber from side ports. The monomers reach sample stage with the help of vacuum system which pulls the monomer towards vacuum outlet. The situated vaporized monomers and oxidants on the stage start the polymerization reaction resulting in conducting polymer thin film.

As mentioned earlier, oCVD has step-growth mechanism during thin film polymerization. First of all, when oxidant molecules encounter evaporated monomer, they create radical cations in monomer molecular structure. Then, two radical cations form dimer of these two monomer. Straight after dimerization reaction, the anions ,which exist in oxidizing agent, take the excess protons of dimer structure in order to stabilize the product. Repeatedly, the oxidizing agent reacts with stable dimer molecules to generate more radical cations. Eventually, huge polymer chain grows by the reaction between oxidizing agent and molecularly large radical cations. After fabrication of uncharged polymer chain, some heterocylic rings become positively charged by anions of oxidizing agent which is called dopants. Consequently, doping process occurs at the end of polymerization steps and the polymer thin film gets electrically conductive due to formation of polaron or bipolaron bands depending on dopant concentration.
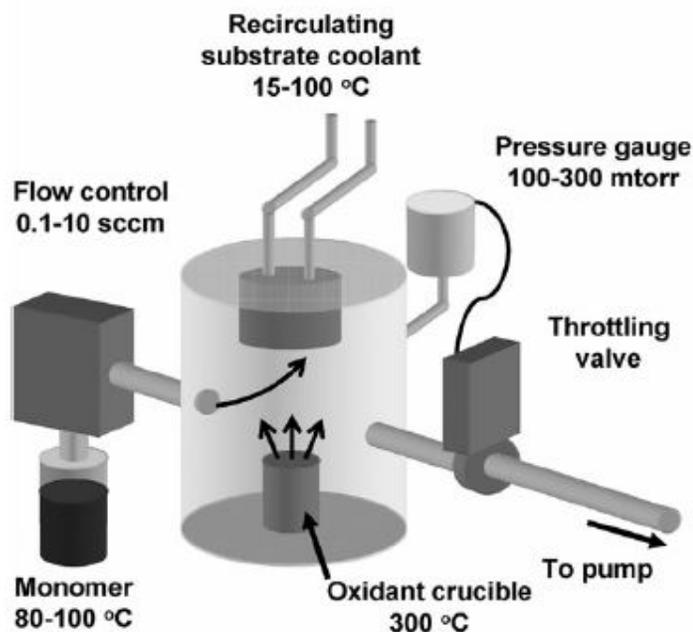
Fig. 12: Schematic Illustration of oCVD reactor's components [88]

Conducting Polymeric Single Nanotubes were fabricated using oxidative chemical vapor deposition technique (oCVD) which is converted from physical vapor deposition (PVD) chamber to 35.5 liter oCVD reactor. Furthermore, resistively heated ceramic crucible and sample stage was added by company (NANOVAK) in order to control stage temperature and solid oxidant flowrate during film deposition. Besides, two monomer pipelines, their heating equipment provided by plastic heating cable and mass flow controllers/ valve system was connected to oCVD chamber as shown in figure 12. The temperature of monomer pipelines was kept at 95 °C to prevent possible condensation due to monomer flow. The homogenous heating and minimum energy loss were obtained by tightly wrapping the aluminum foil. The heater system used in sample stage enabled to control stage temperature in the range of 25 °C and 120 °C. For deposition below 25 °C, LabO branded water chiller is used that has connection from chiller to the top of sample stage. The chamber pressure was monitored using capacitance manometer provided by NANOVAK and manually adjusting the vacuum opening. The solid oxidant placed in ceramic crucible was heated up by applying voltage through highly resistive wire. The deposition temperature of solid oxidant was determined with respect to its evaporation temperature. Besides, liquid oxidant was sent to oCVD chamber from bottom part. Similarly to monomer, liquid oxidant was heated

up to the temperature provided enough vapor pressure using plastic heating cable with power supplier and controlling with automatic temperature controller (Sorensen, Ametek). After setup of oCVD reactor, the minimum leak was measured around 0.002 sccm and base pressure was 15 mTorr
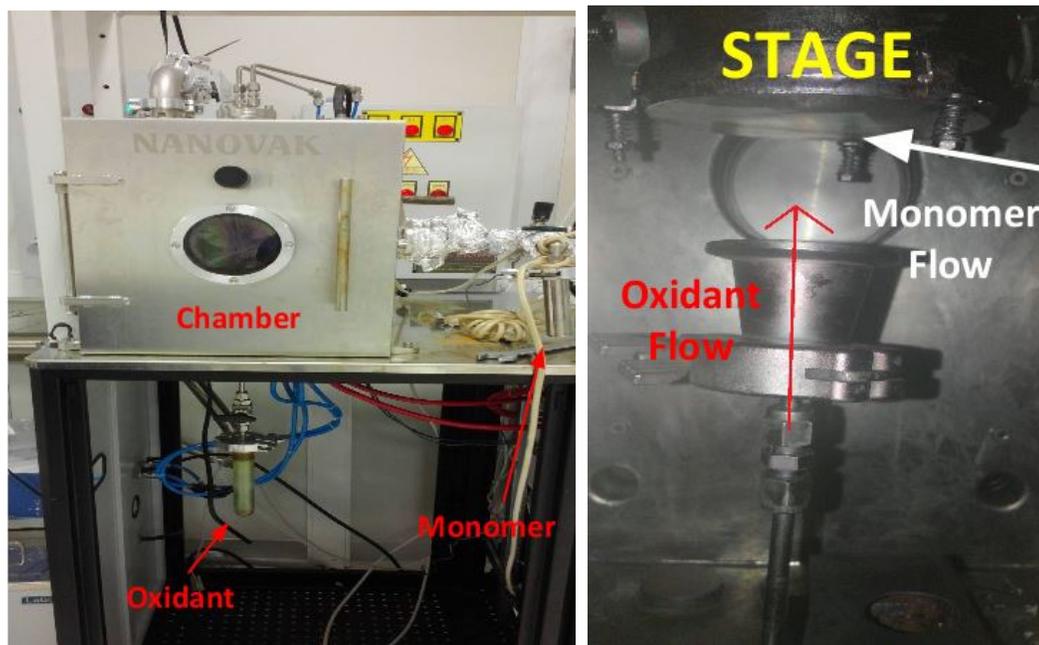
Figure 13: oCVD chamber and components

For conducting polymeric nanotube fabrication, the monomer aniline (Aldrich, 98%) and the oxidant antimony pentachloride ($SbCl_5$) (Aldrich, 98%) were purchased. Both chemicals were used in synthesis process without further purification. The aniline was heated within a metal jar up to 60 °C while $SbCl_5$ was kept at room temperature within a glass jar. Both chemicals were connected to the chamber through metal pipelines. As substrates on the stage, glass slide, Si wafer and AAO template were used. Si wafer and glass slide were used for thin film characterization whereas AAO templates were used for nanotube fabrication. The flowrates was determined as 1.6 sccm for aniline and 1.2 sccm for $SbCl_5$ after several optimization experiment.

Subsequently, four different deposition conditions were performed by only changing stage temperature and keeping constant the chamber pressure and monomer/oxidant flowrates. The stage temperatures were set to 25 °C, 40 °C, 60 °C and 80 °C for each deposition.

All depositions were carried out for 15 minutes at 25 mTorr. The polyaniline coated AAO membranes were exposed to oxygen plasma cleaner with 50 watts for various time depending on thickness of polymer thin film. The membranes were immersed into 0.5 M HCl solution for 48 hours to remove the template without causing damage to polymer nanotubes and release the polymeric nanotubes.

2.6 Flat Polyaniline Film Characterization

For chemical characterization, FTIR and RAMAN spectroscopy was performed on polyaniline coated Si wafer. For FTIR measurement, the spectra was acquired between 400 cm^{-1} and 4000 cm^{-1} with 4 cm^{-1} for 128 scans. RAMAN measurement was taken at 532 nm wavelength (green laser) and 50 mWatt power. Besides, UV-VIS spectrophotometer was used on PANI coated glass slides in order to find the band gap of fabricated PANI and confirm whether conducting state of PANI forms or not by calculating band transition energies. Thickness of PANI thin film on Si wafer and glass were done with a spectroscopic ellipsometer. Measurement angles were adjusted as 65°, 70° and 75° while a range of 300-800 nm was used during ellipsometric measurement. For glass substrate, glass with absorbing film model was used to fit the raw data and then find the film thickness. For PANI on Si wafer, Si with absorbing model was applied to data. Due to high absorbance of conducting polymer on visible light range, absorbing model was generally preferred over the other model options.

Atomic Force Microscopy (AFM):
Atomic Force Microscopy (AFM) (Bruker Multimode 8, ScanAsyst) was used to acquire topography and surface roughness of PANI on Si wafer. To see the effect of annealing on surface roughness, PANI coated small Si wafers were placed into vacuum oven and annealed at 40 °C, 60 °C, 80 °C , 100 °C, 140 °C and 180 °C for 4 hours. Then, all samples were cooled down to room temperatures. AFM measurements were performed with ScanAsyst mode on so that all parameters are automatically given by AFM software (NanoScope 8.15). The scan size was 10 x 10 micron and scan number was 512 to obtain AFM image with higher resolution. After taking measurement, the image post-process software (NanoScope Analysis 1.5) calculated the overall roughness of different PANI samples.

X-Ray Diffraction (XRD):

XRD (Bruker, D8 Advance XRD) was performed to identify the amorphism of PANI and crystalline plane direction. Furthermore, it enabled to make a comparison of crystallinity change between untreated and annealed sample. The measurement was taken on non-annealed PANI coated Si wafer and 80 °C annealed PANI coated Si wafer between the 2Φ angle of 5° and 40° in order to eliminate the peak originated from Si 100 plane. The each measurement takes 4 hours to increase the signal to noise ratio.

4-Point Probe Measurements:

Electrical conduction of PANI thin film was calculated by measuring voltage-current (V-I) curve of samples. Instead of Si wafer, PANI coated glass was chosen to prevent the conductivity originated from Si itself. Before the measurement, all samples were cleaned with N_2 gas to remove the contamination and tiny dusts. Then, non-annealed and each annealed samples (40°C, 60°C, 80°C, 100°C, 140°C and 180°C) were separately placed under 4 probes of equipment. Afterwards, the measurement was taken by touching 4 probes at four different points. While taking measurement, the current was always kept constant at 10^{-7} milliamp (mA). The measurement was performed for 6 times to increase reliability of data. When the measurement finished, the software showed V/I value for each 6 data and converted to sheet resistance (R_s) and resistivity by using several formula which will be explained in following chapters.

To analyze the stability of PANI thin film, electrical conductivity of non-annealed PANI coated glass was examined for 30 days. The measurement was taken at each three days and compared to previous data in order to understand whether conductivity changed over time.

2.7 SRP and CP based Coaxial Nanotube Fabrication

To fabricate coaxial nanotube, it is decided to make outer layer conducting polymer (CP) and inner layer stimuli responsive polymer (SRP) in order not to hinder electrical conduction pathway. Therefore, CP was first coated using oCVD system and iCVD method deposited SRP as inner layer. Before starting iCVD deposition, PANI layer

,which formed during oCVD deposition, on AAO templates was etched by oxygen plasma etcher used at 50 watt for 20 seconds to reopen the AAO pore openings.

HEMA (Aldrich, 99%) , the crosslinker EGDMA (Aldrich, 98%) and the initiator TBPO (Aldrich, 98%) were used during pHEMA synthesis without further purification. The partially PANI filled templates were put along with Si wafer onto the stage of iCVD chamber, where free radical polymerization of HEMA occurs. HEMA and TBPO within two separate metal jars were connected to the iCVD chamber through metal pipelines. HEMA and EGDMA was respectively heated up to 70 °C , 85 °C and TBPO was kept at room temperature. The deposition was achieved at 120 mTorr and stage temperature of 40 °C . The flowrates of HEMA, EGDMA and TBPO was set to 0.8 sccm, 0.11 sccm and 1 sccm, respectively. The thickness of pHEMA layer was monitored using iCVD laser system. After deposition, the samples was again exposed to oxygen plasma at 50 watt for 10 seconds to clean the excess pHEMA layer on AAO membranes.

In order to obtain CP and SRP based polymeric nanotubes, AAO membranes was immersed in 0.5 M HCl solution for 48 hours. Then, the coaxial nanotubes was allowed to dry in the air for 2 days.

2.8 Humidity Sensor Test

The sensitivity of PANI flat film, PANI nanotubes and PANI+pHEMA coaxial nanotubes were measured using 2-point probe (Keithley). Before measurement, each samples were treated by photolithography in order to create circular spots for better gold electrode settlement. In photolithography, all samples were coated by photoresist (AZ5214 E) using spin coating with 4000 rpm for 15 seconds followed by baking of photoresist coated samples at 150°C for 2 minutes. Later, baked samples having circular spots mask with 100 micron diameter were exposed to UV photolithography for 15 seconds. The UV exposed samples were immersed into special photographic developer solution (mixing of NaOH and KOH) for 45 seconds followed by rinsing in DI water for 15 seconds. Eventually, the dot patterned gold electrodes on polymer films appeared after immersing of samples in acetone for 3 hours.

In order to vary ambient humidity, several saturated salt solutions were prepared in DI water that each solution corresponds to specific humid level. Table 6 lists the all salt solution and their humid equivalent at room temperature. Each salt solutions were

placed in sealed box to stop the air flow from outside. The flat PANI, PANI single nanotubes and PANI+pHEMA coaxial nanotubes were respectively put inside of box for 10 minutes for each humid level. The humidity values were checked with standard precalibrated humidity meter (PCE 555). Afterwards, the V-I measurements was performed by touching 2 probes on gold electrodes and keeping the current constant at 10^{-3} amps for each humid level. Each sample was exposed to air for 5 minutes in order to analyze the response rate of samples and second V-I measurement was taken by following the same procedure.

	LiCl	CH_3CO_2K	$MgCl_2$	K_2CO_3	$Mg(NO_3)_2$
Humidity	11.3 %	22.5 %	32.7 %	43.1 %	52.8 %

	NaCl	KCl	KNO_3	K_2SO_4
Humidity	75.2 %	84.3 %	93.5 %	97.3 %

Table 6: 9 different salts and equivalent humid levels [89]

CHAPTER 3

STUDIES ON RELEASE KINETICS

3.1 Single pH Responsive Nanotubes

3.1.1 Flat pMAA Thin Film

The chemical composition of iCVD deposited p(MAA) thin film was studied using FTIR analysis. Figure 14 indicates FTIR spectra of p(MAA) thin film on Si wafer. The peak at 1702 cm^{-1} corresponds to C=O stretching modes originated from carboxyl group of p(MAA) whereas the higher peak at 1730 cm^{-1} shows C=O stretching modes of EGDMA. The dual peak between 2870-3000 cm^{-1} is indication of C-H stretching vibration stems from both MAA and EGDMA molecules. Besides, the broad peak appears at 3100-3400 cm^{-1} corresponds to O-H stretching vibration of p(MAA-co-EGDMA). The absence of any peaks at 1600-1650 cm^{-1} , which is originated from C=C, confirms full polymerization and crosslinking of p(MAA-co-EGDMA) polymer. Table 7 summarizes the peak position of the most significant functional groups of p(MAA). Consequently, it can be stated that iCVD mechanism protects the functional groups ,which is key for stimuli response, and provides fully polymerization during deposition process [90].
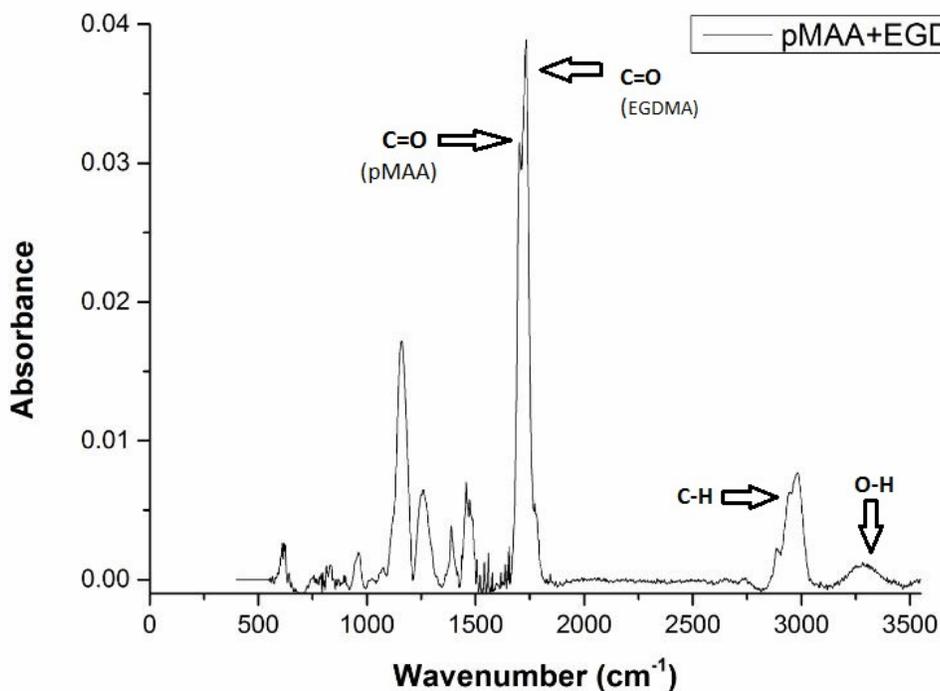
Figure 14 : FTIR spectra of p(MAA) thin film on Si wafer

Stretching Vibration	Wavenumber (cm^{-1})
p(MAA) C=O stretching	1702 cm^{-1} (sharp)
p(EGDMA) C=O stretching	1730 cm^{-1} (sharp)
O-H stretching	3100-3400 cm^{-1} (broad)
C-H stretching	2870-3000 cm^{-1} (broad)

Table 7: FTIR peak position of some important p(MAA-co-EGDMA) functional group

It is possible to calculate the crosslinker (EGDMA) ratio in thin film using FTIR spectra. The Beem-Lambert theory states that the band absorption intensity is directly correlated to concentration of bands. As number of bands per volume increase, the intensity also arises if the power of band IR absorption is the same. Thus, the common C=O peak which is 1730 cm^{-1} for EGDMA and 1702 cm^{-1} for MAA is selected for calculation. Two peaks are fitted with Gaussian fit option and the area under fitted peaks are calculated using Math software (Origin 9.0) (Figure 15). Due to the fact that

EGDMA has two C=O group, the area of peak originated from EGDMA is divided by 2. The formula is given below;

$$\frac{[EGDMA]}{[MAA]} = \frac{A_{C=O(EGDMA)}/2}{A_{C=O\,(MAA)}} \qquad (7)$$
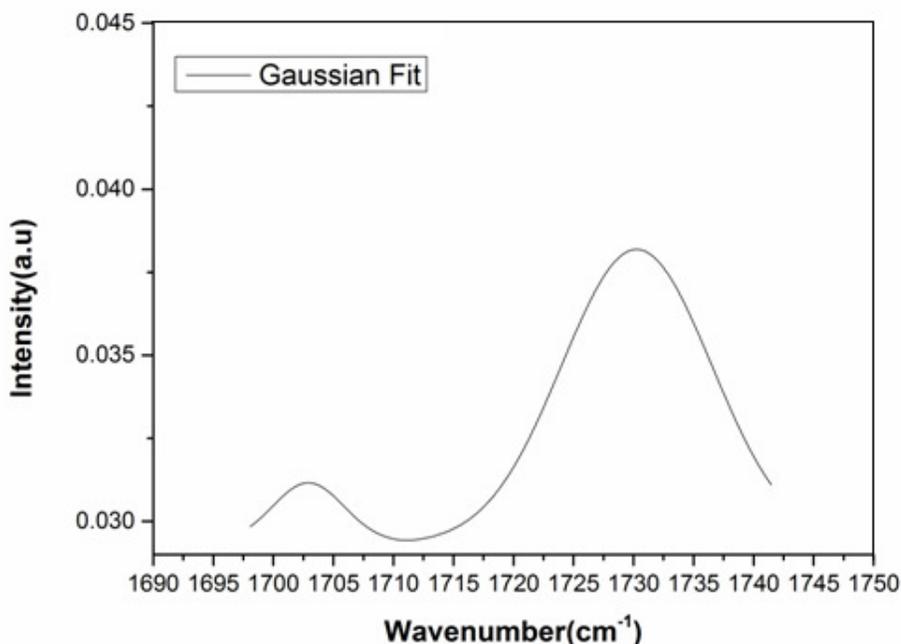
Figure 15: Gaussian Fit of MAA and EGDMA C=O peak

The results indicates that p(MAA-co-EGDMA) thin film includes 56.5% MAA and 43.5% EGDMA in terms of concentration. The reason of existence high crosslinking amount is to enhance the resistivity of film to water and mechanical properties.

In response to the changes in the pH of the medium, the change in the thickness of the p(MAA-co-EGDMA) thin films can be monitored real time using ellipsometric spectroscopy. Figure 16 (a) and (b) shows the thickness change and swelling percentage at pH values of 4 and 8 as a function of time. Films with initial thickness of 300 nm exhibit swelling percentages of up to 35% at pH 8 whereas at pH 4, the swelling is only 3% at the end of 60 minutes. Similar swelling behavior was also observed for iCVD deposited p(MAA-co-EGDMA) by Lau et al. [91] who reported more than 30% swelling in pH 7 and swelling of 5% in acidic medium of pH 1.2-5.

(a)

(b)
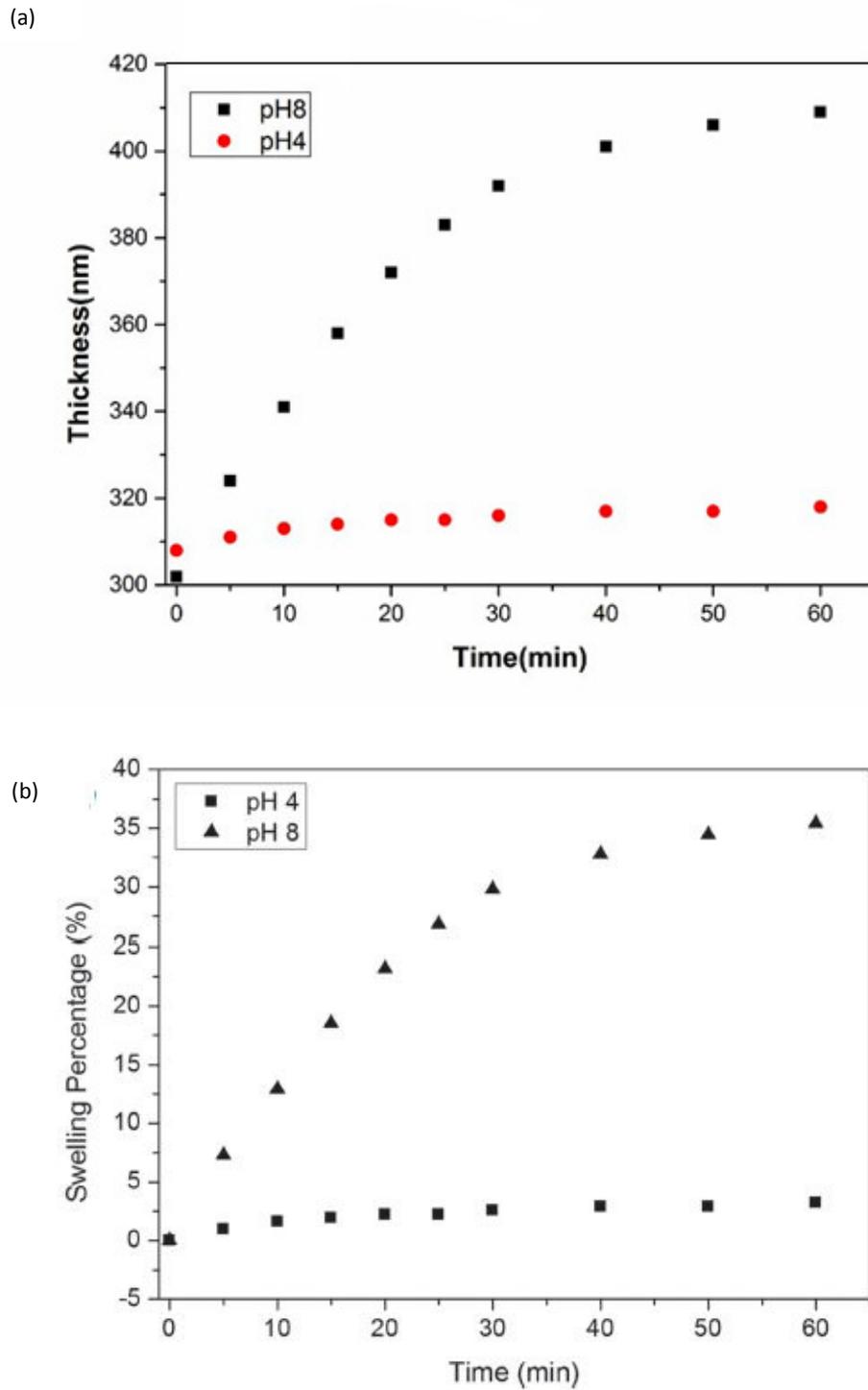
Figure 16: a) Thickness b) Swelling percentages of the p(MAA-co-EGDMA) films in pH 4 and pH 8 as a function of time.

The transport mechanism leading to the observed swelling behavior can be studied by fitting the data to the following formula:

$$\frac{T_t}{T_{eq}} = k * t^n \tag{8}$$

where T_t and T_{eq} represent the difference between the initial dry thickness and the thickness at time t and at equilibrium respectively, and k is a material dependent constant. This simple model which was proposed by Kim et al. [92] to explain the permeant diffusion in hydrogels is used to fit the data below 60% swelling to describe the early time kinetics of transport. The exponent n is related to the dominating transport mechanism; with n values larger than 0.5 indicating non-Fickian transport and n value of 0.5 indicating Fickian type diffusion. In this model, both the relaxation of the polymer chains and the diffusion of water through polymer mesh contribute to the swelling behavior observed. Figure 17 (a) and (b) respectively shows the fits of the data below 60% at pH 4 and pH 8 values to Equation 8. Figure 18 indicates the combination of (a) and (b) in one plot.

(a)

(b)
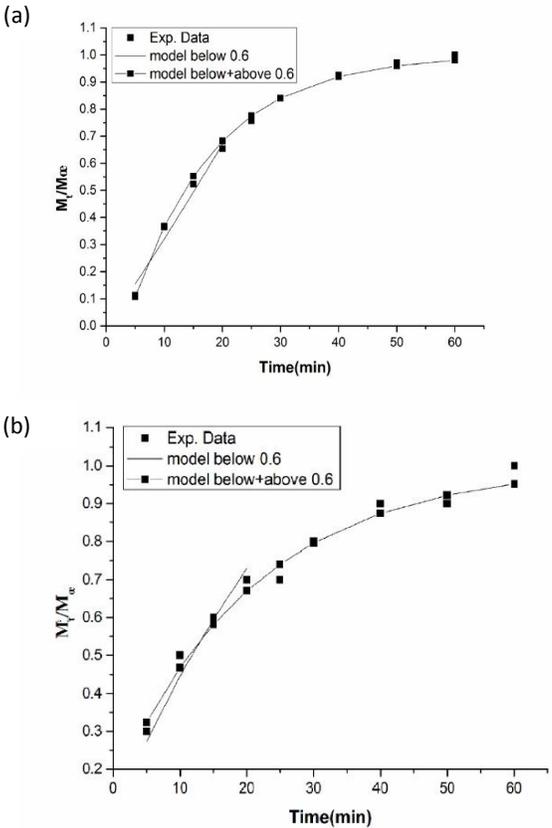
Figure 17: Change of T_t / T_{eq} ratio as a function of time and the fits of data to Equation 8 for pH 4 (a) and pH 8 (b)
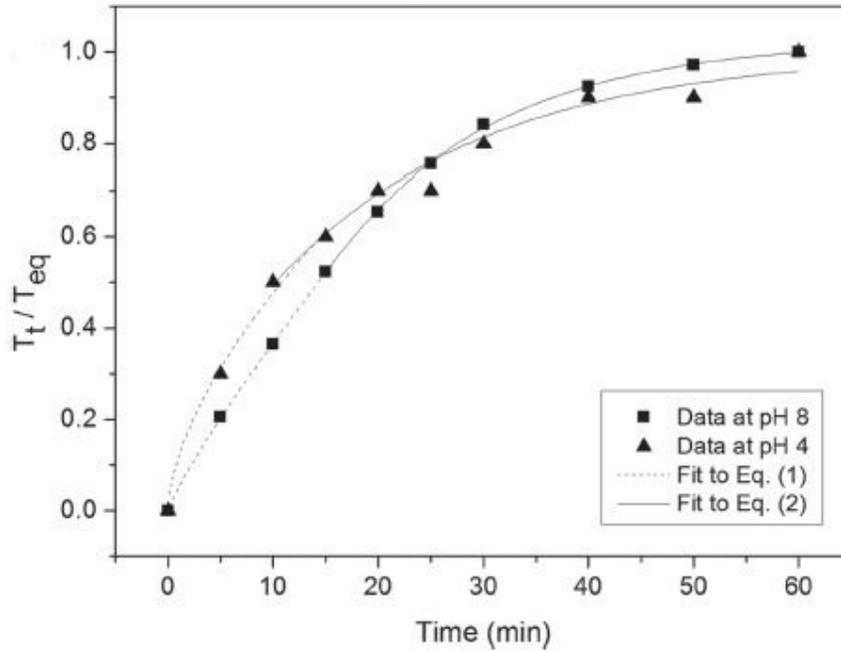
Figure 18: Combination of Figure X (a) and (b) in one plot

The model can successfully fit the data at pH 4 with k value of 0.11 min^{-n} where n is 0.57. On the other hand, at pH 8, the value of k is found as 0.05 min^{-n} where n is 0.86. Comparing the *n* value of 0.57 obtained at pH 4 and 0.86 obtained at pH8, it is observed that for low pH diffusion controlled transport dominates where the relaxation of polymer chain is negligible. As n is approaching to 1, the relaxation of the polymer starts dominating the transport mechanism at high pH values where the swelling of the polymer is significant.

At later times as the swelling rates of polymer reaches equilibrium, the relaxation of the polymer becomes the main mechanism that drives the penetrant transport through the polymer which follows first-order kinetics. Therefore, above 60 % swelling , the data is fitted to the equation [93] :

$$\frac{T_t}{T_{eq}} = 1 - A \exp(-k_2 \, t) \tag{9}$$

where A is an activity constant and k_2 is the relaxation rate constant (Figure 18). By using the fit results, A and k_2 are found as 0.84 and 0.05 min^{-1} at pH 4 whereas at pH 8, A and k_2 values are calculated as 1.31 and 0.08 min^{-1} indicating a

faster relaxation at high pH values. Difference in the relaxation kinetics observed at different pH values will be differentiating factor between the release rates of the p(MAA-co-EGDMA) nanotubes.

3.1.2 pMAA Nanotubes Loading-Release Capacity and Kinetics

SEM images are taken in order to check whether pMAA nanotubes are successfully fabricated after iCVD deposition. Figure 19 (a) and (b) confirm that after removal of the AAO templates, fabrication of hollow nanotubes with having approximately 50 $\mp$ 5 nm diameter are able to be achieved.
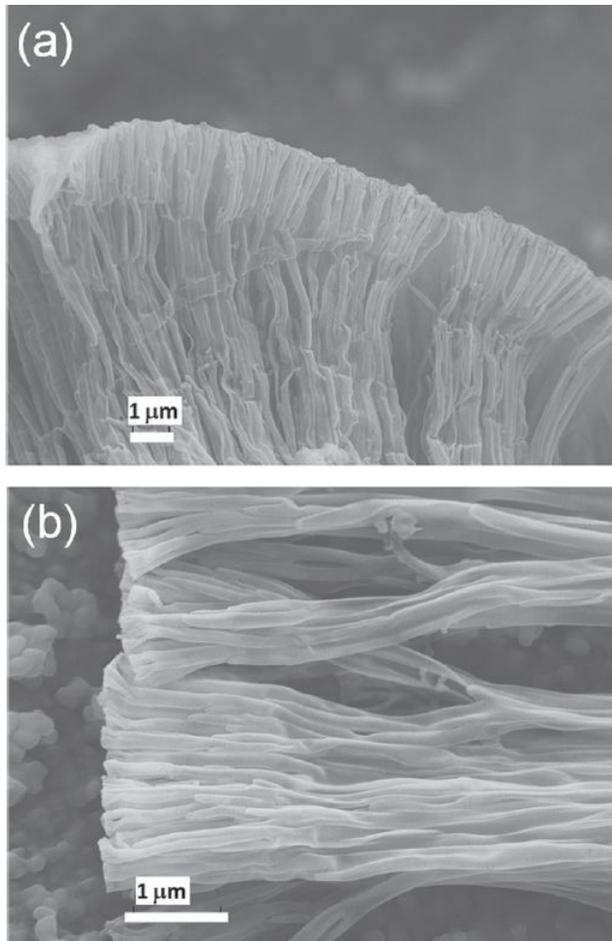
Figure 19: SEM images of the p(MAA-co-EGDMA) nanotubes after removal of the AAO templates [51]

These nanotubes are then loaded with the Phl dye. UV-VIS measurements taken at the end of 24-hour loading process at pH 8 showed that for the amount of samples used approximately 7.5 $\mp$ 0.5 x 10^{-7} moles of Phl was loaded. This corresponds to 8% of the feed concentration and can be further increased by increasing the amount of nanotube

samples. The unloading experiments were performed at pH values of 4 and 8. The changes in the release concentrations as a function of time are separately shown in Figure 20 and Figure 21 at pH 4 and pH 8, respectively. The Figure 22 also indicates the combination of release concentration change at pH 4 and pH 8 and p(EGDMA) control sample release concentration change. At the end of 240 minutes of unloading, 50.4 ∓ 0.8 % of dye released at pH 4, whereas the release was only 9.6 ∓ 0.7 % at pH 8.
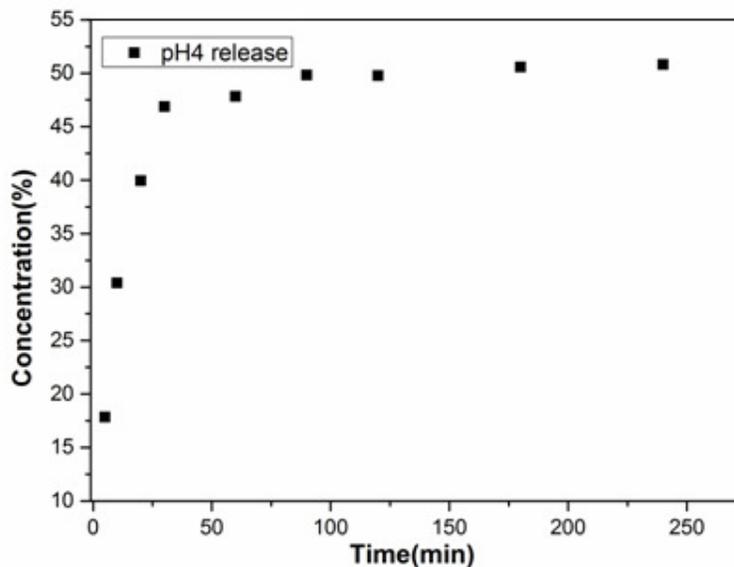
Figure 20: Release concentration change for Phl loaded nanotubes at pH 4
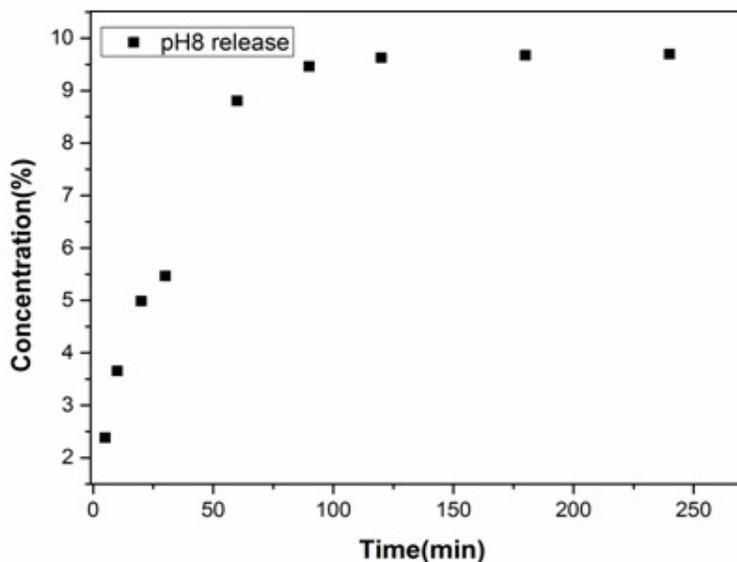
Figure 21: Release concentration change for Phl loaded nanotubes at pH 8
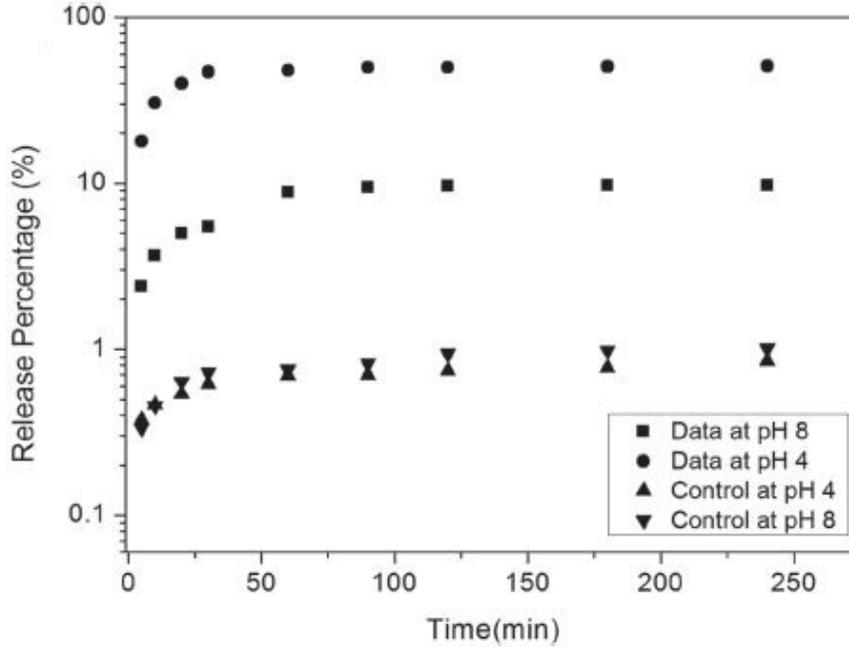
Figure 22: Release percentages of the model dye molecules from p(MAA-co-EGDMA) an p(EGDMA) nanotubes at pH 4 and pH 8 as a function of time

In control experiments, p(EGDMA) nanotubes which are unresponsive to pH changes were used to study the contribution of the dye molecules that physisorb on the polymer to overall release. Same loading and release procedures were followed as that of the p(MAA-co-EGDMA) nanotube samples. For the amount of samples used approximately $3.3 \mp 0.1 \times 10^{-7}$ moles of Phl was loaded which corresponds to 3 % of the feed concentration. At the end of 240 minutes, approximately 1 % of the loaded dye was released both at pH 4 and pH 8 as seen in Figure 22 .The release percentage of p(MAA-co-EGDMA) nanotubes at pH 4 and pH 8 are significantly higher than that of the p(EGDMA) nanotubes. Moreover, changing the pH of the medium did not have a significant effect on dye release from the p(EGDMA) nanotubes.

The overall rates at different pH values were analyzed using an empirical formula below:

$$x(t) = x_f (1 - e^{-kt}) \tag{10}$$

where x(t) is the release percentage at time t, x_f is the final dye release percentage and k is the rate coefficient [94]. Figure 23 shows the fitting of release

data at pH 4 and pH 8 to equation 10, respectively. Fitting the release data at pH 4 and pH 8 with respect to equation 10, the rate coefficient is found as 0.036 for pH 8 and 0.089 for pH 4. In the calculations, measured x_f values of 9.7 ∓ 0.3 and 49.8 ∓ 0.4 are used for pH 8 and pH 4, respectively. The higher release rates observed at pH 4 compared to the release rates at pH 8 are attributed to the shrinking of the polymer in the hydrophobic regime and the subsequent stress-induced burst release of the dye molecules. On the other hand, at pH 8 the release rate of the dye from the swollen polymer is mainly via concentration gradient driven diffusion process. However, the higher release percentages obtained with the swollen p(MAA-co-EGDMA) nanotubes compared to p(EGDMA) nanotubes confirm that dye diffusion through the swollen polymer is the active transport mechanism at high pH values.
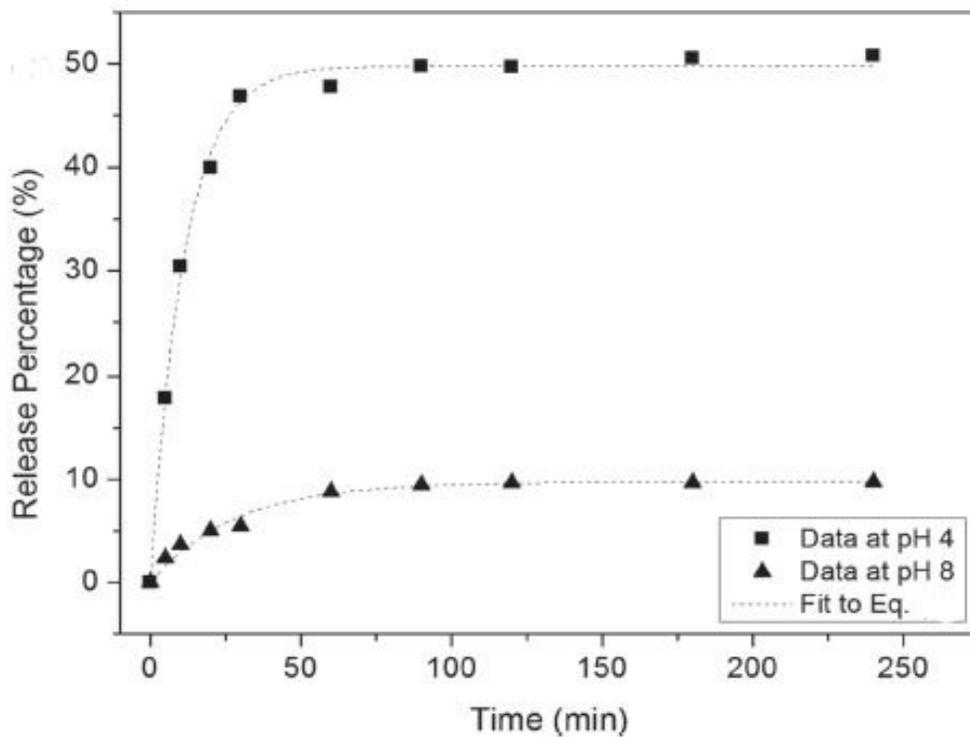
Figure 23: Fitting of the release percentage at pH 4 and pH 8 in one plot

As a result, the vapor phase iCVD technique can successfully be utilized to fabricate the stimuli responsive polymeric nanotubes for controlled release applications. In this chapter, p(MAA-co-EGDMA) which is responsive to changes in the pH of the environment is used to fabricate the nanotubes. The nanotubes are loaded with model dye molecules at pH 8 where the p(MAA-co-EGDMA) is in swollen state, enabling the absorption of the dyes through the polymer mesh. The release of the dye molecules is activated by changing the pH to 4. In acidic medium, the p(MAA-co-EGDMA) polymer shrinks, triggering the stress-induced release of the dye molecules. Release percentages of more than 50 % can be achieved at pH 4, whereas at pH 8, release is less than 10 %. These results confirm that pH responsive polymer nanotubes can be fabricated via iCVD without affecting the functionality of the polymer and the release from these nanotubes can be controlled by changing the pH.

3.2 Coaxial Stimuli Responsive Polymeric Nanotubes

3.2.1 Flat Stimuli Responsive Polymer Thin Film

The chemical composition of iCVD deposited p(MAA), p(HEMA) and p(NIPAAm) thin film was studied using FTIR analysis. The FTIR analysis of iCVD deposited polymers on Si wafers confirms the successful copolymerization of NIPAAm, HEMA and MAA with EGDMA as shown in Figure 24, Figure 25 and Figure 26, respectively.

According to 426, the peaks at 3300 cm^{-1}, 1530 cm^{-1} and 1630 cm^{-1} correspond, respectively, to the N-H stretching vibration, C-N-H bending vibration and C=O vibration of NIPAAm [95]. Besides, there are other significant peaks at 1370-1385 cm^{-1}, 1440 cm^{-1} and 3000 cm^{-1} originated from the doublet isopropyl band, $C(CH_3)_2$ stretching and C-H stretching vibrations. On the other hand, as shown Figure 25, the broad peak between 3150 cm^{-1} and 3550 cm^{-1} is due to O-H stretching vibration and the peak at 1730 cm^{-1} is due to C=O stretching vibration of HEMA [96]. The FTIR analysis of MAA was discussed in previous sub-chapter. Briefly, the peak at 1700 cm^{-1} corresponds to C=O vibration of MAA, whereas the C=O stretching vibration of EGDMA is at 1730 cm^{-1}. The absence of a peak between 1600 and 1650 cm^{-1} confirms the complete polymerization of the monomer adsorbed on the surface. The EGDMA content in the deposited films can be calculated from the ratios of the characteristic peak areas of the monomers as done in previous sub-chapter. For the polymer system used in

this study the EGDMA content in the thin films is calculated to be 22.9 %, 32.1 % and 56.5 % for pNIPAAm , pHEMA and pMAA, respectively. Table 8 indicates the crucial peaks identify the functional group of each polymer.
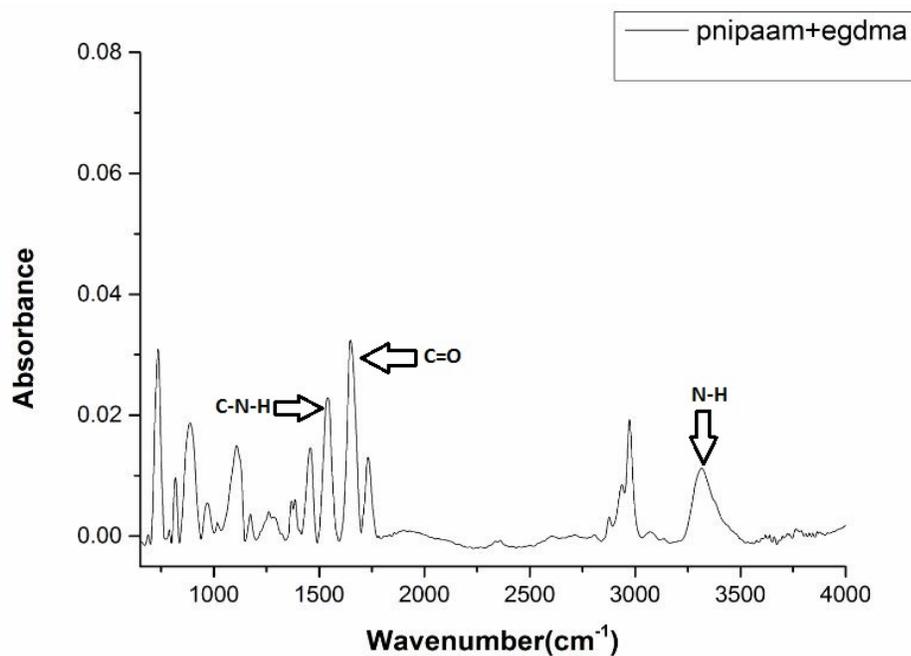
Figure 24: FTIR spectra of pNIPAAM
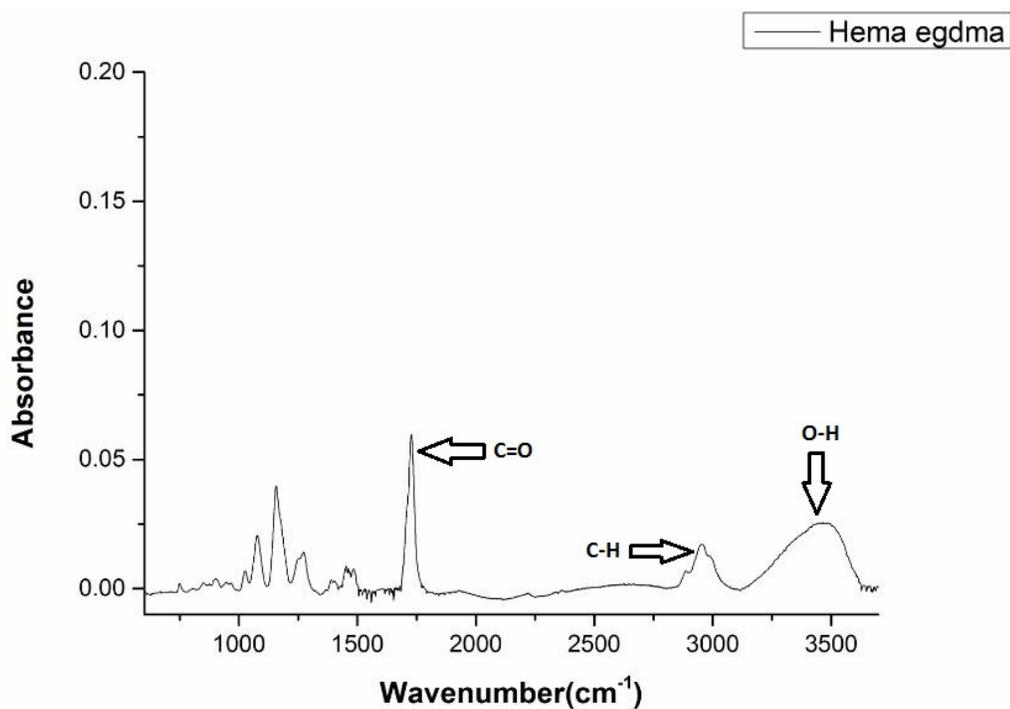
Figure 25: FTIR spectra of pHEMA
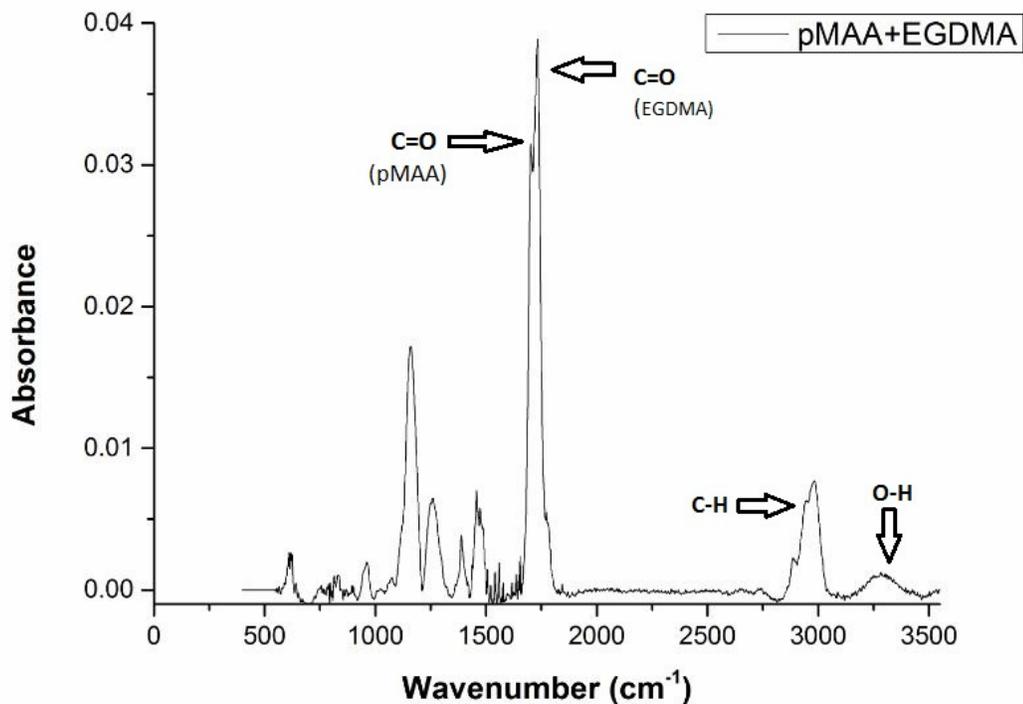
Figure 26: FTIR spectra of pMAA

Vibration Type	Wavenumber (cm^{-1})	Polymer
p(MAA) C=O stretching	1702 cm^{-1} (sharp)	pMAA
p(EGDMA) C=O stretching	1730 cm^{-1} (sharp)	pEGDMA
O-H stretching	3100-3400 cm^{-1} (broad)	pMAA
C-H stretching	2870-3000 cm^{-1} (broad)	pMAA
N-H stretching	3300 cm^{-1} (broad)	pNIPAAm
C-N-H bending	1530 cm^{-1} (sharp)	pNIPAAm
C=O stretching	1630 cm^{-1} (sharp)	pNIPAAm
O-H stretching	3150-3550 cm^{-1} (broad)	pHEMA
C=O stretching	1730 cm^{-1} (sharp)	pHEMA

Table 8: FTIR peak position of some important p(MAA-co-EGDMA), p(NIPAAm-co-EGDMA) and p(HEMA-co-EGDMA) functional groups

The mesh size, ξ, of the deposited polymer thin films in their swollen and collapsed states, which affects the diffusion of the dye molecules through the polymer matrix can be calculated using equation below;

$$\xi = Q^{1/3} \left[2Cn\left(\frac{Mc}{Mr}\right)\right]^{1/2} l \tag{11}$$

where Q is the swelling ratio obtained from ellipsometer studies, l is the C-C bond length (0.154 nm), C_n is the characteristic ratio , M_r is the molecular weight of the monomer and M_c is the average molecular weight between crosslinks, M_c can be calculated as follows;

$$\frac{1}{Mc} = \frac{2}{Mn} - \frac{\frac{v}{V_1}[\ln(1+vs)+vs+x(vs^2)[1-\frac{Mr}{2Mc}vs^{\frac{2}{3}}]^3}{(vs^{\frac{1}{3}}-0.5vs)[1+\frac{Mr}{2Mc}vs^{\frac{1}{3}}]^2} \tag{12}$$

where v is the specific volume of the polymer, x is the Flory-Huggins interaction parameter, V_1 is the molar volume of water (18 cm^3 mol^{-1}), v_s is the ratio of dry thickness to wet thickness (given as 1/Q) and M_n is the number average molecular weight of the polymer. As M_n is significantly larger than M_c , the first term on the right can be ignored. The Flory-Huggins interaction parameters are assumed to be constant for different crosslink ratios range within the range of v_s values obtained.

For pNIPAAm the values of C_n, M_r, v and x used in these equations are, respectively 11.7, 113.16 g mol^{-1}, 0.909 cm^3 g^{-1} [97] and x is 0.51 for NIPAAm-water interaction [98]. For pHEMA the value of C_n is 6.9 [99], M_r is 130.14 g mol^{-1}, v is 0.931 cm^3 g^{-1} and x is 0.8 for HEMA-water interaction [100]. Finally, for pMAA, C_n is 14.6 for MAA [101], M_r is 86.09 g mol^{-1} , v is 0.984 cm^3 g^{-1} and x is 0.59 for MAA-water interaction. By inserting these values to equation 11 and 12, the mesh size of each polymer is found as 7.1 A°, 14.35 A°, 10.35 A°, 8.32 A° and 32.3 A° for pNIPAAm (at 40 °C) , pNIPAAm (at 25 °C), pHEMA, pMAA (at pH 4) and pMAA (at pH 8), respectively. The table 9 shows the mesh size values of each polymer system.

	ξ (A°)	Q or $1/\boldsymbol{v}_s$	M_c (g mol^{-1})
pNIPAAm (40 °C)	7.1	1.03	105.67
pNIPAAm (25 °C)	14.35	1.88	276.98
pHEMA	10.35	8.77	101.66
pMAA (pH 4)	8.32	1.08	81.88
pMAA (pH 8)	32.3	2.43	722.62

Table 9: Mesh sizes, ξ, swelling ratio Q and the average molecular weight between the crosslinks M_c of the polymers at different temperatures and pH values.

3.2.2 Coaxial Nanotubes Loading-Release Capacity and Kinetics

The SEM images of the coaxial nanotubes NIPAAm +MAA (NIMA) are shown in Figure 27 (a). Due to the similarity in their polymer structure, the inner and outer layers cannot be distinguished in the SEM. The SEM images show that the nanotubes are approximately 200 nm in diameter and 10-20 micron in length. The tubes are hollow inside with 30 $\mp$ 5 nm of wall thickness (Figure 27 (b)). The SEM images of NIMA samples with wall thickness of 50 $\mp$ 10 nm and NIMA samples with closed ends are shown in Figure 27 (c) and (d).
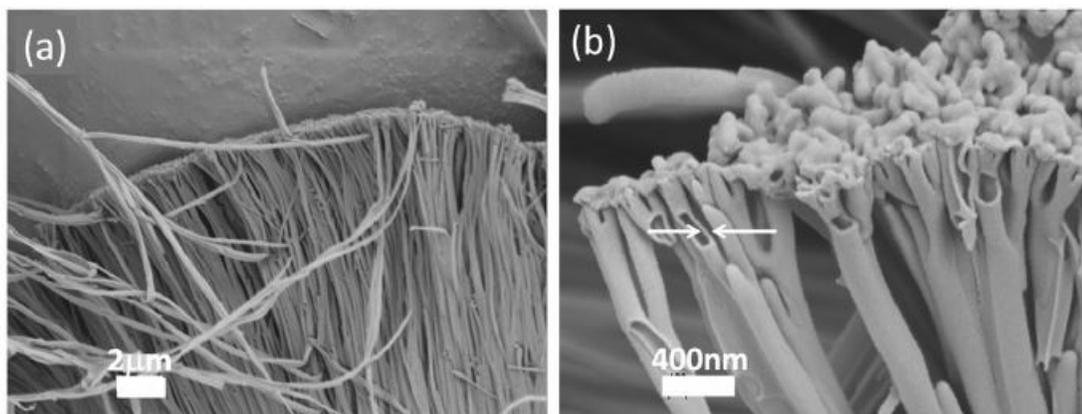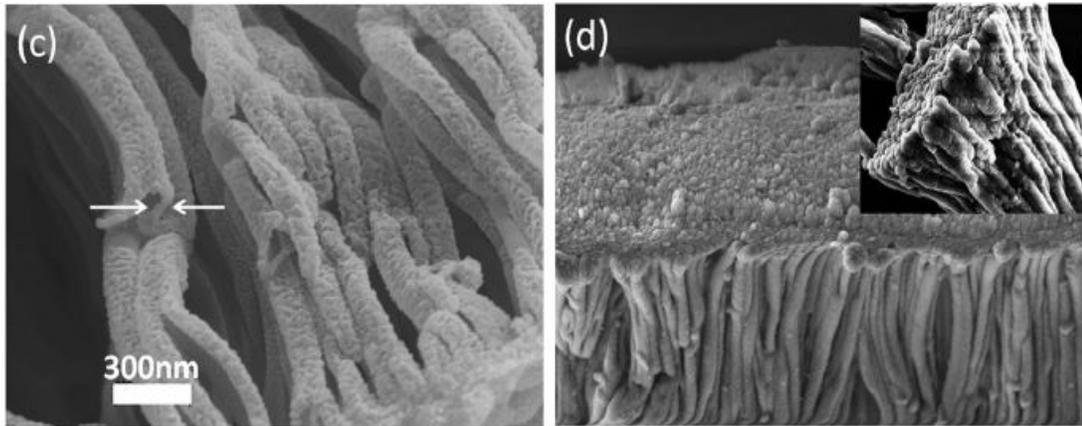
Figure 27: **(a and b) SEM images of the NIMA nanotubes at different lengthscales. c) SEM images of the NIMA nanotubes with thicker wall d) SEM images of the NIMA nanotubes with closed ends [52]**

The loading and release of Phl molecules from the polymer nanotubes were systematically studied using UV-VIS characterization details of which were given early chapter. The Phl dye molecules that are used in these studies have a solvent excluded volume of 90.42 $A^{\circ 3}$ [102], which corresponds to an approximate diameter of 5.7 A°, smaller than the mesh sizes of the studied polymers. Figure 28, Figure 29 and Figure 30 show the released dye percentages as a function of time for NI, NIHE and NIMA samples, respectively. As the loaded dye amount depends strongly on the amount of nanotubes in the solution, the loading concentrations may differ between samples; therefore, percentages are used to compare different samples. In none of the samples tested, release percentages higher than 50 % could be obtained , which can be explained by the hydrophilic dye molecules being entrapped in the polymer mesh of the hydrophilic. As for the control samples, pEGDMA nanotubes, which are not responsive to pH or temperature changes, are used.
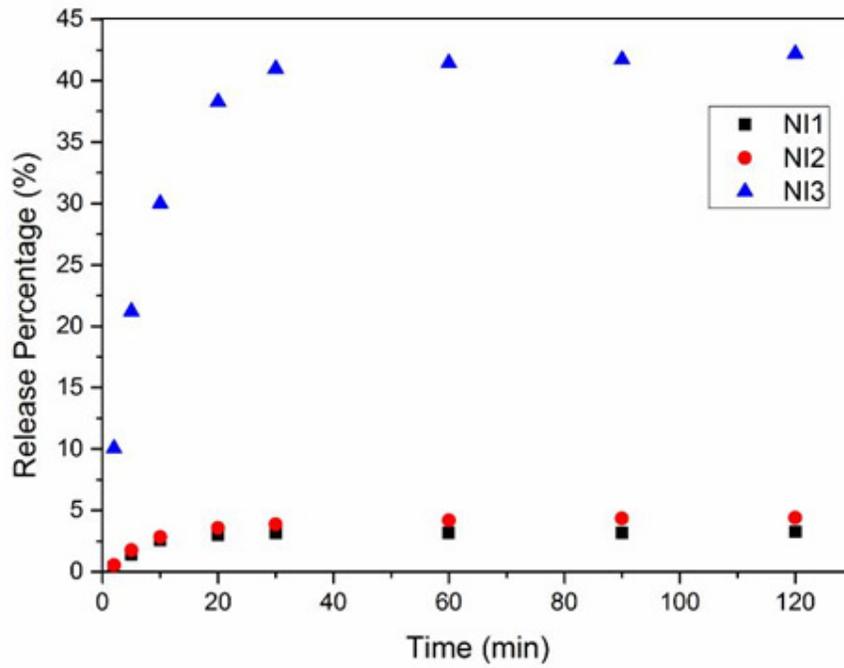
Figure 28: Dye release percentages of NI nanotubes
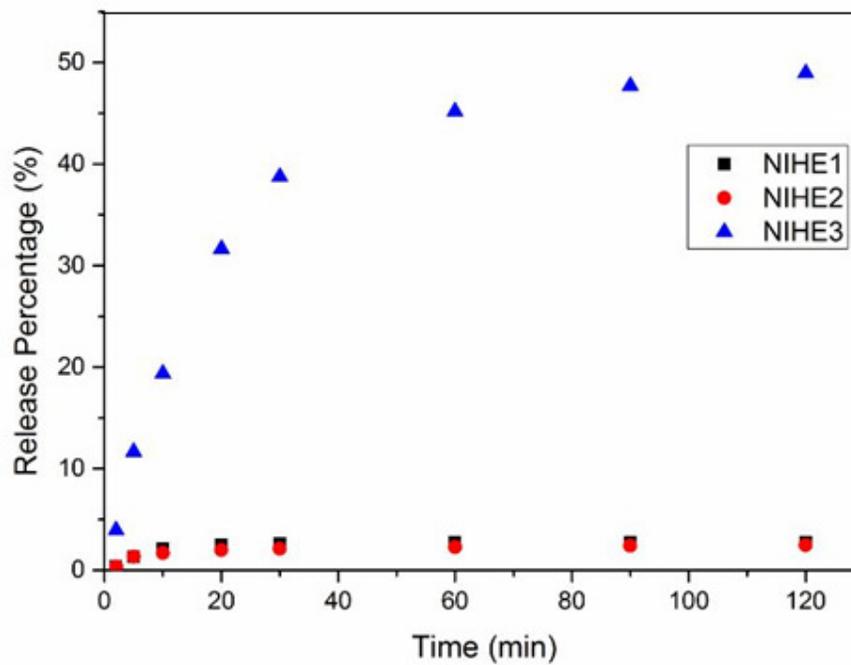
Figure 29: Dye release percentages of NIHE nanotubes
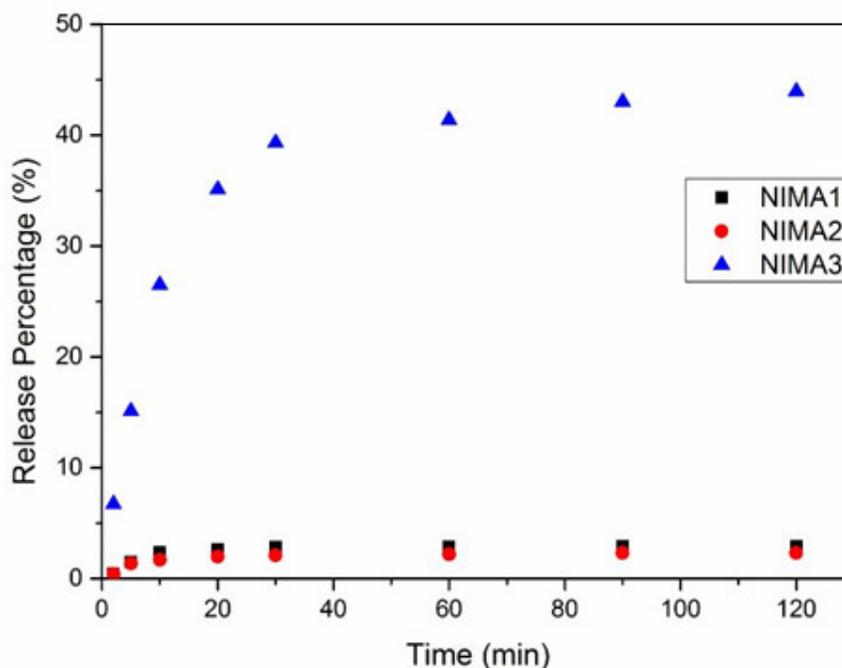
Figure 30: Dye release percentages of NIMA nanotubes

The following experimental results were obtained with open-ended nanotubes. At the end of 120 minutes, 42.1 % of the dye loaded was released by NI3, whereas only 3.2 % and 4.3 % were released by NI1 and NI2, respectively. The difference in the release percentages of NI1 and NI2 samples was insignificant and did not depend on the loading percentages. The significant difference in the release percentages between NI3 and other samples can be attributed to the hydrophobic nature of the pNIPAAm polymer at high temperatures; above the LCST of 32 °C, indicating that low surface energy of the polymer nanotubes at high temperatures increased the release of the Phl molecules. The lower release percentages at 25 °C, on the other hand, are due to hydrophilic interactions between the dye molecules and the pNIPAAm polymer. The release from the control samples is observed to be less than 2 % due to non-responsive nature of the pEGDMA nanotubes.

As for NIHE samples with a pHEMA inner layer , 2.7 %, 2.4 % and 48.9 % of the loaded dye were released by NIHE1, NIHE2 and NIHE3, respectively. The same experimental conditions were applied to NIHE samples as that of NI samples. Considering that the pHEMA polymer is not temperature responsive, release behavior similar to that of NI samples was observed, such that release increased at high temperatures and was independent from the loading temperatures.

For a better control of the release kinetics, another responsive polymer, pMAA, was used as the inner layer of the NIMA coaxial nanotubes. Changing the pH of the medium had an effect on the release kinetics of NIMA samples where the pMAA inner layer is the pH responsive polymer, which is hydrophilic at high pH values and hydrophobic at low pH values. At the end of 120 minutes, 2.93 %, 2.31 % and 43.9 % of the loaded Phl were released by NIMA1, NIMA2 and NIMA3, respectively. Loading experiments were performed at high pH , where the pMAA polymer is hydrophilic, to improve the loading of hydrophilic dye due to hydrophilic-hydrophilic interaction between the dye molecules and the polymer. Release experiments, on the other hand, were performed at low pH values where the polymer is hydrophobic, enhancing the release of the hydrophilic dye molecules. Maximized release percentages with the NIMA coaxial nanotubes were observed at low pH values and high temperatures, where both inner pMAA and outer pNIPAAm layers were hydrophobic. When the outer layer was hydrophilic, the release percentages decreased significantly, as observed with NIMA1 and NIMA2.

For all the samples studied, the highest release percentages obtained were less than 50 %. This can be attributed to dye molecules that are trapped between adjacent nanotubes, and which are not washed off during the rinsing procedure. Although these dye molecules may be released during unloading, they are not expected to have a big impact on the overall release percentages. The burst release observed as a result of changes in the stimuli suggests that mostly dye molecules that are loaded inside the nanotubes are released and the release is mainly through the tube openings. The release of the dyes attached on the walls would be less affected by the changes in the stimuli and would be at a slower rate than observed for burst release. Comparing the percentage of dyes released from different polymers, the highest release percentage of 48.9 % was obtained with NIHE3, whereas the release percentage of NI3 and NIMA3 were similar and 42.1% and 43.9%, respectively. The lower release percentage of the NI3 and NIMA3 compared to that of NIHE3 may be related to the smaller mesh sizes of pMAA and pNIPAAm when collapsed. Mesh sizes of approximately 0.7 nm and 0.8 nm of pNIPAAm and pMAA in the hydrophobic state are close to the size of the Phl dye (0.57 nm). Therefore, the dye molecules diffusing through the polymer mesh in the nanotube walls are trapped when the polymer collapses. On the other hand, pHEMA has a mesh size of 1 nm under all conditions and this larger mesh size compared to the size of the dye molecules enables the release of the dye molecules through the nanotube walls.

The dominant release mechanism can be determined by comparing the release percentages of the open and closed end nanotubes. The release of the dye molecules from close-end nanotubes is mainly via diffusion through the polymer mesh, whereas in open-ended nanotubes, bulk release of dyes from the tube openings is also active. The results showed that NIMA3 nanotubes with closed ends had release percentages of $10 \mp 4 \%$ (Figure 31) while NIMA3 samples with open ends had $40 \mp 2 \%$ release. Higher release percentages indicate that the release is mainly from the open ends of the nanotubes activated by changes in the polymer wall dimensions.
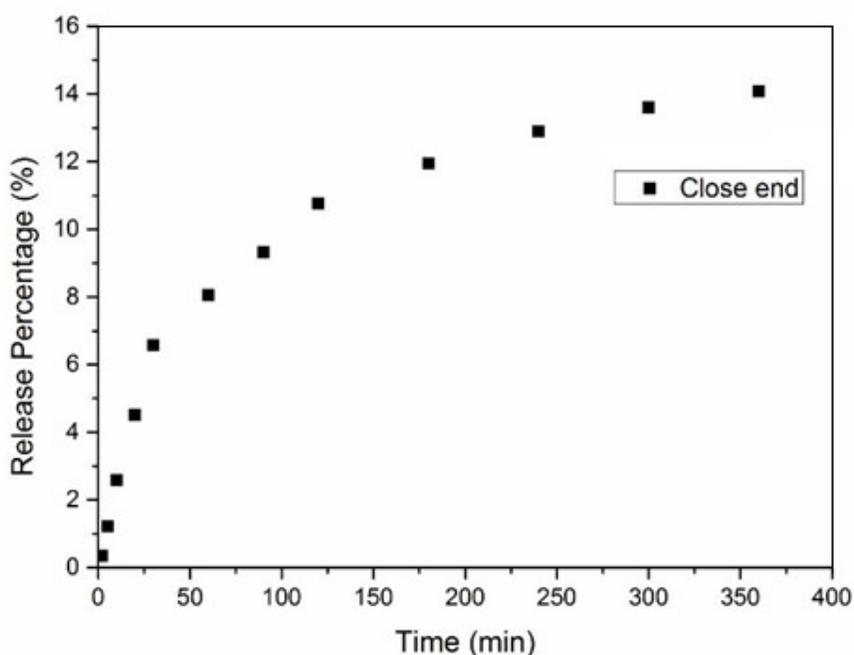
Figure 31: Dye release percentages of NIMA3 nanotubes with close end

The kinetics of the release from the nanotubes was studied by using the equation 10 in previous subtitle. The time release data of NI3, NIHE3 and NIMA3 can be fit to equation 10 in order to find the rate constants, k (Figure 32, Figure 33 and Figure 34). From the fits, the rate constants, k, are found to be 0.134 min^{-1}, 0.052 min^{-1} and 0.089 min^{-1} for NI3, NIHE3 and NIMA3, respectively. The significantly faster release kinetics observed with NI3 can be attributed to the hydrophobic nature of pNIPAAm at a release temperature of 40 °C. At high temperatures, the hydrophilic PhI molecules are released faster from the hydrophobic pNIPAAm polymer. On the other hand, the low release rate of NIHE3 is due to hydrophilic nature of the pHEMA both at low and high temperatures. Although the larger mesh size of the pHEMA layer facilitates the process

increasing the amount of the dye molecules released, the hydrophilic nature of the polymer, slows down the rate of the dye release from the nanotubes. Therefore, burst-type release is not observed with NIHE3 nanotubes
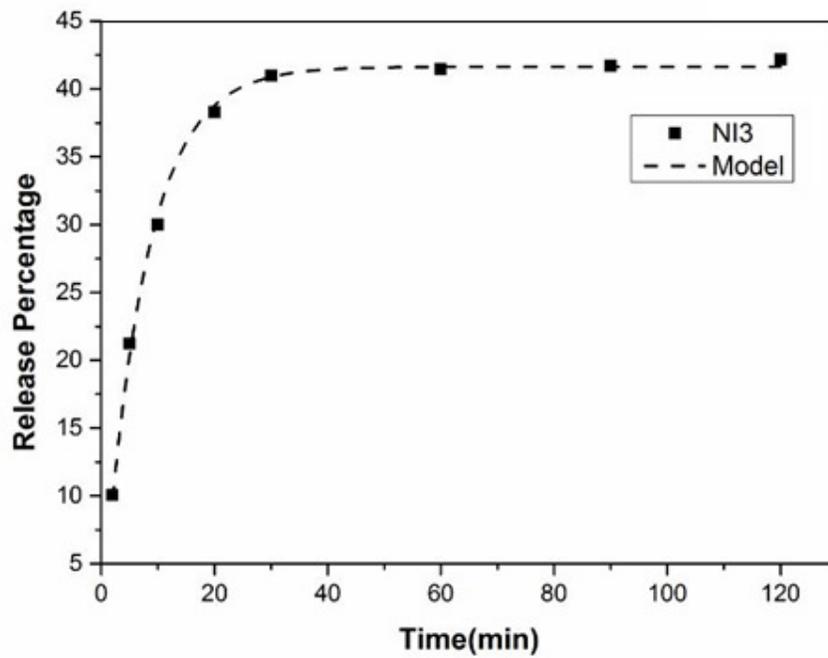
Figure 32: **Fitting of NI3 to first order kinetics**
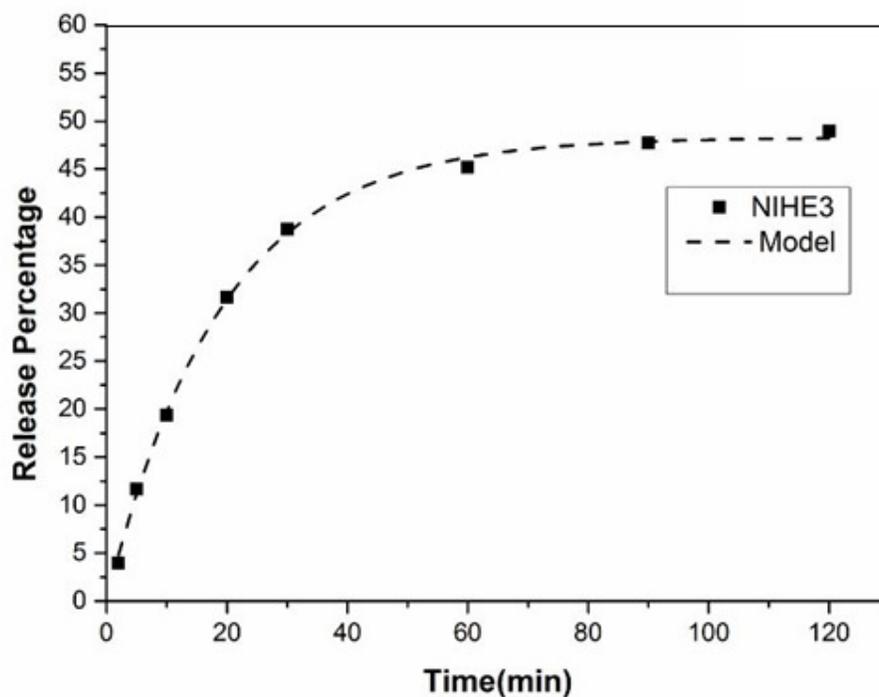
Figure 33: **Fitting of NIHE3 to first order kinetics**
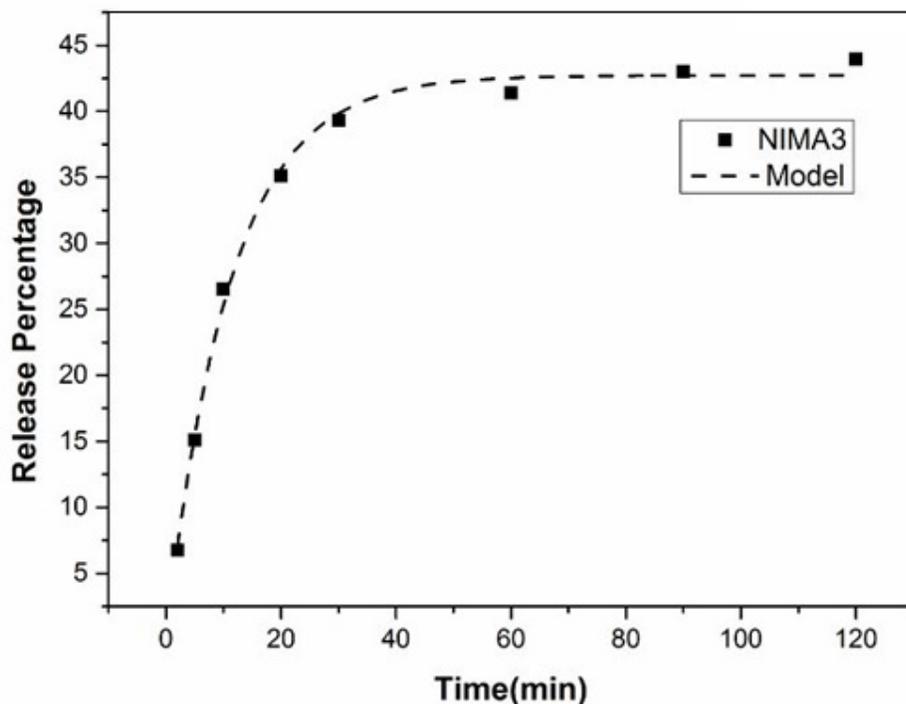
Figure 34: **Fitting of NIMA3 to first order kinetics**

NIMA3 samples, on the other hand, demonstrate release kinetics that is faster than NIHE3, due to the hydrophobic nature of pMAA at low pH values, leading to the collapse of the inner polymer layer. However, the release rates of NIMA3 are slower than that of NI3 although both samples are hydrophobic during release of the dye molecules. The collapse rates of pNIPAAm and pMAA thin films are 0.15 min^{-1} and 0.12 min^{-1}, respectively, as measured using the ellipsometer. The slow collapse rates of pMAA compared to pNIPAAm may explain the lower release rates of NIMA3 than that of NI3. Although both NIMA3 and NI3 collapse, the slower response of the inner layer of NIMA3 results in lower dye release rates compared to NI3.

Nanotubes with thicker walls (~50 nm) generally have lower release percentages and slower kinetics. Release percentages of 31.9 % and release rates of 0.06 min^{-1} were obtained with NI3 samples with thicker walls (Figure 35), whereas for thinner samples release percentages and rates were 42.1 % and 0.13 min^{-1}, respectively. Similarly, NIMA3 samples with thicker and thinner walls had release percentages of 28.6 % (Figure 36) and 43.9 % and release rates of 0.05 min^{-1} and 0.09 min^{-1}, respectively. As discussed earlier, although the dominant release mechanism is burst release from the tube openings, the lower rate constants obtained with nanotubes of thicker walls suggest

that diffusion through the polymer mesh is also an active release mechanism. Furthermore, as the wall thickness increases, the amount of dye molecules trapped within the polymer mesh increases, leading to reduced release percentages.
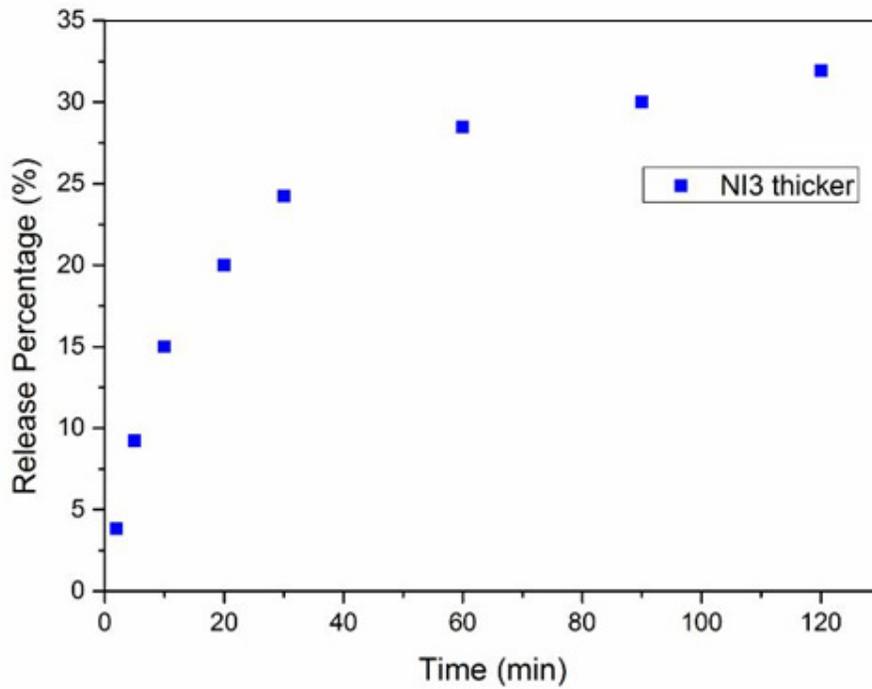
Figure 35: Dye release percentages of NI3 with thicker walls
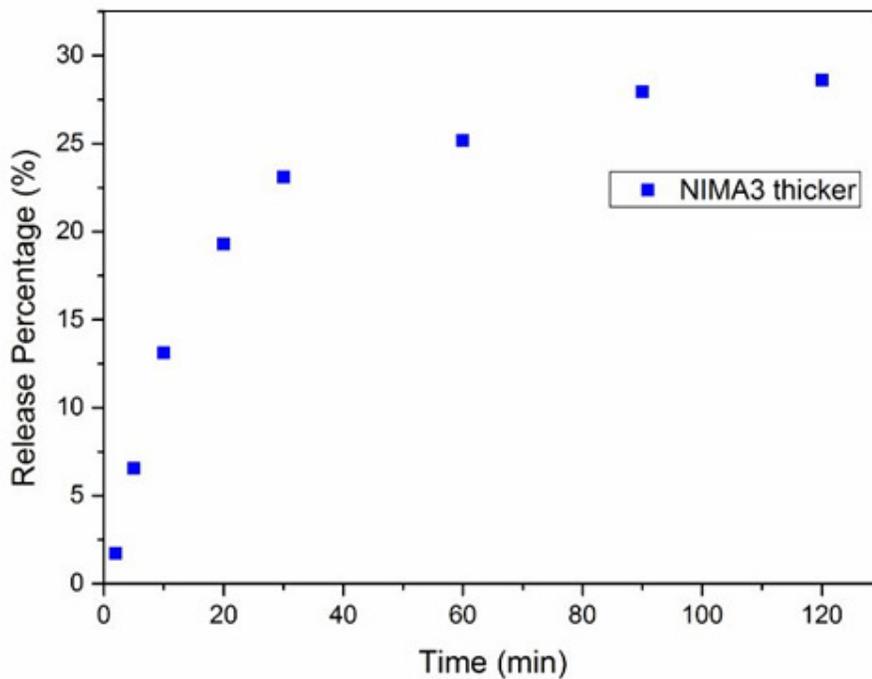
Figure 36: Dye release percentages of NIMA3 with thicker walls

In order to study the stability of the nanotubes, the same experiments were repeated three times and the release percentages as a function of time for each cycle were monitored. Figure 37 shows the release percentages at the end of 120 minutes for NI, NIHE and NIMA coaxial nanotubes after each cycle. In all samples, a drop in the overall release percentage of less than 10 % was observed after each cycle, indicating accumulation of dye molecules in the nanotubes, which can be due to the hydrophilic interactions between the dye molecules. These dye release rates of the nanotubes did not change significantly between cycles, confirming that the stimuli-responsive nature of the polymers was maintained.
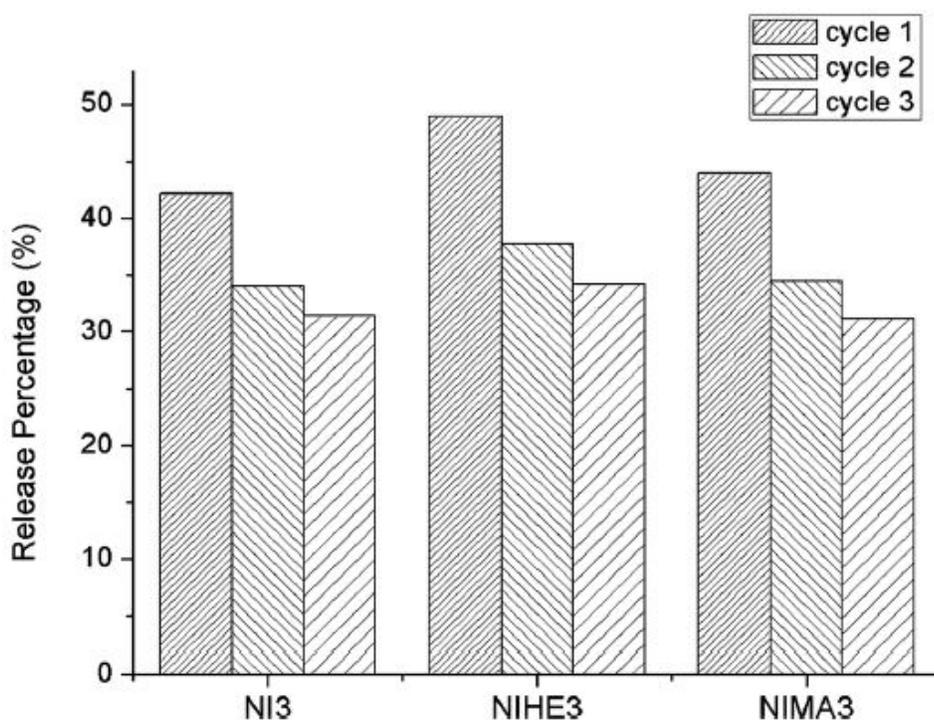
Figure 37: Percentage releases obtained at the end of cyclic release studies of NI3, NIHE3 and NIMA3

The main aim in this study was to design coaxial nanotubes with controllable release kinetics. Our previous studies with single component stimuli responsive nanotubes showed that burst release of loaded molecules could be achieved in response to changes in the stimuli. However, release rates depend heavily on the polymers. The release rates of 0.089 min^{-1} and 0.013 min^{-1} were obtained with single layer pMAA and pNIPAAm nanotubes, respectively, confirming the strong dependence of the release kinetics on the polymers used. In this chapter, released rates ranging between 0.052 min^{-1} and 0.134

min^{-1} were achieved, confirming that by combining two stimuli responsive polymers in one system, release rates could be tuned.

In conclusion, stimuli responsive polymeric nanotubes are fabricated using the templated iCVD technique and the release of a model dye from these nanotubes is systematically studied. The conformal nature of the iCVD process enables fabrication of coaxial nanotubes with layers of different stimuli responsive polymers. The release rates of the polymeric nanotubes depend on the polymers used to fabricate different layers. While pNIPAAm nanotubes have faster release rates, coaxial nanotubes with pMAA inner layers demonstrate slower release due to the difference in the swelling rates of the polymers. These results show that the release rates of the nanotubes can be tuned for different applications by designing coaxial nanotubes for SRP polymers. The amount of dye released, on the other hand, is approximately 50 % of the loaded amount. This low performance can be attributed to the trapping or accumulation of the dye molecules inside the nanotubes, which needs to be improved by tailoring the mesh sizes of the polymers.

CHAPTER 4

HUMIDITY SENSOR STUDY

4.1 Flat Polyaniline Thin Film

The chemical composition of oCVD deposited polyaniline thin film (PANI) was analyzed using FTIR and RAMAN spectroscopy. The FTIR analysis of PANI emeraldine phase confirms that the step-growth polymerization is achieved in oCVD chamber. Besides, RAMAN spectroscopy is used as complementary to FTIR in order to identify the functional groups with higher accuracy.

Figure 38 indicates FTIR spectra of PANI thin film on Si wafer. The broad peaks at 2850-3100 cm^{-1} and 3100-3600 cm^{-1} correspond, respectively, to CH_2-CH_3 and N-H stretching vibration. The strong peak at 1590 cm^{-1} shows C=C vibration in benzene group due to quinoid deformation, while, the peak at 1495 cm^{-1} indicates C-C stretching in benzene ring because of benzenoid deformation. On the other hand, the peak at 1591 cm^{-1} corresponds to C=N stretching vibration outside of benzene ring [103]. Table 10 represents the significant peaks and their corresponding functional groups for PANI emeraldine salt.
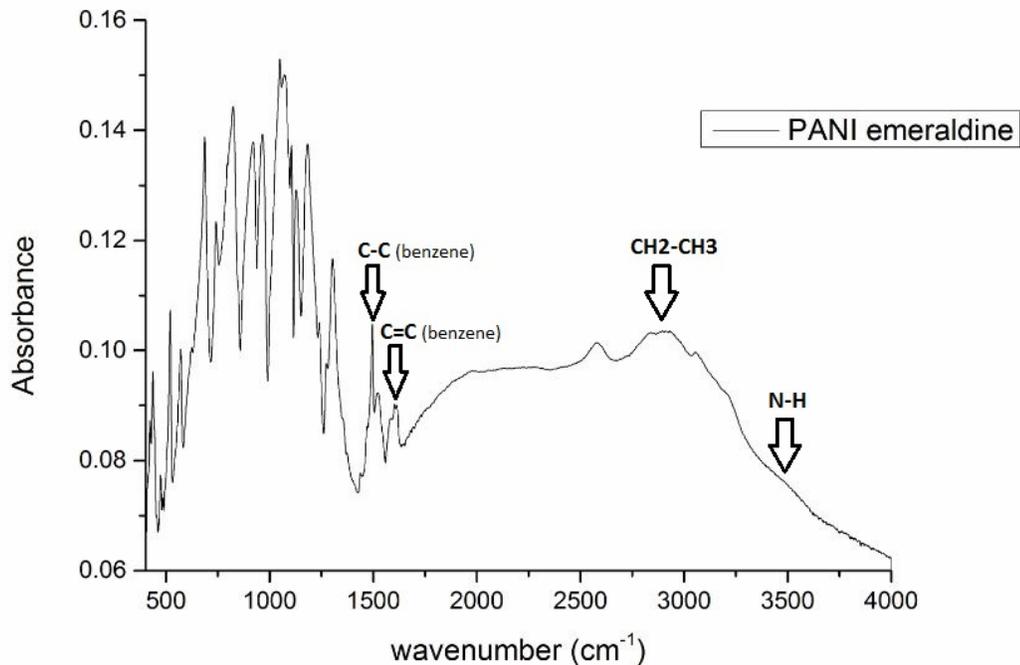
Figure 38: FTIR spectra of PANI emeraldine thin film on Si wafer

Stretching Vibration	Wavenumber (cm^{-1})
CH$_2$-CH$_3$ stretching	2850-3100 cm^{-1} (broad)
N-H stretching	3100-3600 cm^{-1} (broad)
C=C in benzene	1590 cm^{-1} (sharp)
C-C in benzene	1495 cm^{-1} (sharp)
C=N stretching	1591 cm^{-1} (sharp)

Table 10: FTIR peaks of functional groups in PANI emeraldine salt [77]

RAMAN spectra (Figure 39) was acquired in order to ensure that polaronic structure can be simultaneously achieved during doping process in oCVD deposition. Although the RAMAN spectra is noisy due to low PANI film thickness on Si wafer, the critical peaks can be identified at the spectra. The peak at 1193 cm^{-1}, 1223-1272 cm^{-1}, 1458 cm^{-1} correspond, respectively, to C-H bending in benzoid rings, N-H group and C=N stretching in quinoid rings. Besides, the sharp peak at 1569 cm^{-1} shows C=C stretching in quinoid rings, whereas, C-C stretching in benzoid rings can be comprehensible looking at the peak at 1638 cm^{-1} [104]. The two peak at 1332-1376 cm^{-1} indicates the presence of delocalized polaronic structure which is created by doping process and points out the achievement of oCVD deposition and doping.

Table 11 summarizes some important RAMAN peaks of PANI emeraldine salt.
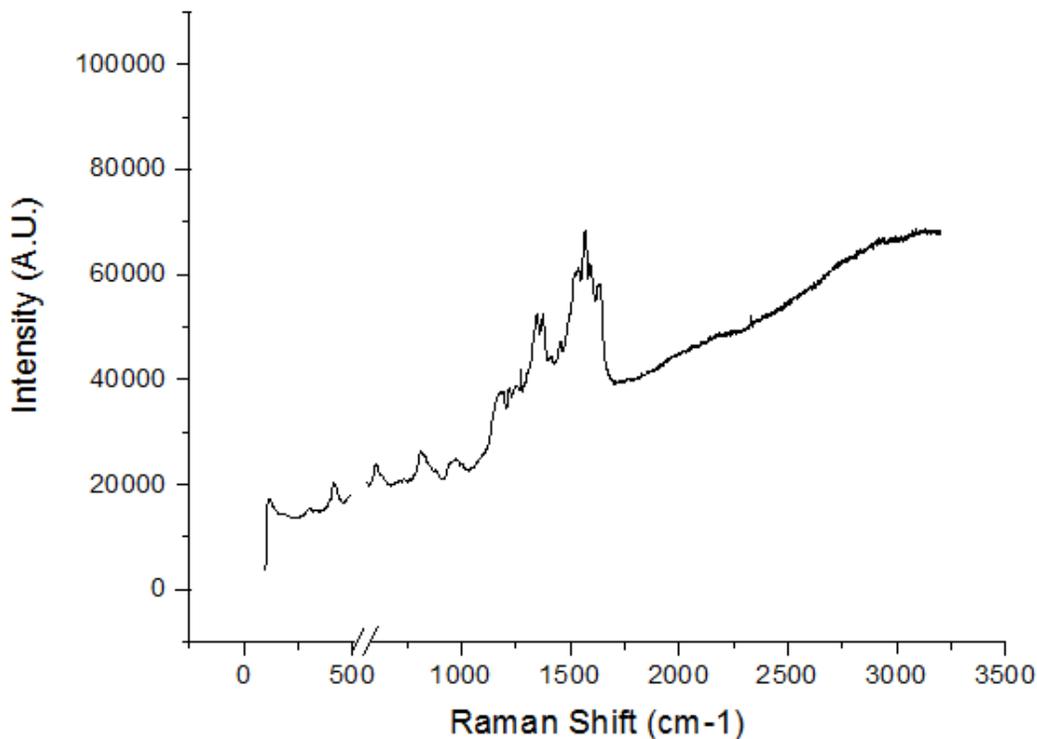
Figure 39: RAMAN spectra of PANI emeraldine thin film on Si wafer

Type of Vibration	Raman Shift (cm^{-1})
C-H bending in benzoid ring	1193 cm^{-1}
N-H bending	1223-1272 cm^{-1}
Delocalized polaronic structure	1332-1376 cm^{-1}
C=N stretching in quinoid ring	1458 cm^{-1}
C=C stretching in quinoid ring	1569 cm^{-1}
C-C stretching in benzoid ring	1638 cm^{-1}

Table 11: RAMAN peaks of functional groups in PANI emerealdine salt

UV-VIS spectrophotometric analysis was performed in order to reveal electronic structure of PANI emeraldine salts. Figure 40 and Figure 41, respectively, demonstrates the UV-VIS of PANI coated glass at different annealed temperatures, 25 °C and 80 °C. The peaks at wavelength of 360 nm and 790 nm indicate the formation of a polaron

band transition. On the other hand, the peak at 430 nm is originated from polaron-bipolaron band transition [105].
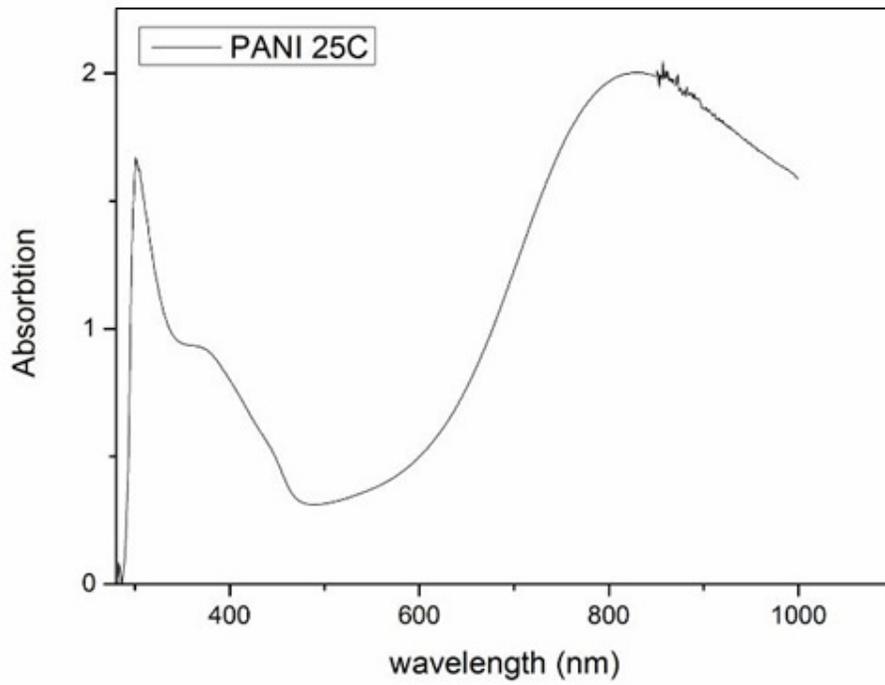
Figure 40: UV-VIS spectra of PANI coated glass (non-treated)
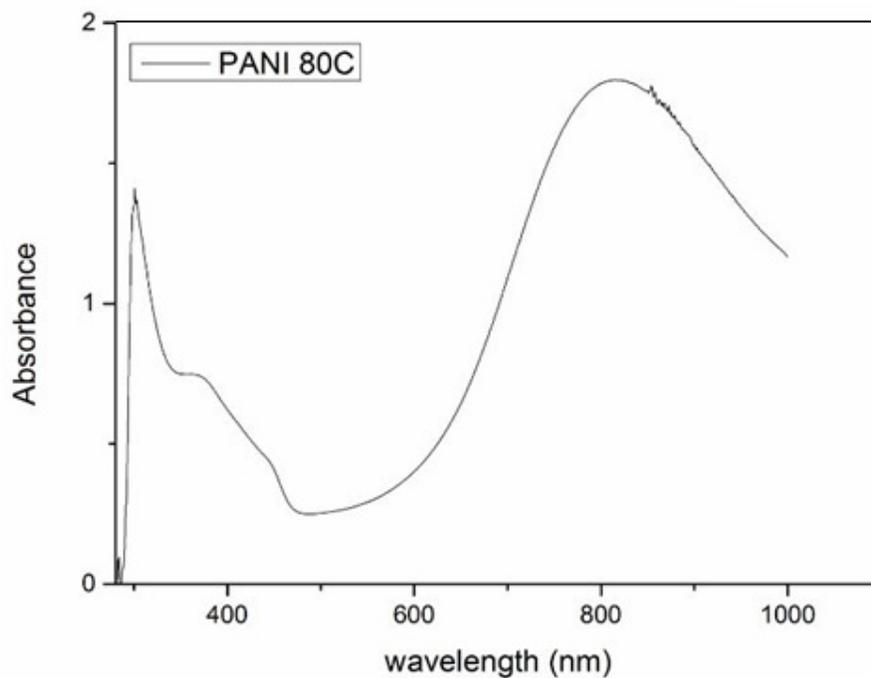
Figure 41: UV-VIS spectra of PANI coated glass (annealed at 80°C)

The band gap of both non-treated and annealed PANI sample is calculated using the equation below ;

$$E_g = \frac{1240}{\lambda}$$

(13)

In order to find band gap of PANI thin film, the line which is tangential to point of inflection of parabola increasing from 490 nm to 360 nm is drawn. The extrapolation of the line to the point, where y axis is zero , is performed. The x-axis interception point is called as band gap (E_g) which is the forbidden gap between first polaron band and conduction level. Figure 42 demonstrates E_g of non-treated and annealed PANI sample at 80 °C. The E_g of non-treated and annealed samples was calculated as 2.21 eV and 2.03 eV, respectively. The slight decrease in band gap with increasing annealing temperature is consistent with the previous PANI studies [106]. Joshi et al. found that the band gap of PANI decreases as annealing temperature increases at a certain point (80-100°C) due to formation of new crystalline region and rearrangement of present crystalline region. However, the annealing at temperature above 80-100 °C initiates deformation and causes damage in crystalline structure of PANI polymer chains resulting in increase of the band gap energy.
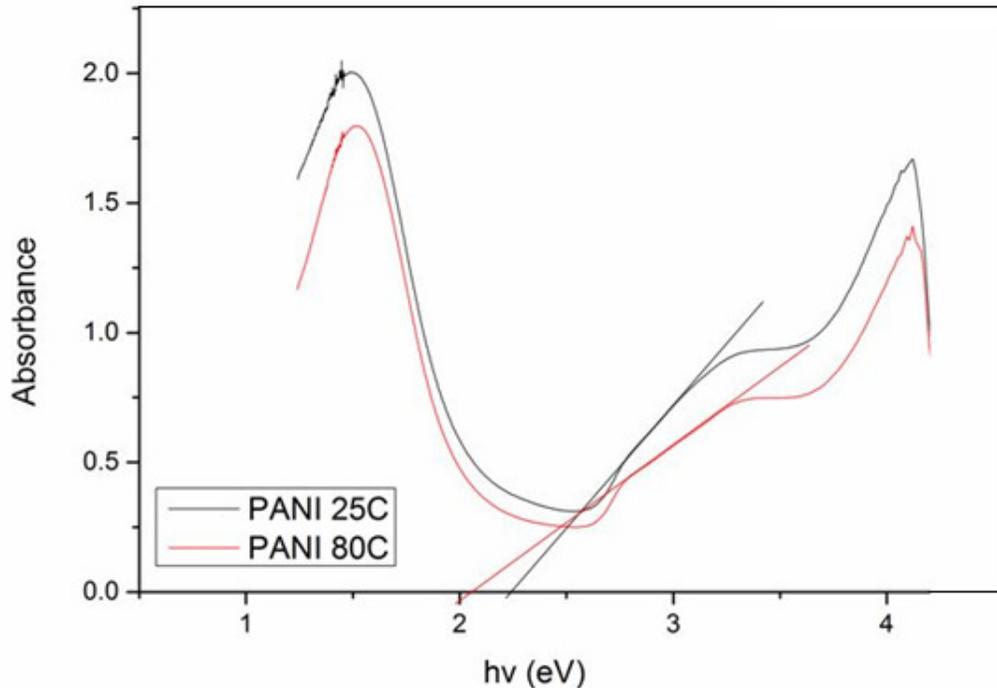
Figure 42: Band gap of non-treated and annealed PANI thin film

To investigate the change of surface roughness of PANI thin film after heating treatment, AFM measurements were performed on non-treated sample and samples annealed at 40°C, 60°C and 80°C. Figure 43 (a) (b) (c) and (d) show raw AFM images of PANI coated glass annealed at different temperatures. Although it seems that there is no distinct difference in the AFM images in terms of surface roughness, the average roughness of 6 points (R_q) (Figure 44) was calculated as 29.875 nm, 26.575 nm, 24.025 nm and 22.825 nm for 250 nm PANI coated glass annealed at 25°C, 40°C, 60°C and 80°C, respectively. The high surface roughness is originated from the excess residual oxidant on the surface after oCVD deposition which can be eliminated by cleaning PANI sample in methanol for 5 minutes. The decrease in surface roughness with arising temperature can be explained by rearrangement of amorphous part of polymer chains and formation of new crystalline region on the surface that reduce the irregularity and increase the percentage of crystalline pack on the surface.
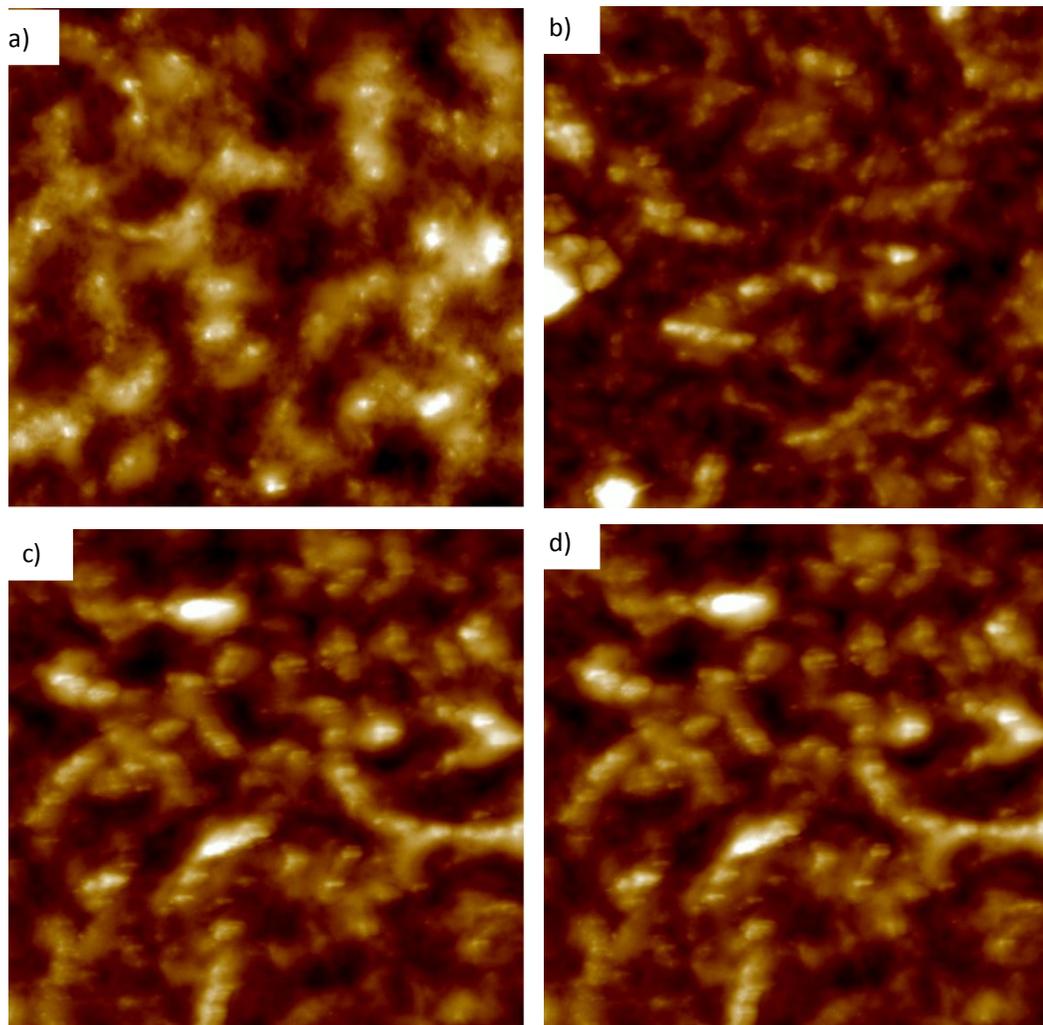
Figure 43: AFM images of PANI thin film annealed at 25°C,40°C,60°C and 80°C
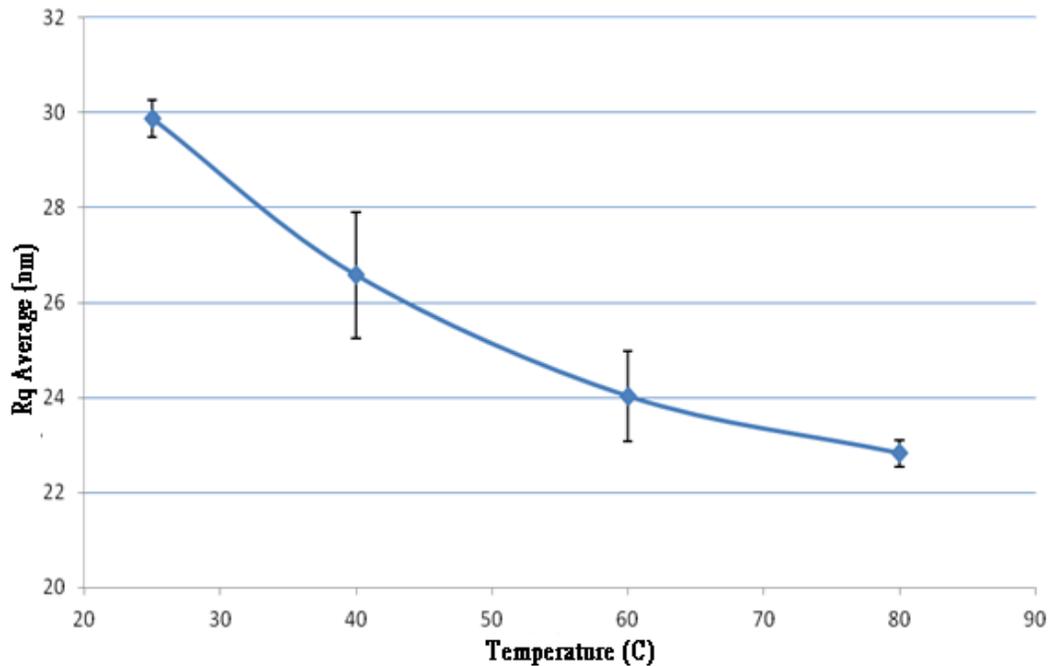
Figure 44: Surface roughness of PANI thin film annealed at 25°C,40°C,60°C and 80°C

XRD measurements were taken in order to analyze the crystalline plane direction of as-deposited PANI thin film and PANI thin film annealed at 80 °C. Figure 45 shows XRD spectra of PANI thin films which are non-annealed and annealed. XRD spectra of annealed sample has peaks at ~16° and ~25° which correspond to (011) and (200) crystalline plane direction in polymer chain, whereas, as-deposited PANI sample lacks any distinct peak, indicating the amorphous structure. The low signal/noise ratio arises from both low thickness of PANI film and high percentage of amorphous region compared to crystalline region. Nevertheless, consequently, it may be stated that annealing at 80°C increases the crystallinity of PANI chains due to rearrangement of amorphous region and formation of new crystalline plane at (011) and (200) direction.
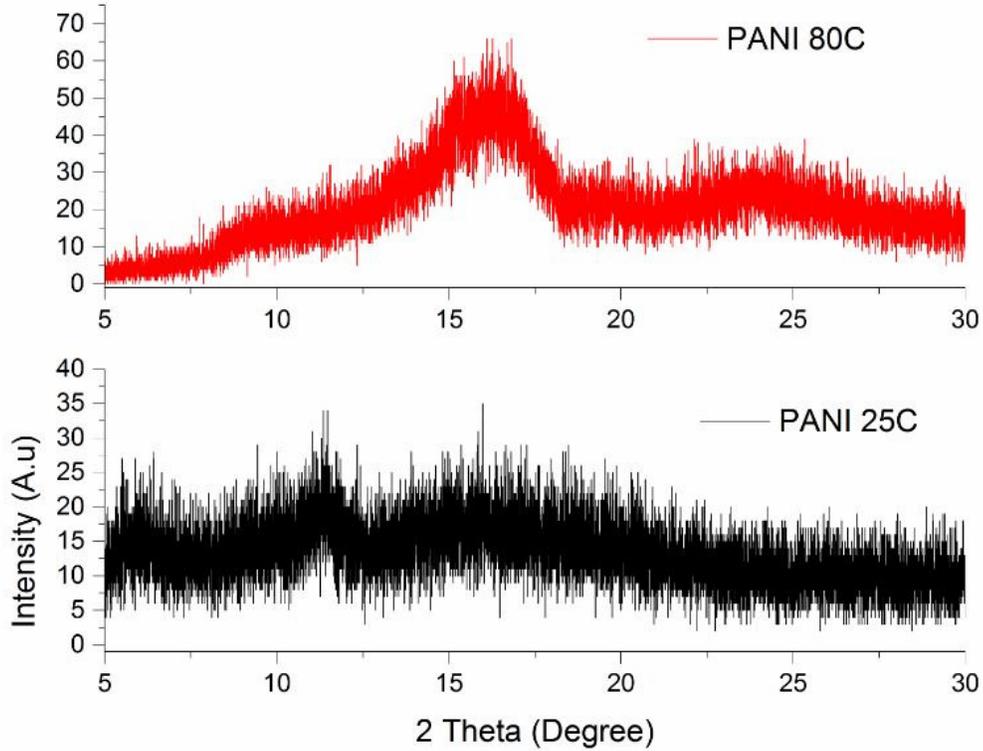
Figure 45: XRD spectra of as-deposited PANI and annealed PANI thin films

For electrical conductivity measurements, 4-point probe conductivity test was performed on PANI coated glass slides which are used as-deposited and as annealed at 25°C, 40°C, 60°C, 80°C, 100°C,140°C and 180°C. The electrical conductivities are calculated using sheet resistance formula;

$$R_S = 4.532 * V/I \tag{14}$$

$$R_S = \rho * d \tag{15}$$

$$\sigma = 1/\rho \tag{16}$$

where R_s is sheet resistance, ρ is resistivity, d is film thickness and σ is electrical conductivity. Figure 46 indicates the conductivities of 400 nm PANI coated glass samples with respect to change of annealing temperature. Electrical conductivities were found as 1.02 S/cm , 2.65 S/cm, 4.54 S/cm, 9.64 S/cm, 25.68 S/cm, 8.72 S/cm and 0.43 S/cm for as-deposited, annealed at 40°C, 60°C, 80°C, 100°C, 140°C and 180°C, respectively. The abrupt increase in the conductivity at 80°C and 100°C stems from the

rearrangement of amorphous part of polymer chain and formation of new crystalline regions that decreases the irregularity and hopping distance between each polymer chain which facilitates the electrons/holes movement and increases charge carrier mobility. Therefore, all PANI nanotubes and thin films were annealed at 100°C for the rest of the study.
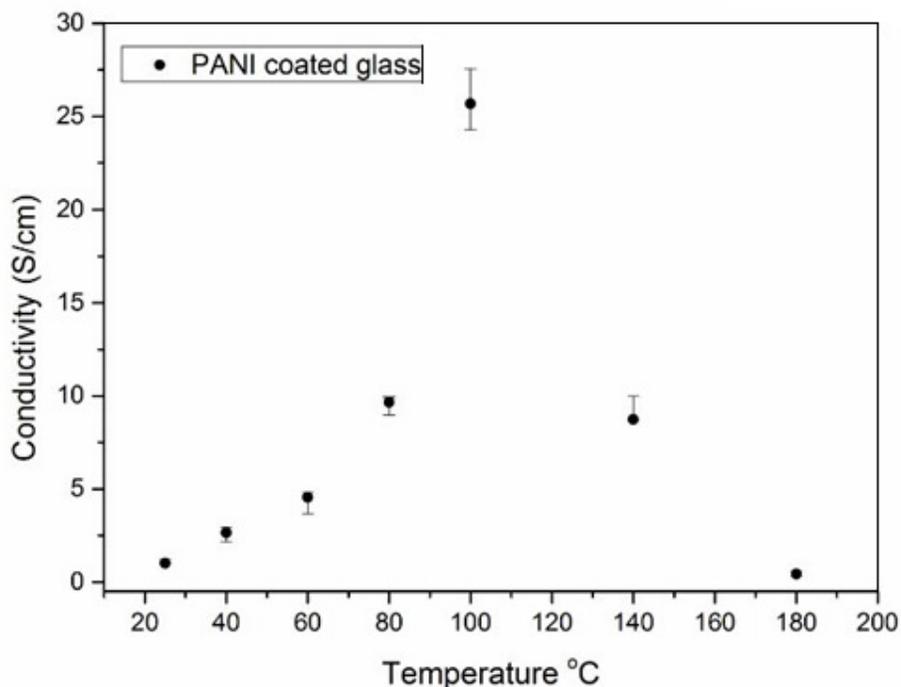
Figure 46: Electrical conductivity of PANI at different annealed temperature

The stability of PANI thin film in air was studied by checking sheet resistance and conductivity change with time. The results (Figure 47) indicate that the conductivity remains at similar level at the end of 30 days compared to its initial value. For example, the initial conductivity of PANI annealed at 80°C is 6.131 S/cm and it reduces to the conductivity of 5.451 S/cm with less than 15% change at the end of 30 days. Consequently, oCVD coated PANI samples show reasonable resistance to the air that making them good candidates for various long-term applications.
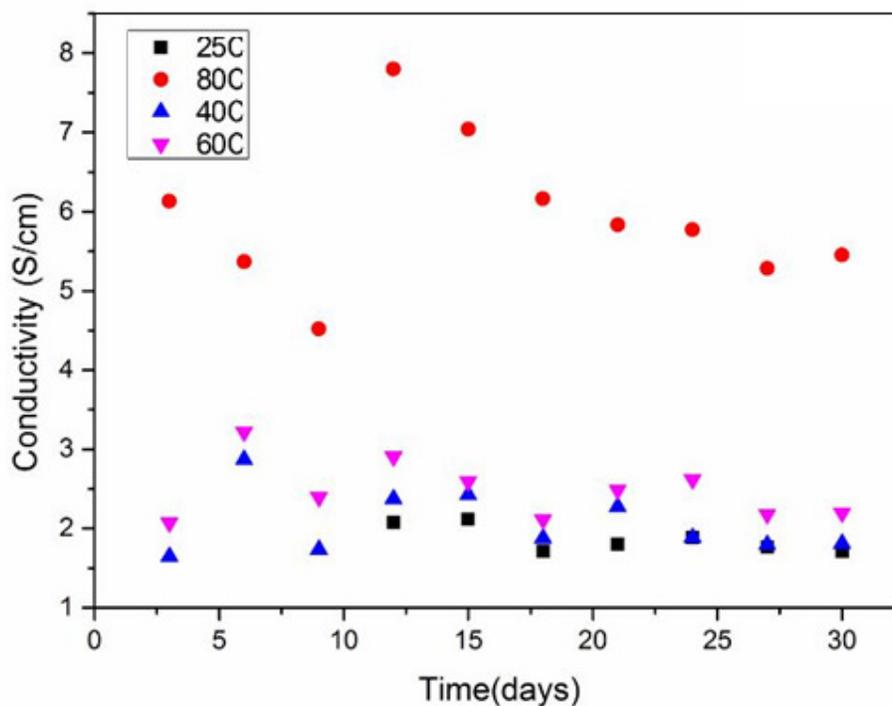
Figure 47: Electrical conductivity change of PANI with time

4.2 PANI Single Nanotube Sensors

SEM images of PANI nanotubes (Figure 48) indicate that oCVD deposition on AAO enabled the successful fabrication of nanotubes with having approximately 30 ∓ 10 nm diameter.
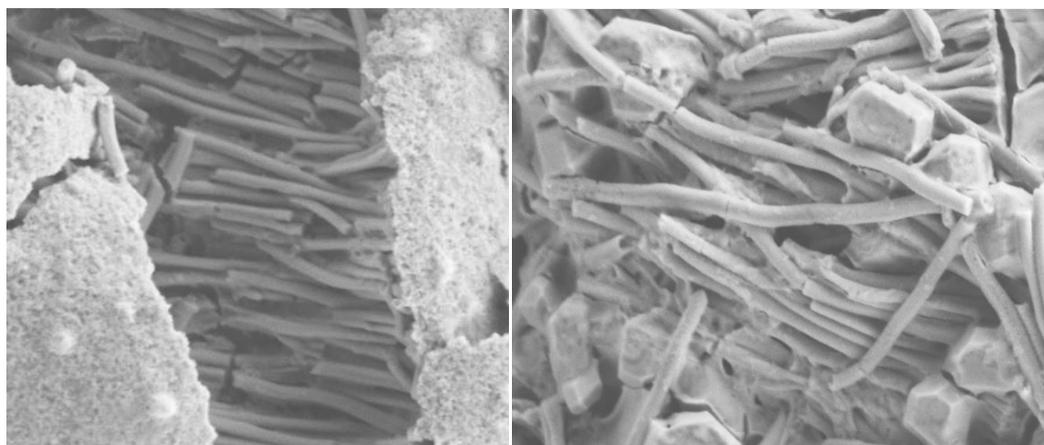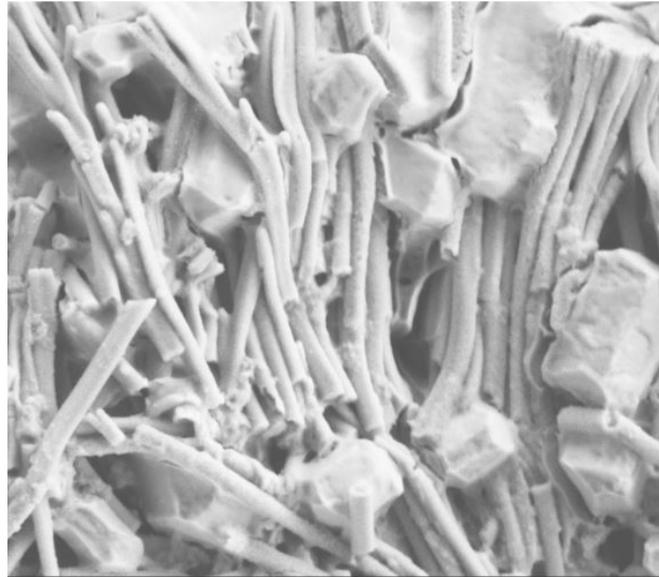
Figure 48: SEM images of PANI nanotubes

The resistance change of gold spots coated PANI nanotubes and flat film at different humidity levels was measured using 2-point probe equipment. Figure 49 shows the location of circular gold spots (light green) and aniline part (dark green). The size of gold electrode was measured 200 micron, as expected. This size was optimized in order to provide better DC resistance.
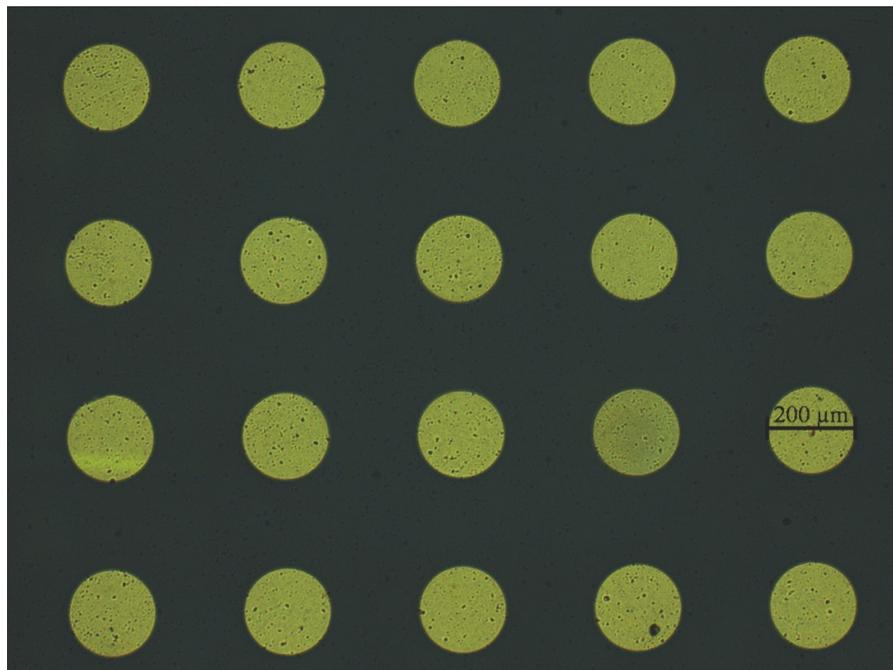
Figure 49: Optical microscopy image of gold electrodes and PANI thin film

For PANI flat film, the normalized resistance value (R/R_0) versus relative humidity (RH%) were plotted in Figure 50 . Initial resistance (R_0) is used for the resistance of PANI thin film at 11.3%. The R/R_0 value of PANI thin film was respectively 1, 0.95, 0.88, 0.83, 0.81,0.76, 0.75, 0.78 and 0.79 for 11.3 %, 22.5%, 32.7%, 43.1%, 52.8%, 75.2%, 84.3%, 93.5% and 97.3%. According to the results, the resistance slightly decreases as RH% increases up to a certain value (RH= 84.3%). However, this trend becomes reversed beyond RH= 84.3% and the resistance increases ~3-4 % of its value at RH= 84.3 %. The maximum resistance of 4372 kΩ was obtained at 11.3% ,whereas the minimum was obtained at 84.3% which is 3301 kΩ. The lower resistance of PANI coated glass compared to the PANI flat film without electrode can be explained by the effect of gold electrode which decreases the contact resistance between PANI polymer and probes of the equipment.
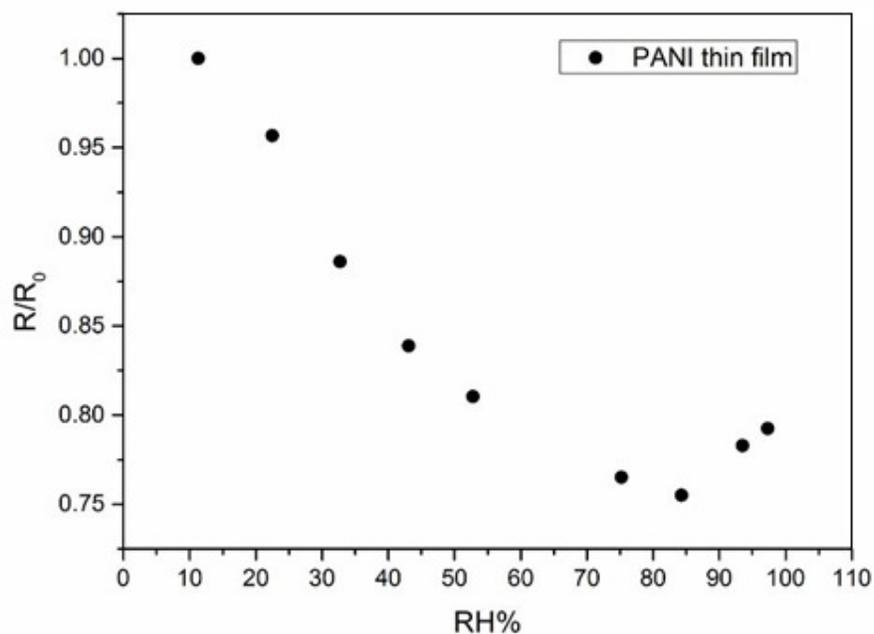
Figure 50: Normalized resistance change of PANI thin film with relative humidity

For PANI single nanotubes, R/R_0 change at different relative humidity was shown in Figure 51. Again, R_0 was used as the resistance value at RH= 11.3% in order to normalize the resistance data. The maximum resistance which is obtained at 97.3% is 1023 kΩ while the minimum resistance was measured as 75 kΩ at 52.8 %. The significant resistance difference between PANI nanotubes and PANI thin film stems from alignment of polymer nanotubes more regularly than polymer thin film that directly affects the hopping distance and reduces the resistance between each chain which facilitates the mobility of charge carrier. At this time, the decreasing trend of resistance become reversed at RH= ~50% as opposed to PANI thin film. The reason of this reversing can be explained by doping and swelling mechanism due to water molecules in the environment. Since, water molecules are ionisable, it can divide into positive proton and negative hydroxyl ions when entering to polymer chain. The positive proton (H^+) ions act as dopant when encountering the undoped region of PANI emeraldine salt. Therefore, it increases the doping level of PANI film up to certain value due to limited undoped region. When the doping level reaches the maximum and undoped part is filled by H^+ ions, the other effect become dominated which is called swelling effect. As polymer chains swell due to excess water in the ambient, the distance between each chain increases which results in higher hoping distance/resistance and also creates distortion in polymer chains that increase electrical resistance. Briefly, the competition between doping effect and swelling effect determines the minimum point of resistance for conducting polymer [76]. The cause of distinct reverse point for PANI thin film and nanotubes (84.3% and 52.8%, respectively) can be explained by the huge difference in their surface-to-volume ratios. The nanotube structure has higher surface-to-volume ratio than flat thin film so that water molecules can more easily contact with each polymer chain of the nanotubes. Even lower humidity levels enable the undoped region of polymer chain of the nanotubes to be filled by H^+ ions, but not for flat thin films. Thus, reverse point of PANI nanotubes is at 52.8% while it is at 84.3% for flat thin film.
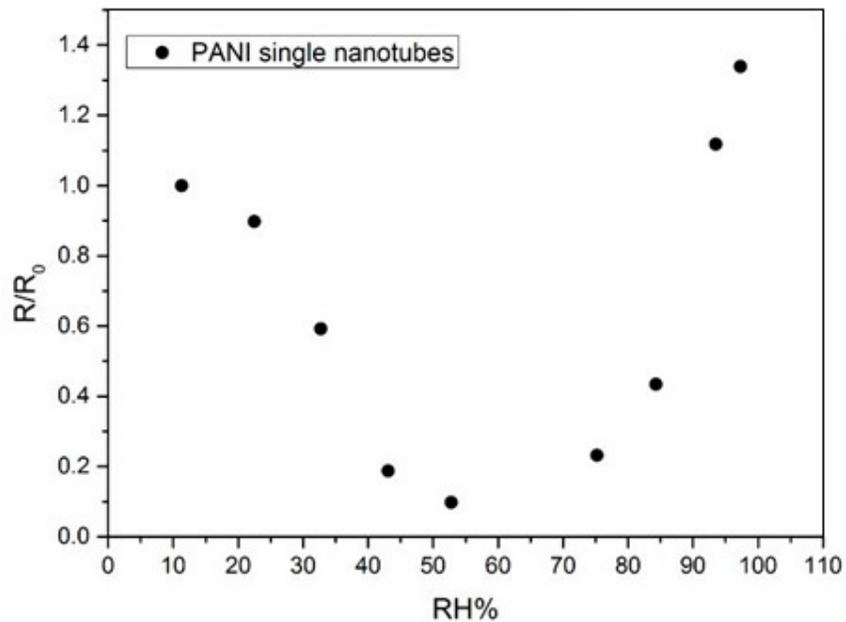
Figure 51: Normalized resistance change of PANI single nanotubes with relative humidity

Figure 52 indicates the comparison of normalized resistance between PANI nanotubes and thin film. The variation of resistance with different RH% condition is greater for PANI nanotubes than PANI thin film. The normalized resistance of nanotubes changes from 1 to 0.09 whereas it is only between 1 and 0.75 for PANI thin film. Therefore, it can be stated that PANI nanotubes show better sensor sensitivity than PANI thin film. The reason of this behavior is similar to explanation of different reverse point. The higher surface-to-volume ratio of nanotubes provide greater area for water molecules which interact with polymer chains. Thus, more water molecules can contact with PANI nanotubes rather than thin film that increases the variation of electrical resistance with ambient relative humidity change.
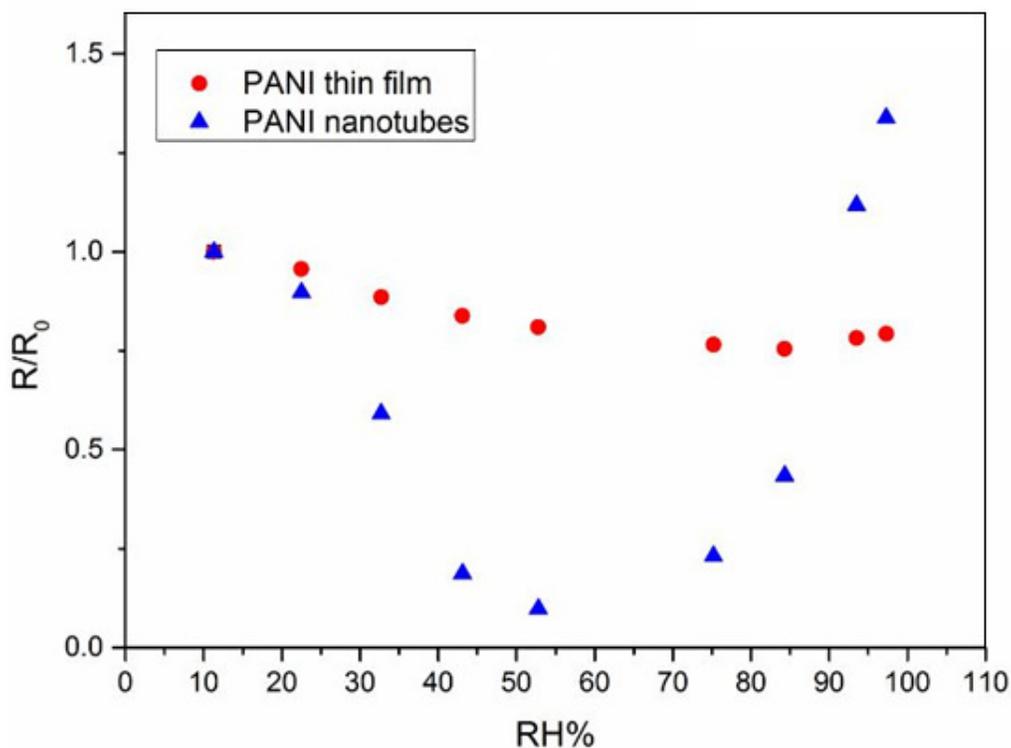
Figure 52: Comparison of PANI nanotubes and thin film R/R$_0$ variation

To check the stability of PANI nanotubes sensor, the cyclic measurement was performed at air and RH= 52.8% (optimal condition) for 10 times. Figure 53 shows the resistance change between two condition. In the first cycle, the resistance was measured as 336 kΩ and 79 kΩ at air humidity level and RH=52.8%, respectively. In the tenth cycle, the PANI resistance was 334 kΩ and 87 kΩ, at air and 52.8%. The change of conductivities is lower than ~10% that indicates the resistances at air and 52.8% remains the same level at the end of 10 cycle. In each cycle, the response time of PANI nanotubes ,from lower conductivity to higher, was measured 100 seconds which is consistent with the literature. Therefore, it can be concluded that PANI nanotubes can be suitable in the application of sensors for long-term usage.
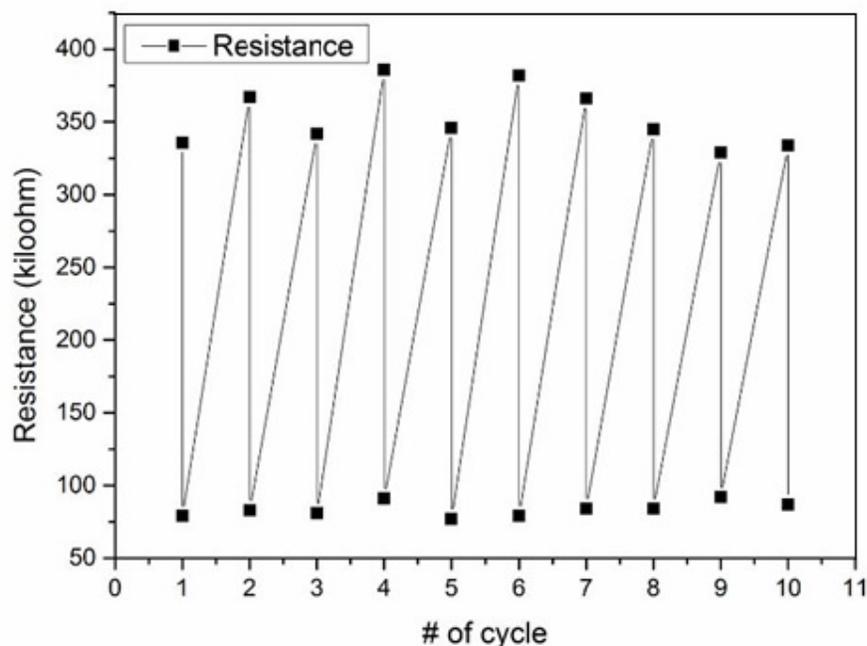
Figure 53: Stability of PANI nanotubes at different RH%

4.3 PANI+HEMA Coaxial Nanotubes Sensors

PANI+ HEMA coaxial nanotubes were fabricated in order to analyze the effect of SRP layer on the performance of humidity sensor. Similarly to the process performed on PANI nanotubes, all PANI+ HEMA coaxial nanotubes were coated by gold and gold spots with having the diameter of 200 micron were obtained on the nanotubes as an electrode.

For PANI+ HEMA coaxial nanotubes, the normalized resistance value (R/R_0) versus relative humidity (RH%) were plotted in Figure 54 . Initial resistance (R_0) is used for the resistance of PANI thin film at 97.3% at this time. According to the results, the resistance shows parabolic rise with increasing humidity level. The increase of normalized resistance is very limited between the humidity of 11.3% and 32.7%, however, it shows significant resistance rise until RH= 97.3%. The maximum resistance of 4027 kΩ was obtained at 97.3%, whereas, the minimum resistance was 957 kΩ at the humidity level of 22.5%.
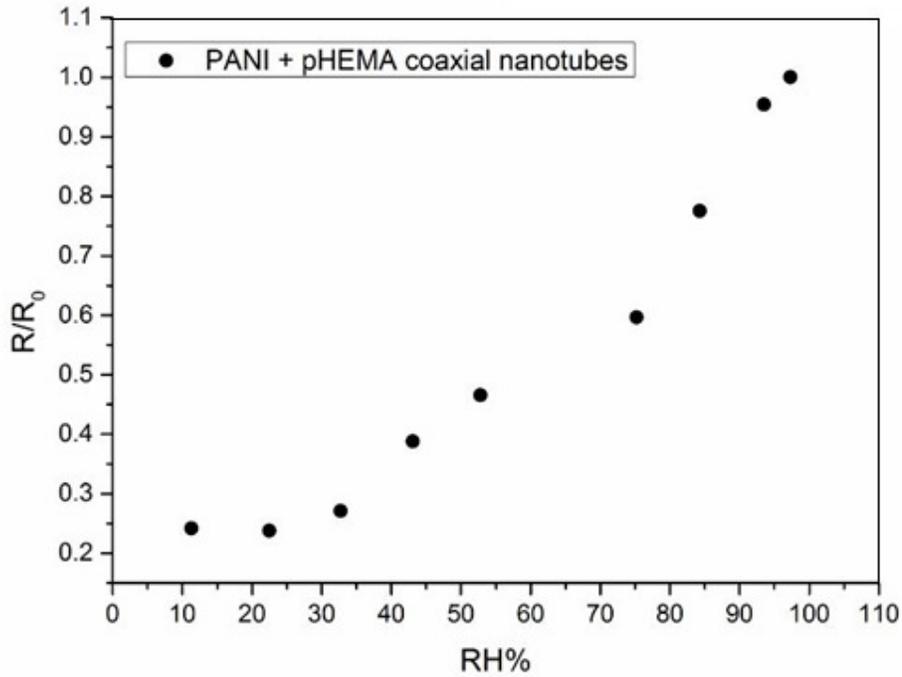
Figure 54: Normalized resistance change of PANI+HEMA coaxial nanotubes with relative humidity

To compare the R/R_o trend of PANI nanotubes and PANI+HEMA coaxial nanotubes, normalized resistance versus RH% were plotted for two type of nanotubes in one figure (Figure 55). The significant difference between the trend of normalized resistance change with increasing humidity level stems from the existence of SRP polymer of pHEMA in the coaxial nanotubes. As stated earlier, pHEMA is water-responsive polymer that swells or deswells with respect to the water level in the ambient. As humidity increases, the pHEMA swells that results in higher distance between each polymer chains which affects the electronic structure of the whole nanotubes. The higher distance between polymer chains increases the hoping resistance of polymer structure so that the resistance of coaxial nanotubes rises with increasing humidity level. At this time, the doping effect is dominated by swelling effect due to pHEMA layer on the nanotube. The doping effect can only beat the swelling effect at lower humidity level , between 11.3% and 22.5%, that causes slight decrease in resistance from 973 kΩ to 957 kΩ. However, this trend becomes reversed at 32.7% which electrical resistance shows a continuous increase until 97.3%. Consequently, addition of pHEMA layer on PANI polymer decreases relative humidity level ,which provides the minimum resistance, from 52. 8% to 22.5%.
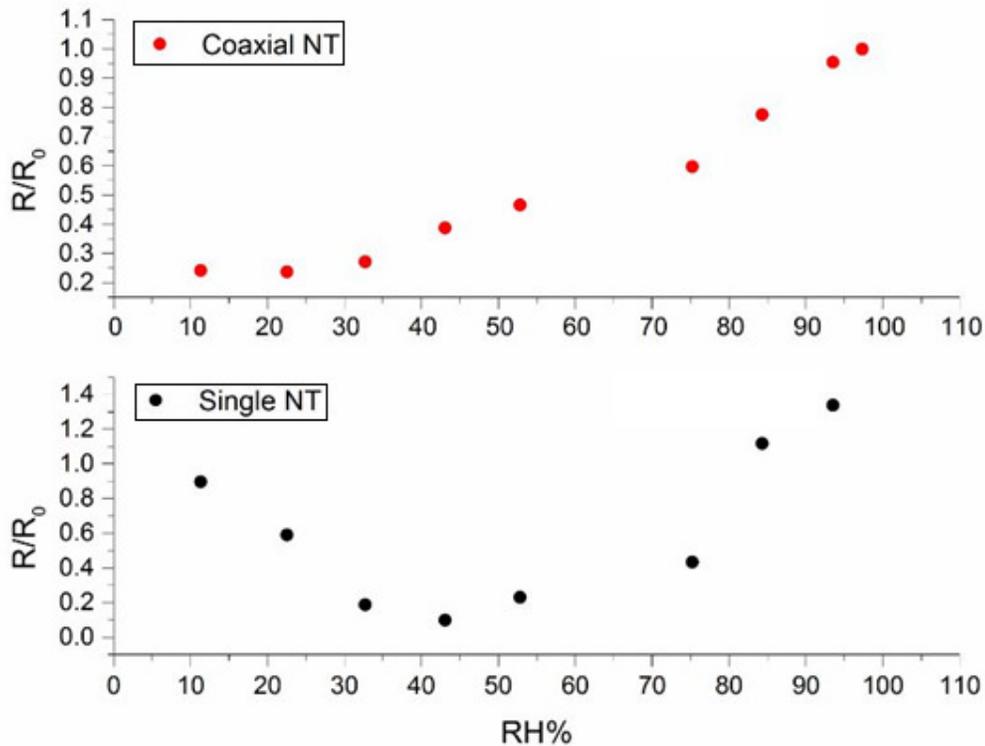
Figure 55: Comparison of PANI+HEMA coaxial nanotubes and PANI nanotubes R/R_0 variation

For the stability of PANI+HEMA coaxial nanotubes sensor, the cyclic measurement was performed at air and RH= 22.5% (lowest resistance) for 10 times. Figure 56 indicates the resistance change between two condition. In the first cycle, the resistance was measured as 1154 kΩ and 943 kΩ at air humidity level and RH=22.5%, respectively. In the tenth cycle, the PANI resistance was 1246 kΩ and 983 kΩ, at air and 22.5%. The change of conductivities is lower than ~10% that indicates the resistances at air and 52.8% remains the same level at the end of 10 cycle. In each cycle The response time of PANI+HEMA nanotubes ,from lower conductivity to higher, was measured 60 seconds which is better response rate than PANI nanotubes due to fast swelling rate of pHEMA rather than PANI. Therefore, it can be concluded that PANI+HEMA nanotubes can be used for several cycles without any performance loss. Furthermore, the better response time can be great advantage for humidity sensor applications.
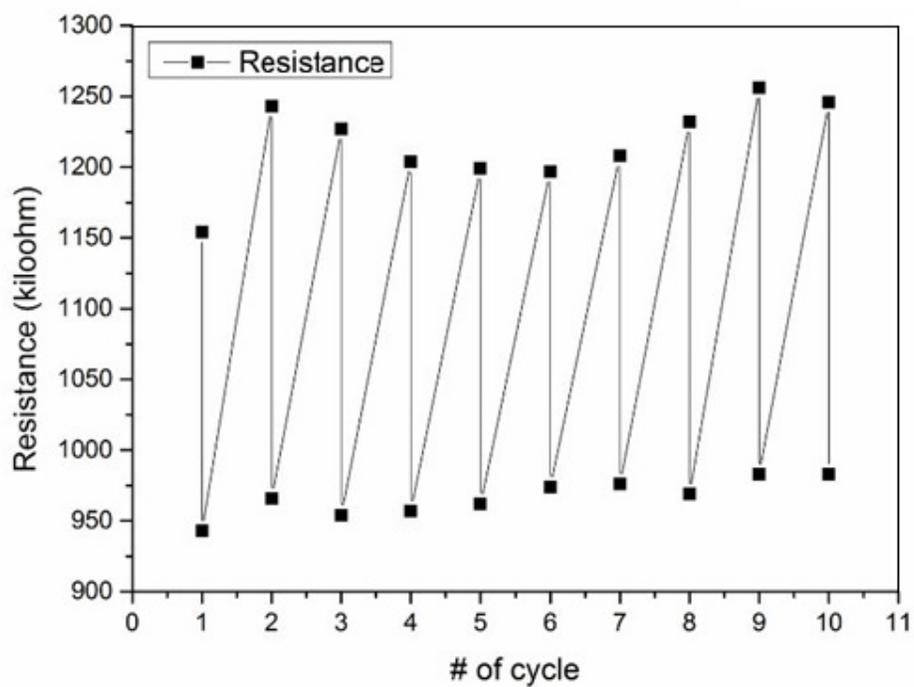
Figure 56: Stability of PANI+HEMA nanotubes at different RH%

CONCLUSION

Within the scope of this thesis, the fabrication of SRP and CP based polymeric single and coaxial nanotubes was achieved using two types of chemical vapor deposition technique, initiated chemical vapor deposition (iCVD) and oxidative chemical vapor deposition (oCVD).

The aim of this thesis is to control the loading/release kinetics and enhance humidity sensor sensitivity changing the polymer and tuning the type of polymer layer of the nanotubes. For this purpose, firstly, pH responsive (pMAA) single nanotubes and pNIPAAm based SRP coaxial nanotubes were fabricated using initiated chemical vapor deposition (iCVD) for release studies. The maximum release amount of the nanotubes were calculated after several UV-VIS characterization measurement. Subsequently, release kinetics were calculated using first order kinetic model for pH responsive nanotubes and coaxial nanotubes. This study shows that while pNIPAAm or pH responsive single nanotubes have faster release rates, coaxial nanotubes with pMAA or pHEMA inner layers demonstrate slower release due to the difference in the swelling rates of the polymers. The results also indicate that the release rates of the nanotubes can be tuned for different applications by designing coaxial nanotubes for SRP polymers.

In the last chapter of the thesis, PANI single nanotubes and PANI+HEMA coaxial nanotubes were synthesized using both oxidative chemical vapor deposition and initiated chemical vapor deposition techniques. The effect of annealing on PANI was analyzed using several characterization techniques. According to the results, annealing up to 80-100 °C decreases the band gap and roughness while increases the crystallinity and electrical conductivity of PANI polymer. However, higher annealing temperatures damage and deform polymer structure which decreases the electronic conductivity of PANI. Thus, the optimal annealing point of 100 °C was selected for all PANI nanotubes to obtain better conductivity in the sensor application. After characterization on PANI thin film, the sensitivity of PANI flat film, PANI nanotubes and PANI+HEMA coaxial nanotubes were analyzed using 2-point probe equipment. The results show that the best sensitivity is obtained with PANI nanotubes. However, the interesting trend was observed in the resistance measurement of all nanotubes. As relative humidity increases up to certain point, the resistance firstly decreases, then it reaches reverse point and

become increasing. This trend is caused by the competition between the doping effect and swelling effect of PANI due to water in the environment. PANI+HEMA coaxial nanotubes show lower reverse point due to existence of water-responsive HEMA layer on polymer nanotubes. Besides, cyclic tests were performed on both PANI nanotubes and PANI+HEMA coaxial nanotubes in order to analyze the stability of nanotube sensors for long-term applications. The results indicate that the nanotubes can be used for several times without any performance loss.

BIBLIOGRAPHY

1) C. Petruczok, et al. (2014).Macromolecular Rapid Communication 35: 1345-1350.

2) E.S Gil and S. M. Hudson (2004), Prog. Polym. Sci. 29(12): 1173-1222.

3) S.T Grainger and M. El-Sayed (2010). Stimuli-sensitive particles fordrug delivery. biologically-responsive hybrid biomaterials: a reference for material scientists and bioengineers. Danvers, World Scientific Publishing Co. Pte. Ltd.

4) Y. Liu, et al. (2013). Asian Journal of Pharmaceutical Sciences 8: 159-167.,

5) I.Y. Galaev and B. Mattiasson (2008). Smart Materials, CRC Press.,14-24

6) S.J.P McInnes, et al. (2012). ACS Appl. Mater. Interfaces 4: 3566.

7) S.R Macewan, et al. (2010). Nanomedicine UK 5(5): 793-806.

8) R. Liu, et al. (2009). Colloid and Polymer Science 287(6): 627-643.

9) X. Li, et al. (2014). Soft Matter 10: 2008-2015.

10) K. Tauer, et al. (2009). Colloid Polym. Sci. 287(299-312).

11) M. Heskins and J. E. Guillet (1968). J. Macromol. Sci., Part A: Pure Appl. Chem. 2: 1441-1455.

12) Z. Shen, et al. (2008). Eur. J. Pharm. Sci. 35: 271-282.

13) X. Zhang, et al. (2004). Biomaterials 25: 3793-3805.

14) Y.Y. Li, et al. (2007). Nanotechnology 18: 215605.

15) V. Mittal, et al. (2007). European Polymer Journal 43: 4868-4881.

16) M.C. Koetting, et al. (2015). Material Science and Engineering R 93: 1-49.

17) N.A Peppas and E. W. Merrill (1977). J. Appl. Polym. Sci. 21: 1763-1770.

18) E. Garcia-Millan, et al. (2015). International Journal of Pharmaceutics 487: 260-269.

19) G. Ozaydin-İnce, et al. (2010). Soft Matter 6: 1635-1639.

20) C.K Chiang, et al. (1977). "Electrical Conductivity in Doped Polyacetylene " Phys. Rev. Lett. 39: 1098.

21) Kroschwitze, J. I. (1988). Electronical and Electronic properties of polymer, John Wiley and Sons INC P57.

22) Kareema, M. Z. (1997). The electrical and optical properties conducting polymers (PT, PT/PVCand PT/PTFE) of and Their application in Rechargeable Batteries. Basrah,Iraq, University of Basrah. PhD Thesis.

23) Camurlu, P. (2014). RSC Adv. 4: 55832.

24) J.E. Yoo, et al. (2007). J.Mater.Chem 17: 1268-1275.

25) Y. Zhang and G. C. Rutledge (2012). Macromolecules 45: 4238-4246.

26) K. M. Molapo, et al. (2012). Int. J. Electrochem. Sci. 7: 11859-11875.

27) A. K. Gaharwar et al. (2014), Biotechnol. Bioeng, 111,:441-453.

28) N. Rapoport (2007), Prog. Polym. Sci., 32: 962–990.

29) S. F. Peteu et al. (2010) Polymers, 2: 229–251

30) S. Ganta et al. (2008), J. Controlled Release: 126, 187.

31) H. M. C. Azeredo et al. (2011), In Tech, edited by B. Reddy, DOI: 10.5772/14437

32) P. Krogstrup, et al. (2013). Nature Photonics 7: 306-310.

33) G. Ozaydin-Ince, et al. (2011), PNAS, 108: 2656

34) F. S. Du et al. (2010), Soft Matter,6: 835-848

35) J. Chen et al.(2014), Chem. Commun. ,50 :14482–14493

36) H. Masuda and K. Fukuda (1995), Science, 268 :1466–1468

37) M. Yoshizawa et al. (2009), Angew. Chem., Int. Ed., 48: 3418–3438

38) S. Ganta et al. (2008), J. Controlled Release, 126: 187.

39) S. Mura et al. (2013), Nat. Mater., 12,:991.

40) Z. Deng et al. (2011), Biomaterials, 32: 4976.

41) K. C. Hribar et al. (2011), ACS Nano, 5: 2948.

42) G. L. Li et al. (2013) ACS Nano, 7: 2470

43) G. Chen et al. (2014), *J. Mater. Chem.,* 2, 1327

44) E. Garcia-Millan, et al. (2015). International Journal of Pharmaceutics 487: 260-269

45) J.H. Chang, et al. (2004). Bull.Korean Chem. Soc. 25: 1257-1260.

46) G. Baochun et al. (2008), *Applied Surface Science,* 255, 2715–2722

47) G. Chen, et al. (2014). J. Mater. Chem B. 2: 1327.

48) G. Cavallaro et al. (2015). J. Phys. Chem. C 119: 8944-8951.

49) S. J. P. McInnes et al. (2012), *ACS Appl. Mater. Interfaces,4, 3566-3574.*

50) G. Ozaydin-İnce, et al. (2010), Soft Matter, 6: 1635-1639

51) E. Armagan, et al. (2015). Nanoscience and Nanotechnology Letters 7: 79-83.

52) E. Armagan and G. Ozaydin-İnce (2015). Soft Matter 11: 8069-8075.

53) J. Jang and H. Yoon (2005). Langmuir 21: 11484-11489

54) J. Jang, et al. (2005). Adv. Mater. 17: 1616-1620.

55) G. Li and Z. Zhang (2004). Macromolecules 37: 2683-2685.

56) Y.K. Koo, et al. (2004). Mol. Cryst. Liq. Cryst 425: 55-60.

57) T. Higuchi, et al. (2015). Microscopy 64: 205-212

58) J. Huang, et al. (2010). J. Mater. Chem 20: 1117-1121.

59) S. Nejati, et al. (2014). ACS Nano 8: 5413-5422.

60) S. N Habisreutinger et al. (2014). Nano Lett 14: 5561-5568.

61) S. Peng et al. (2012). RSC Adv. 2: 652-657.

62) A. Sumboja et al. (2015). Adv. Mater. Interfaces 2: 1400154.

63) M. Chen-Liu et al. (2009). Sensors 9: 869-880.

64) M.R. Abidian et al. (2006). Adv. Mater. 17: 405-409.

65) O. S Kwon et al. (2012). Nano Lett. 12(2797-2802).

66) Ishpal and A. Kaur (2013). Journal of Applied Physics 113: 094504.b

67) F. Wang et al. (2008). J. Am. Chem. Soc. 130: 5392-5393.

68) A. Mohammedi et al. (1986), Synth. Met., 14: 189.

69) B. Winther-Jensen et al. (2004). Macromolecules 37: 5930-5935.

70) A. Sumboja et al. (2015). Adv. Mater. Interfaces 2: 1400154.

71) S. Virji et al. (2004) Nano Letters 4: 491-496.

72) P. Y. Stakhira et al. (2005), Phys. Chem. Solid State, 6: 96-98

73) M. R. Anderson et al. (1991), Science,252: 1412-1415

74) M. Chen-Liu et al. (2009). Sensors 9: 869-880.

75) J. Wang et al. (2004), Nano Lett.,4 : 1693-1697

76) F. W Zeng et al. (2010). Sensors and Actuators 143: 530-534.

77) Q. Lin et al. (2012). Sensors and Actuators B 161: 967-972.

78) N. Parvatikar et al (2006). Journal of Applied Polymer Science 102: 5533-5537.

79) K. K. Gleason et al. (2007), Surface and Coatings Technology, 201: 9400-9405

80) K. K. Gleason et al. (2010), Advanced Materials, 22: 1993-2027

81) T. Cikim et al. (2014). Journal of Heat Transfer 136: 081504.

82) G. Ozaydin-İnce, et al. (2010), Soft Matter, 6: 1635-1639

83) N. J. Trujilo et al. (2010), J. Mater. Chem., 20: 3968-3972

84) J.P Lock et al. (2006), Macromolecules, 39: 5326-5329

85) R. M Howden et al. (2013). J.Mater.Chem A 1: 1334.

86) S. Nejati , and K.K.S. Lau (2011), Langmuir, 27(24): 15223-15229.

87) D. Bhattacharyya et al. (2012) J. Polym. Sci, Part:B Polym Phys.,50: 1329-1351.

88) S. H. Baxamusa et al. (2009). Phys. Chem. Chem. Phys 11: 5227-5240.

89) A. Wexler and S. Hasegawa (1954). Journal of Research of the National Bureau of Standarts 53: 20-26

90) E. Armagan, et al. (2015). Nanoscience and Nanotechnology Letters 7: 79-83.

91) K.K.S Lau and K. K. Gleason (2007). Macromol. Biosci. 7: 429-434.

92) K. Bumsang et al. (2003), Journal of Applied Polymer Science, 89: 1606-1613

93) A. R. Berens and H. B. Hopfenberg (1978), Polymer 19: 489

94) G. Chen et al. (2014), J. Mater. Chem., 2: 1327

95) J. Wang et al. (2012), J. Colloid Interface Sci., 369: 231-237

96) C. G. Gomez et al. (2003), J. Biochem. Biophys. Methods, 55: 23-26

97) T. Trongsatitkul and B. M. Budhlall (2012) Polym. Chem., 4: 1502–1516.

98) C. Erbil et al. (2000) Polym. Int., 49: 795–800.

99) S. Yarimkaya and H. Basan (2007) J. Macromol. Sci., Part A: Pure Appl.Chem., 44: 939–946.

100)   K. Tauer et al. (2005), Colloid Polym. Sci., 283: 351–358

101)   C. L. Bell and N. A. Peppas (1996) Biomaterials, 17: 1203–1218

102)   A. Asatekin and K. K. Gleason, (2011) Nano Lett., 11: 677–686.

103)   M. Campos et al. (2014). J. Appl. Polym. Sci. 131: 40688.

104)   E. C Gomes and M. A. S. Oliveira (2012). American Journal of Polymer Science 2: 5-13.

105)   B.S Flavel et al. (2009). Soft Matter 5: 164-172.

106)   G. P. Joshi et al. (2006). Indian J Pure& Appl Phys 44: 786-790.